On Skin Cyanotic Appearances and Spectral Responses Elicited by Methemoglobinemia and Sulfhemoglobinemia

by

Stephen Askew

A thesis
presented to the University of Waterloo
in fulfillment of the
thesis requirement for the degree of
Master of Mathematics
in
Computer Science

Waterloo, Ontario, Canada, 2018

I hereby declare that I am the sole author of this thesis. This is a true copy of the thesis, including any required final revisions, as accepted by my examiners.

I understand that my thesis may be made electronically available to the public.

Abstract

Methemoglobinemia and sulfhemoglobinemia are potentially life-threatening blood disorders characterized by similar symptoms and markedly distinct treatment procedures. In this thesis, we investigate the causal relationship between these disorders and the onset of cyanosis (purple or bluish skin coloration). More specifically, we perform controlled experiments to elicit cyanotic appearances resulting from different severity levels of these disorders and varying physiological conditions. We note that such experiments cannot be induced in living subjects without posing risks to their health. Accordingly, we have resorted to an *in silico* experimental approach supported by biophysical data reported in the biomedical literature. Besides bringing new insights about cyanotic chromatic variations elicited by methemoglobinemia and sulfhemoglobinemia, our investigation provides the basis for the proposition of a cost-effective protocol for the noninvasive detection and differentiation of these disorders. Our experimental results indicate that its sensitivity range exceeds the range of similar technologies, which are in general associated with high operational costs. We believe that these aspects make the proposed protocol particularly suitable for incorporation into noninvasive disease screening/diagnostic systems, particularly those deployed at the point of care of medical settings with limited access to laboratory resources.

Acknowledgements

I would like to thank my supervisor Gladimir V. G. Baranoski for his positivity and guidance throughout the development of this thesis. In addition, I would like to thank the rest of the Natural Phenomena Simulation Group, both alumni and current members, for their support.

Table of Contents

List of Tables vii

List of Figures xiii

1 Introduction 1

2 Biophysical Background 5

2.1 Skin Overview 5

2.2 Cyanosis Optics Overview 7

2.3 Relevant Radiometric Concepts 8

3 Investigation Framework 10

3.1 In Silico Experimental Set-up 10

3.2 Specimen Characterization Data 11

3.3 Swatch Generation and Analysis 14

4 Investigation Findings 17

4.1 Methemoglobinemia and Sulfhemoglobinemia Spectral Responses 17

4.2 Cyanotic Appearance Changes 18

4.3 Proposed Detection and Differentiation Protocol 25

5 Conclusion and Future Prospects 32

References 34

Alphabetical Index 44

APPENDICES 46

A RGB Data 47

B Additional Dysfunctional Reflectance Curves 49

C Reflectance Data 62

D Reflectance Data Subjected to Random Fluctuations 71

E Swatch Generation 80

List of Tables

3.1 Parameters employed in the characterization of a palmar fingertip. The acronyms SC, SG, SS, SB, PD and RD refer to the skin layers considered by HyLIoS: stratum corneum, stratum granulosum, stratum spinosum, stratum basale, papillary dermis and reticular dermis, respectively. 12

3.2 MetHb and functional hemoglobin concentrations (in g/L) used in the simulation of distinct levels (represented by percentages of MetHb with respect to total hemoglobin content) of methemoglobinemia severity. 14

3.3 SHb and functional hemoglobin concentrations (in g/L) used in the simulation of distinct levels (represented by percentages of SHb with respect to total hemoglobin content) of sulfhemoglobinemia severity. 14

4.1 Second derivative signs (at 620 nm) of the dysfunctional reflectance curves resulting from our *in silico* experiments considering v_{blood}^{rd} equal to 2%. The signs were obtained using Equation 4.2 and the reflectance values extracted from these curves. These values are provided in Tables C.1 to C.4 (Appendix C). The curves were computed using the Hylios model [65], the specimen's characterization parameter values presented in Table 3.1 and considering four angles of incidence (0°, 15°, 30° and 45°) as well as distinct severity levels of methemoglobinemia and sulfhemoglobinemia (10% to 80%). The concentrations of dysfunctional (MetHb and SHb) and functional hemoglobins associated with these levels are provided in Tables 3.2 and 3.3. 27

4.2 Second derivative signs (at 620 nm) of the dysfunctional reflectance curves resulting from our *in silico* experiments considering v_{blood}^{rd} equal to 5%. The signs were obtained using Equation 4.2 and the reflectance values extracted from these curves. These values are provided in Tables C.5 to C.8 (Appendix C). The curves were computed using the Hylios model [65], the specimen's characterization parameter values presented in Table 3.1 and considering four angles of incidence (0°, 15°, 30° and 45°) as well as distinct severity levels of methemoglobinemia and sulfhemoglobinemia (10% to 80%). The concentrations of dysfunctional (MetHb and SHb) and functional hemoglobins associated with these levels are provided in Tables 3.2 and 3.3. 28

4.3 Second derivative signs (at 620 nm) of the dysfunctional reflectance curves resulting from our *in silico* experiments considering v_{blood}^{rd} equal to 10%. The signs were obtained using Equation 4.2 and the reflectance values extracted from these curves. These values are provided in Tables C.9 to C.12 (Appendix C). The curves were computed using the Hylios model [65], the specimen's characterization parameter values presented in Table 3.1 and considering four angles of incidence (0°, 15°, 30° and 45°) as well as distinct severity levels of methemoglobinemia and sulfhemoglobinemia (10% to 80%). The concentrations of dysfunctional (MetHb and SHb) and functional hemoglobins associated with these levels are provided in Tables 3.2 and 3.3. 28

4.4 Second derivative signs (at 620 nm) of the dysfunctional reflectance curves resulting from our *in silico* experiments considering v_{blood}^{rd} equal to 15%. The signs were obtained using Equation 4.2 and the reflectance values extracted from these curves. These values are provided in Tables C.13 to C.16 (Appendix C). The curves were computed using the Hylios model [65], the specimen's characterization parameter values presented in Table 3.1 and considering four angles of incidence (0°, 15°, 30° and 45°) as well as distinct severity levels of methemoglobinemia and sulfhemoglobinemia (10% to 80%). The concentrations of dysfunctional (MetHb and SHb) and functional hemoglobins associated with these levels are provided in Tables 3.2 and 3.3. 29

4.5 Reflectance values at 605, 620 and 635 nm extracted from dysfunctional curves computed using the HyLIoS model [25], the specimen's characterization parameter values presented in Table 3.1 and accounting for the presence of random noise ($\pm 1\%$) in our simulations. In the computation of these curves, we considered an angle of incidence of 15°, a reticular blood content (v_{blood}^{rd}) equal to 15% and distinct severity levels of methemoglobinemia and sulfhemoglobinemia (10% to 80%). The concentrations of dysfunctional (MetHb and SHb) and functional hemoglobins associated with these levels are provided in Tables 3.2 and 3.3. 30

4.6 Second derivative values computed using the reflectance values provided in Table 4.5 and Equation 4.2 for distinct severity levels of methemoglobinemia and sulfhemoglobinemia (10% to 80%). The concentrations of dysfunctional (MetHb and SHb) and functional hemoglobins associated with these levels are provided in Tables 3.2 and 3.3. 30

A.1 RGB values computed for the swatches depicted in Fig. 4.5. 47

A.2 RGB values computed for the swatches depicted in Fig. 4.6. 48

A.3 RGB values computed for the swatches depicted in Fig. 4.7. 48

A.4 RGB values computed for the swatches depicted in Fig. 4.8. 48

C.1 Reflectance values extracted from dysfunctional curves obtained considering the blood content of the reticular dermis (v_{blood}^{rd}) equal to 2% and the angle of incidence equal to 0°. 62

C.2 Reflectance values extracted from dysfunctional curves obtained considering the blood content of the reticular dermis (v_{blood}^{rd}) equal to 2% and the angle of incidence equal to 15°. 63

C.3 Reflectance values extracted from dysfunctional curves obtained considering the blood content of the reticular dermis (v_{blood}^{rd}) equal to 2% and the angle of incidence equal to 30°. 63

C.4 Reflectance values extracted from dysfunctional curves obtained considering the blood content of the reticular dermis (v_{blood}^{rd}) equal to 2% and the angle of incidence equal to 45°. 64

C.5 Reflectance values extracted from dysfunctional curves obtained considering the blood content of the reticular dermis (v_{blood}^{rd}) equal to 5% and the angle of incidence equal to 0°. 64

C.6 Reflectance values extracted from dysfunctional curves obtained considering the blood content of the reticular dermis (v^{rd}_{blood}) equal to 5% and the angle of incidence equal to 15°. 65

C.7 Reflectance values extracted from dysfunctional curves obtained considering the blood content of the reticular dermis (v^{rd}_{blood}) equal to 5% and the angle of incidence equal to 30°. 65

C.8 Reflectance values extracted from dysfunctional curves obtained considering the blood content of the reticular dermis (v^{rd}_{blood}) equal to 5% and the angle of incidence equal to 45°. 66

C.9 Reflectance values extracted from dysfunctional curves obtained considering the blood content of the reticular dermis (v^{rd}_{blood}) equal to 10% and the angle of incidence equal to 0°. 66

C.10 Reflectance values extracted from dysfunctional curves obtained considering the blood content of the reticular dermis (v^{rd}_{blood}) equal to 10% and the angle of incidence equal to 15°. 67

C.11 Reflectance values extracted from dysfunctional curves obtained considering the blood content of the reticular dermis (v^{rd}_{blood}) equal to 10% and the angle of incidence equal to 30°. 67

C.12 Reflectance values extracted from dysfunctional curves obtained considering the blood content of the reticular dermis (v^{rd}_{blood}) equal to 10% and the angle of incidence equal to 45°. 68

C.13 Reflectance values extracted from dysfunctional curves obtained considering the blood content of the reticular dermis (v^{rd}_{blood}) equal to 15% and the angle of incidence equal to 0°. 68

C.14 Reflectance values extracted from dysfunctional curves obtained considering the blood content of the reticular dermis (v^{rd}_{blood}) equal to 15% and the angle of incidence equal to 15°. 69

C.15 Reflectance values extracted from dysfunctional curves obtained considering the blood content of the reticular dermis (v^{rd}_{blood}) equal to 15% and the angle of incidence equal to 30°. 69

C.16 Reflectance values extracted from dysfunctional curves obtained considering the blood content of the reticular dermis (v^{rd}_{blood}) equal to 15% and the angle of incidence equal to 45°. 70

D.1 Reflectance values extracted from dysfunctional curves obtained considering the blood content of the reticular dermis equal to 2% and the angle of incidence equal to 0°. 71
D.2 Reflectance values extracted from dysfunctional curves obtained considering the blood content of the reticular dermis equal to 2% and the angle of incidence equal to 15°. 72
D.3 Reflectance values extracted from dysfunctional curves obtained considering the blood content of the reticular dermis equal to 2% and the angle of incidence equal to 30°. 72
D.4 Reflectance values extracted from dysfunctional curves obtained considering the blood content of the reticular dermis equal to 2% and the angle of incidence equal to 45°. 73
D.5 Reflectance values extracted from dysfunctional curves obtained considering the blood content of the reticular dermis equal to 5% and the angle of incidence equal to 0°. 73
D.6 Reflectance values extracted from dysfunctional curves obtained considering the blood content of the reticular dermis equal to 5% and the angle of incidence equal to 15°. 74
D.7 Reflectance values extracted from dysfunctional curves obtained considering the blood content of the reticular dermis equal to 5% and the angle of incidence equal to 30°. 74
D.8 Reflectance values extracted from dysfunctional curves obtained considering the blood content of the reticular dermis equal to 5% and the angle of incidence equal to 45°. 75
D.9 Reflectance values extracted from dysfunctional curves obtained considering the blood content of the reticular dermis equal to 10% and the angle of incidence equal to 0°. 75
D.10 Reflectance values extracted from dysfunctional curves obtained considering the blood content of the reticular dermis equal to 10% and the angle of incidence equal to 15°. 76
D.11 Reflectance values extracted from dysfunctional curves obtained considering the blood content of the reticular dermis equal to 10% and the angle of incidence equal to 30°. 76

D.12 Reflectance values extracted from dysfunctional curves obtained considering the blood content of the reticular dermis equal to 10% and the angle of incidence equal to 45°. 77
D.13 Reflectance values extracted from dysfunctional curves obtained considering the blood content of the reticular dermis equal to 15% and the angle of incidence equal to 0°. 77
D.14 Reflectance values extracted from dysfunctional curves obtained considering the blood content of the reticular dermis equal to 15% and the angle of incidence equal to 15°. 78
D.15 Reflectance values extracted from dysfunctional curves obtained considering the blood content of the reticular dermis equal to 15% and the angle of incidence equal to 30°. 78
D.16 Reflectance values extracted from dysfunctional curves obtained considering the blood content of the reticular dermis equal to 15% and the angle of incidence equal to 45°. 79

List of Figures

1.1 Photograph showing hands depicting a cyanotic appearance [42], notably on the fingertips. It can be a symptom of a number of medical conditions, from a disorder of the blood vessels (as it is the case for this patient) known as Raynaud's phenomenon [42] to disorders affecting the blood's capability to transport oxygen known as methemoglobinemia and sulfhemoglobinemia. Reprinted by permission from Springer. 2

2.1 Diagram depicting the spatial organization of the cutaneous tissues (from the outermost to the innermost) and their main layers. 6

2.2 Absorption spectra of the hemoglobins. (a) Molar extinction coefficient curves for the functional hemoglobins [76]. (b) Molar extinction coefficient curves for the dysfunctional hemoglobins [77, 82, 103]. 8

3.1 Components of the convolution process employed to generate a skin swatch depicting a palmar fingertip in its normal (baseline) state. (a) The relative spectral power distribution of the CIE standard D65 illuminant. (b) The baseline reflectance curve computed using the parameter values depicted in Table 3.1. (c) Greyscale texture of a palmar fingertip. (d) Resulting swatch. 16

4.1 Graphs depicting reflectance curves resulting from increasing amounts of methemoglobin (MetHb) and sulfhemoglobin (SHb) in a skin specimen characterized by a reticular blood content (v_{blood}^{rd}) equal to 2%. These curves were obtained using the HyLIoS [25] model and considering an angle of incidence equal to 15°. Each graph corresponds to a distinct severity level of methemoglobinemia and sulfhemoglobinemia: (a) 10%, (b) 20%, (c) 30%, (d) 40%, (e) 50%, (f) 60%, (g) 70% and (h) 80%. The concentrations of dysfunctional and functional hemoglobins associated with these levels are provided in Tables 3.2 and 3.3. The remaining parameters values used in the specimen's characterization are provided in Table 3.1. 19

4.2 Graphs depicting reflectance curves resulting from increasing amounts of methemoglobin (MetHb) and sulfhemoglobin (SHb) in a skin specimen characterized by a reticular blood content (v_{blood}^{rd}) equal to 5%. These curves were obtained using the HyLIoS [25] model and considering an angle of incidence equal to 15°. Each graph corresponds to a distinct severity level of methemoglobinemia and sulfhemoglobinemia: (a) 10%, (b) 20%, (c) 30%, (d) 40%, (e) 50%, (f) 60%, (g) 70% and (h) 80%. The concentrations of dysfunctional and functional hemoglobins associated with these levels are provided in Tables 3.2 and 3.3. The remaining parameters values used in the specimen's characterization are provided in Table 3.1. 20

4.3 Graphs depicting reflectance curves resulting from increasing amounts of methemoglobin (MetHb) and sulfhemoglobin (SHb) in a skin specimen characterized by a reticular blood content (v_{blood}^{rd}) equal to 10%. These curves were obtained using the HyLIoS [25] model and considering an angle of incidence equal to 15°. Each graph corresponds to a distinct severity level of methemoglobinemia and sulfhemoglobinemia: (a) 10%, (b) 20%, (c) 30%, (d) 40%, (e) 50%, (f) 60%, (g) 70% and (h) 80%. The concentrations of dysfunctional and functional hemoglobins associated with these levels are provided in Tables 3.2 and 3.3. The remaining parameters values used in the specimen's characterization are provided in Table 3.1. 21

4.4 Graphs depicting reflectance curves resulting from increasing amounts of methemoglobin (MetHb) and sulfhemoglobin (SHb) in a skin specimen characterized by a reticular blood content (v_{blood}^{rd}) equal to 15%. These curves were obtained using the HyLIoS [25] model and considering an angle of incidence equal to 15°. Each graph corresponds to a distinct severity level of methemoglobinemia and sulfhemoglobinemia: (a) 10%, (b) 20%, (c) 30%, (d) 40%, (e) 50%, (f) 60%, (g) 70% and (h) 80%. The concentrations of dysfunctional and functional hemoglobins associated with these levels are provided in Tables 3.2 and 3.3.The remaining parameters values used in the specimen's characterization are provided in Table 3.1. 22

4.5 Skin swatches generated using the dysfunctional reflectance curves provided in Fig. 4.1, which were obtained considering skin specimen characterized by a reticular blood content (v_{blood}^{rd}) equal to 2% and increasing amounts of methemoglobin (MetHb) and sulfhemoglobin (SHb), from 10% to 80%. The bottom row presents the the CIELAB $\Delta E_{ab}^{\star}$ differences for each pair of MetHb and SHb swatches. The RGB values associated with each swatch depicted above can be found in Table A.1 in Appendix A. 23

4.6 Skin swatches generated using the dysfunctional reflectance curves provided in Fig. 4.2, which were obtained considering skin specimen characterized by a reticular blood content (v_{blood}^{rd}) equal to 5% and increasing amounts of methemoglobin (MetHb) and sulfhemoglobin (SHb), from 10% to 80%. The bottom row presents the the CIELAB $\Delta E_{ab}^{\star}$ differences for each pair of MetHb and SHb swatches. The RGB values associated with each swatch depicted above can be found in Table A.2 in Appendix A. 23

4.7 Skin swatches generated using the dysfunctional reflectance curves provided in Fig. 4.3, which were obtained considering skin specimen characterized by a reticular blood content (v_{blood}^{rd}) equal to 10% and increasing amounts of methemoglobin (MetHb) and sulfhemoglobin (SHb), from 10% to 80%. The bottom row presents the the CIELAB $\Delta E_{ab}^{\star}$ differences for each pair of MetHb and SHb swatches. The RGB values associated with each swatch depicted above can be found in Table A.3 in Appendix A. 24

4.8 Skin swatches generated using the dysfunctional reflectance curves provided in Fig. 4.4, which were obtained considering skin specimen characterized by a reticular blood content (v_{blood}^{rd}) equal to 15% and increasing amounts of methemoglobin (MetHb) and sulfhemoglobin (SHb), from 10% to 80%. The bottom row presents the the CIELAB $\Delta E_{ab}^{\star}$ differences for each pair of MetHb and SHb swatches. The RGB values associated with each swatch depicted above can be found in Table A.4 in Appendix A. 24

B.1 Graphs depicting reflectance curves resulting from increasing amounts of methemoglobin (MetHb) and sulfhemoglobin (SHb) in a skin specimen characterized by a reticular blood content (v_{blood}^{rd}) equal to 2%. These curves were obtained using the HyLIoS [25] model and considering an angle of incidence equal to 0°. Each graph corresponds to a distinct severity level of methemoglobinemia and sulfhemoglobinemia: (a) 10%, (b) 20%, (c) 30%, (d) 40%, (e) 50%, (f) 60%, (g) 70% and (h) 80%. The concentrations of dysfunctional and functional hemoglobins associated with these levels are provided in Tables 3.2 and 3.3. The remaining parameters values used in the specimen's characterization are provided in Table 3.1. 50

B.2 Graphs depicting reflectance curves resulting from increasing amounts of methemoglobin (MetHb) and sulfhemoglobin (SHb) in a skin specimen characterized by a reticular blood content (v_{blood}^{rd}) equal to 5%. These curves were obtained using the HyLIoS [25] model and considering an angle of incidence equal to 0°. Each graph corresponds to a distinct severity level of methemoglobinemia and sulfhemoglobinemia: (a) 10%, (b) 20%, (c) 30%, (d) 40%, (e) 50%, (f) 60%, (g) 70% and (h) 80%. The concentrations of dysfunctional and functional hemoglobins associated with these levels are provided in Tables 3.2 and 3.3. The remaining parameters values used in the specimen's characterization are provided in Table 3.1. 51

B.3 Graphs depicting reflectance curves resulting from increasing amounts of methemoglobin (MetHb) and sulfhemoglobin (SHb) in a skin specimen characterized by a reticular blood content (v_{blood}^{rd}) equal to 10%. These curves were obtained using the HyLIoS [25] model and considering an angle of incidence equal to 0°. Each graph corresponds to a distinct severity level of methemoglobinemia and sulfhemoglobinemia: (a) 10%, (b) 20%, (c) 30%, (d) 40%, (e) 50%, (f) 60%, (g) 70% and (h) 80%. The concentrations of dysfunctional and functional hemoglobins associated with these levels are provided in Tables 3.2 and 3.3. The remaining parameters values used in the specimen's characterization are provided in Table 3.1. 52

B.4 Graphs depicting reflectance curves resulting from increasing amounts of methemoglobin (MetHb) and sulfhemoglobin (SHb) in a skin specimen characterized by a reticular blood content (v_{blood}^{rd}) equal to 15%. These curves were obtained using the HyLIoS [25] model and considering an angle of incidence equal to 0°. Each graph corresponds to a distinct severity level of methemoglobinemia and sulfhemoglobinemia: (a) 10%, (b) 20%, (c) 30%, (d) 40%, (e) 50%, (f) 60%, (g) 70% and (h) 80%. The concentrations of dysfunctional and functional hemoglobins associated with these levels are provided in Tables 3.2 and 3.3. The remaining parameters values used in the specimen's characterization are provided in Table 3.1. 53

B.5 Graphs depicting reflectance curves resulting from increasing amounts of methemoglobin (MetHb) and sulfhemoglobin (SHb) in a skin specimen characterized by a reticular blood content (v_{blood}^{rd}) equal to 2%. These curves were obtained using the HyLIoS [25] model and considering an angle of incidence equal to 30°. Each graph corresponds to a distinct severity level of methemoglobinemia and sulfhemoglobinemia: (a) 10%, (b) 20%, (c) 30%, (d) 40%, (e) 50%, (f) 60%, (g) 70% and (h) 80%. The concentrations of dysfunctional and functional hemoglobins associated with these levels are provided in Tables 3.2 and 3.3. The remaining parameters values used in the specimen's characterization are provided in Table 3.1. 54

B.6 Graphs depicting reflectance curves resulting from increasing amounts of methemoglobin (MetHb) and sulfhemoglobin (SHb) in a skin specimen characterized by a reticular blood content (v_{blood}^{rd}) equal to 5%. These curves were obtained using the HyLIoS [25] model and considering an angle of incidence equal to 30°. Each graph corresponds to a distinct severity level of methemoglobinemia and sulfhemoglobinemia: (a) 10%, (b) 20%, (c) 30%, (d) 40%, (e) 50%, (f) 60%, (g) 70% and (h) 80%. The concentrations of dysfunctional and functional hemoglobins associated with these levels are provided in Tables 3.2 and 3.3. The remaining parameters values used in the specimen's characterization are provided in Table 3.1. 55

B.7 Graphs depicting reflectance curves resulting from increasing amounts of methemoglobin (MetHb) and sulfhemoglobin (SHb) in a skin specimen characterized by a reticular blood content (v_{blood}^{rd}) equal to 10%. These curves were obtained using the HyLIoS [25] model and considering an angle of incidence equal to 30°. Each graph corresponds to a distinct severity level of methemoglobinemia and sulfhemoglobinemia: (a) 10%, (b) 20%, (c) 30%, (d) 40%, (e) 50%, (f) 60%, (g) 70% and (h) 80%. The concentrations of dysfunctional and functional hemoglobins associated with these levels are provided in Tables 3.2 and 3.3. The remaining parameters values used in the specimen's characterization are provided in Table 3.1. 56

B.8 Graphs depicting reflectance curves resulting from increasing amounts of methemoglobin (MetHb) and sulfhemoglobin (SHb) in a skin specimen characterized by a reticular blood content (v_{blood}^{rd}) equal to 15%. These curves were obtained using the HyLIoS [25] model and considering an angle of incidence equal to 30°. Each graph corresponds to a distinct severity level of methemoglobinemia and sulfhemoglobinemia: (a) 10%, (b) 20%, (c) 30%, (d) 40%, (e) 50%, (f) 60%, (g) 70% and (h) 80%. The concentrations of dysfunctional and functional hemoglobins associated with these levels are provided in Tables 3.2 and 3.3. The remaining parameters values used in the specimen's characterization are provided in Table 3.1. 57

B.9 Graphs depicting reflectance curves resulting from increasing amounts of methemoglobin (MetHb) and sulfhemoglobin (SHb) in a skin specimen characterized by a reticular blood content (v_{blood}^{rd}) equal to 2%. These curves were obtained using the HyLIoS [25] model and considering an angle of incidence equal to 45°. Each graph corresponds to a distinct severity level of methemoglobinemia and sulfhemoglobinemia: (a) 10%, (b) 20%, (c) 30%, (d) 40%, (e) 50%, (f) 60%, (g) 70% and (h) 80%. The concentrations of dysfunctional and functional hemoglobins associated with these levels are provided in Tables 3.2 and 3.3. The remaining parameters values used in the specimen's characterization are provided in Table 3.1. 58

B.10 Graphs depicting reflectance curves resulting from increasing amounts of methemoglobin (MetHb) and sulfhemoglobin (SHb) in a skin specimen characterized by a reticular blood content (v_{blood}^{rd}) equal to 5%. These curves were obtained using the HyLIoS [25] model and considering an angle of incidence equal to 45°. Each graph corresponds to a distinct severity level of methemoglobinemia and sulfhemoglobinemia: (a) 10%, (b) 20%, (c) 30%, (d) 40%, (e) 50%, (f) 60%, (g) 70% and (h) 80%. The concentrations of dysfunctional and functional hemoglobins associated with these levels are provided in Tables 3.2 and 3.3. The remaining parameters values used in the specimen's characterization are provided in Table 3.1. 59

B.11 Graphs depicting reflectance curves resulting from increasing amounts of methemoglobin (MetHb) and sulfhemoglobin (SHb) in a skin specimen characterized by a reticular blood content (v_{blood}^{rd}) equal to 10%. These curves were obtained using the HyLIoS [25] model and considering an angle of incidence equal to 45°. Each graph corresponds to a distinct severity level of methemoglobinemia and sulfhemoglobinemia: (a) 10%, (b) 20%, (c) 30%, (d) 40%, (e) 50%, (f) 60%, (g) 70% and (h) 80%. The concentrations of dysfunctional and functional hemoglobins associated with these levels are provided in Tables 3.2 and 3.3. The remaining parameters values used in the specimen's characterization are provided in Table 3.1. 60

B.12 Graphs depicting reflectance curves resulting from increasing amounts of methemoglobin (MetHb) and sulfhemoglobin (SHb) in a skin specimen characterized by a reticular blood content (v_{blood}^{rd}) equal to 15%. These curves were obtained using the HyLIoS [25] model and considering an angle of incidence equal to 45°. Each graph corresponds to a distinct severity level of methemoglobinemia and sulfhemoglobinemia: (a) 10%, (b) 20%, (c) 30%, (d) 40%, (e) 50%, (f) 60%, (g) 70% and (h) 80%. The concentrations of dysfunctional and functional hemoglobins associated with these levels are provided in Tables 3.2 and 3.3. The remaining parameters values used in the specimen's characterization are provided in Table 3.1. 61

Chapter 1

Introduction

A number of medical conditions, including arterial thrombosis and heart failure, can have as one of their most noticeable initial symptoms cyanosis [10, 62, 17], a characteristic purple or bluish coloration of the mucosal membranes, nail beds and skin. In its early stages, it can also appear as a grey cutaneous discoloration [38]. Although cyanosis is often elicited by the presence of high levels of deoxygenated hemoglobin in blood-perfused cutaneous tissues [61, 35], it can also be prompted by the presence of abnormal amounts of dysfunctional forms of hemoglobin (which are characterized by not having the capability to bind reversibly with oxygen [31, 44]) in these tissues [17]. In the latter case, cyanosis may indicate the occurrence of two potentially life-threatening dyshemoglobinemia disorders, namely methemoblobinemia and sulfhemoglobinemia [36, 41, 44]. These disorders, in turn, are associated with excessive amounts of dysfunctional forms of hemoglobin known as methemoglobin (MetHb) and sulfhemoglobin (SHb), respectively, in the blood stream [30, 59]. Under normal physiological conditions, the blood circulating in the body transports primarily the functional forms of hemoglobin (oxygenated and deoxygenated).

We note that another form of dysfunctional hemoglobin, known as carboxyhemoglobin (COHb), can also be found in blood-perfused cutaneous tissues [82]. In fact, carbon monoxide poisoning may result in high levels of COHb [50]. Above a 40% level, the patient's skin may start to depict a cherry red coloration [43]. Beyond a 60% level, it may lead to her/his death [43, 50]. Since COHb is not associated with the onset of cyanosis and its presence in the blood stream can be detected and differentiated from other forms of hemoglobin in a relatively straightforward manner [50], it is not further examined in this work.

Both methemoglobinemia and sulfhemoglobinemia can be caused by similar chemical agents and be characterized by similar symptoms, which worsen as the MetHb and SHb

Figure 1.1: Photograph showing hands depicting a cyanotic appearance [42], notably on the fingertips. It can be a symptom of a number of medical conditions, from a disorder of the blood vessels (as it is the case for this patient) known as Raynaud's phenomenon [42] to disorders affecting the blood's capability to transport oxygen known as methemoglobinemia and sulfhemoglobinemia. Reprinted by permission from Springer.

levels increase. In the case of methemoglobinemia, a high mortality rate is often observed when the MetHb level is superior to 70% of the total hemoglobin content [44]. In the case of sulfhemoglobinemia, end-organ damage and death can occur when the SHb level is superior to 60% of the total hemoglobin content [38, 36]. In most cases, methemoglobinemia is reversible through the administration of a substance known as methylene blue [40]. There have been reports, however, of unusual cases in which it did not respond to this treatment [80, 73]. Sulfhemoglobinemia, on the other hand, is not reversible and its management often requires blood transfusions that may pose additional risks to the patient [38, 12]. Thus, if sulfhemoglobinemia is misdiagnosed as methemoglobinemia, the use of methylene blue as antidote will be ineffective [28]. In addition, it may lead to other medical problems such as renal failure [99].

These aspects highlight the importance of the early detection and differentiation of these dyshemoglobinemia disorders. Although devices like co-oximeters and blood gas analysers can be employed, to detect the abnormal presence of MetHb and SHb in blood samples [39, 36], there are two issues that need to be examined when considering this approach, namely cost and effectiveness. With respect to cost limitations, it is worth noting that these detection tests are not performed routinely in most intensive care units and need to be ordered specifically [39]. Hence, one can expect their availability to be even more limited in low-resource clinical settings. With respect to effectiveness, it has been reported that the readings provided by these devices can diverge significantly from actual MetHb and SHb

values [63, 28, 36]. Moreover, available co-oximeters often have difficulties to differentiate between SHb and MetHb [12, 28], and most blood gas analysers do not report SHb levels [28, 36]. Although other technologies, such as the use of optoacoustic sensors [74] or dedicated spectral sensors [91], have been proposed to detect the presence of dysfunctional hemoglobins in the blood stream, they also depend on the collection of blood samples. This invasive procedure is not only potentially painful, but it may also pose additional risks to the patient. These may include, for example, a significant blood loss if multiple blood samplings are required. Such a situation may be particularly worrisome in the case of preterm infants [53].

Ideally, one would like to employ noninvasive and low-cost approaches in the detection and differentiation of methemoglobinemia and sulfhemoglobinemia, particularly at the point of care. These include the visual assessment of cyanosis [12]. However, the extent to which this assessment can contribute for the effective detection and differentiation of these disorders remains an open problem. This can be largely attributed to the relatively limited amount of experimental information about the impact of different levels of MetHb and SHb on skin appearance available in the biomedical literature. Oftentimes works relating cyanosis to abnormal levels of MetHb and SHb refer to *in vitro* experiments performed considering only a handful of test cases [36]. In fact, to date, the small number of reported cases of methemoglobinemia and sulfhemoglobinemia and the consequent scarcity of supporting chromatic and spectral data associated with the onset of cyanotic skin appearances represent major obstacles for advances in this area [12, 36, 63, 39]. Besides these data limitations, controlled *in vivo* quantitative investigations of cyanosis caused by dyshemoglobinemia disorders would involve a relatively large number of biophysical parameters that would need to be kept fixed during the experiments. This would represent another technical challenge.

Nowadays, controlled *in silico* experiments performed through predictive computer simulations are being extensively employed in biomedical research [93, 95]. In the specific case of light interactions with human skin, the information derived from *in silico* experiments contributes not only to the elucidation of scientific questions about these phenomena, but also to the development of more effective procedures aimed at the noninvasive diagnosis and treatment of diseases [88, 12]. Besides its flexibility and the absence of the health-related risks normally associated with *in vivo* experiments, such an investigation approach mitigates the impact of the data and technical constraints mentioned above. For example, as many test cases as necessary can be carried out *in silico*, i.e., they are not bound by a limited set of experimental conditions and on the availability of living subjects. In addition, specific biophysical parameters of interest can be varied while the remaining ones can be treated as constants without incurring in significant logistic overhead.

For these reasons, we also resorted to an *in silico* approach in the work described in this thesis. More precisely, we performed controlled *in silico* experiments to closely investigate the impact of key biophysical factors on the onset of cyanosis elicited by methemoglobinemia and sulfhemoglobinemia. Our findings, in addition to broadening the current knowledge about this complex causal relationship, enabled us to propose a cost-effective protocol for the noninvasive detection and differentiation of these life-threatening disorders. The proposed protocol is expected to outperform technologies currently used in these tasks, not only in terms of effectiveness to cost ratio, but also with respect to sensitivity range.

The remainder of this thesis, whose main contents have also been made available in a journal publication [7], is organized as follows. In Chapter 2 we concisely review biophysical concepts and terminology relevant for this work. In Chapter 3, we describe the methods and data employed in this investigation. In Chapter 4, we present our findings, discuss their practical implications and propose a protocol for the noninvasive detection and differentiation of methemoglobinemia and sulfhemoglobinemia. Finally, in Chapter 5, we conclude the thesis and comment on future prospects in this area.

Chapter 2

Biophysical Background

In this chapter, we review fundamental biophysical information associated with our investigation. We begin by concisely describing the main characteristics of human skin in Section 2.1. We then outline the main optical factors responsible for cyanotic skin appearances in Section 2.2. Finally, in Section 2.3, we introduce radiometric concepts employed in our *in silico* experiments described in Chapter 2.

2.1 Skin Overview

Human skin is usually considered to be composed of three distinct tissues (Fig. 2.1), namely the stratum corneum, the epidermis and the dermis [101]. The stratum corneum and the epidermal layers (stratum granulosum, stratum spinosum and stratum basale, from the outermost to the innermost) are primarily composed of stratified cells [27]. In thick regions of the skin, such as the soles, a clear epidermal layer, known as stratum lucidum, can be found immediately below the stratum corneum [27]. The dermis forms the bulk of the full thickness of skin (Fig. 2.1). It can be divided into the papillary dermis and reticular dermis [6]. Compared to the reticular dermis, the papillary dermis is relatively thin and contains smaller-sized structural fibers. The dermis also contains a network of blood vessels, with wider vessels being located in the reticular dermis [11].

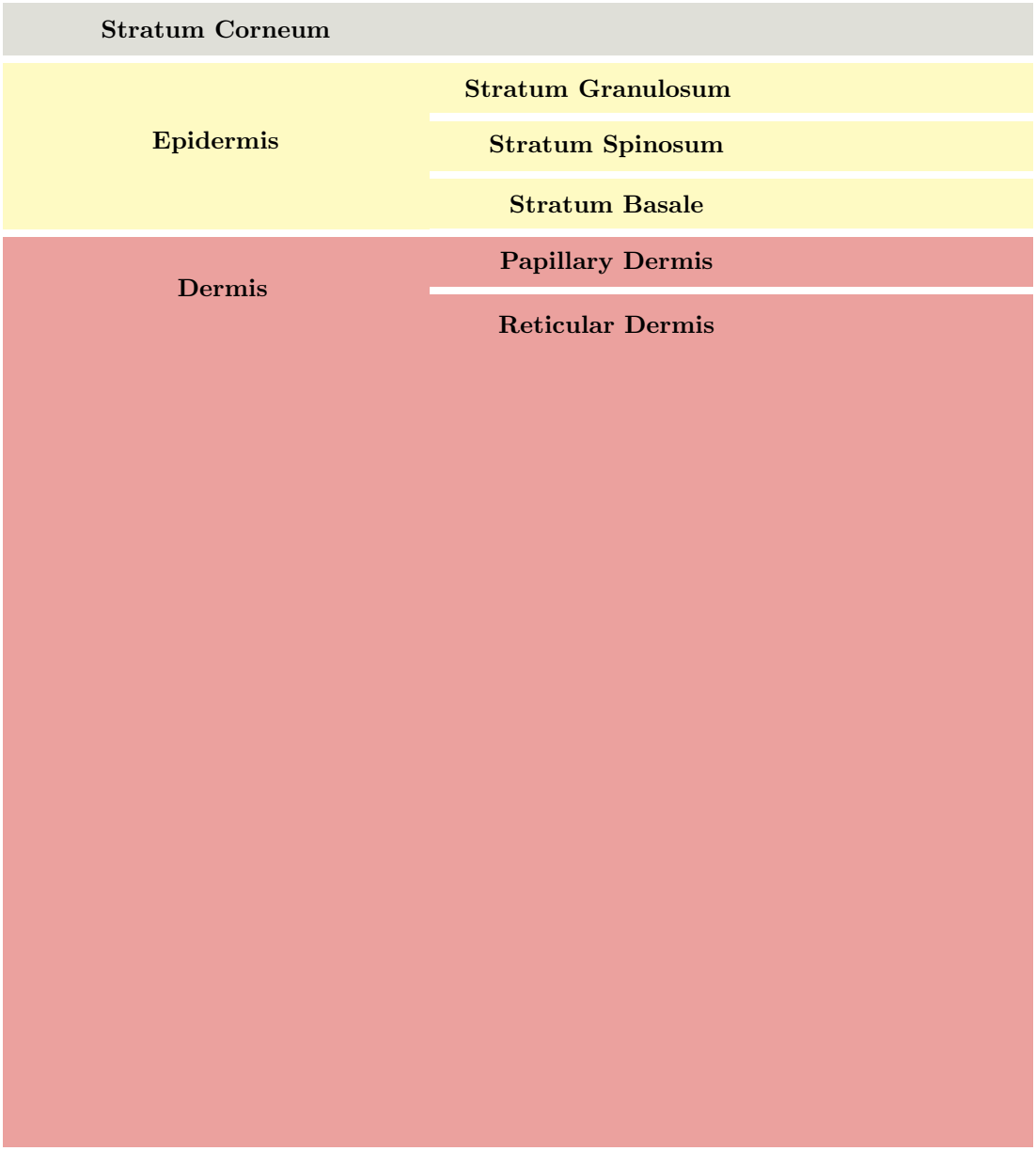

Figure 2.1: Diagram depicting the spatial organization of the cutaneous tissues (from the outermost to the innermost) and their main layers.

Light impinging on the skin surface can be reflected back to the environment or transmitted into its internal tissues. Once light is transmitted into the skin tissues, it can be further attenuated by their constituent materials, either through absorption or scattering events [17]. Relevant absorbing materials acting in the ultraviolet (UV) and visible regions of the light spectrum are situated within the stratum corneum and epidermis. Examples include include DNA, keratin, urocanic acid and melanin. The latter may occur in two forms within human skin: the brown-black eumelanin and the yellow-red pheomelanin [23]. Blood-borne pigments (*e.g.*, hemoglobin, bilirubin and beta-carotene) found in the dermal layers are also relevant absorbers in the visible domain [105]. Water and lipids found throughout the skin dominate the absorption of light in the infrared region of the light spectrum [11].

Within the cutaneous tissues, light is mostly scattered by heterogeneous structures, such as cells, organelles, fibers and fibrils [6]. Among these structures, the melanin-containing organelles, known as melanosomes, have a central role in the attenuation of UV and visible light travelling within the cutanueous tissues [55]. The dermal layers contain dense connective tissue. Light traversing the papillary dermis may be subjected to Rayleigh scattering (which has a stronger effect at the "blue" end (400 to 500 nm) of the visible spectrum) caused by the presence of collagen fibrils [90]. As light penetrates deeper into the more turbid reticular dermis, it becomes progressively diffuse [49].

Eventually, the light traversing the dermis may reach the hypodermis, a subcutaneous tissue that consists mostly of white fat cells that contain lipid droplets [3]. Various studies have indicated that the majority of the visible light that reaches this tissue is likely to be scattered by these droplets and remitted into the cutaneous tissues, notably the reticular dermis.

2.2 Cyanosis Optics Overview

A hemoglobin molecule encapsulates four heme (an iron-containing compound) porphyrin rings (linked group of organic compounds with a central metal atom), each with a centrally localized iron atom [12]. These iron atoms are capable of binding with oxygen when they are in a ferrous state. However, if an iron atom is oxidized (loses an electron) to a ferric state, it can no longer bind to oxygen. The functional forms of hemoglobin, namely oxyhemoglobin and deoxyhemoglobin, stored in the red blood cells (RBCs) can bind oxygen reversibly, However, dysfunctional forms of hemoglobin also stored in the RBCs, such as MetHB and SHb, do not have this capability [12]. While MetHb corresponds to a reversible type of

oxidized hemoglobin, SHb corresponds to an irreversible type (it lasts the lifetime of the RBC) that results from the incorporation of a sulfur atom in its porphyrin ring [103, 38].

From an optics perspective, cyanotic chromatic attributes have been often associated with the light absorption properties of the hemoglobins, with several authors incorrectly attributing the typical cyanotic bluish hue to an allegedly blue appearance of deoxygenated blood (*e.g.*, [62, 9]). However, one has to consider the fact that the hemoglobins are strong absorbers in the blue end of the visible spectrum (Fig. 2.2). In addition, light traveling within the skin tissues may also be strongly attenuated by the melanins. Thus, arterial blood appears bright red, while venous blood appears dark red, almost black, but not blue [54, 104]. In the case of arterial blood containing high amounts of MetHB or SHb, it would appear brown or green [99, 103], respectively. Hence, the purple or bluish coloration of cyanotic skin must be also associated with other light attenuation phenomena besides the absorption by pigments like the hemoglobins. It has been recently demonstrated [17, 18] that Rayleigh scattering taking place in the papillary dermis can play a pivotal role in the onset of typical cyanotic purple and bluish coloration.

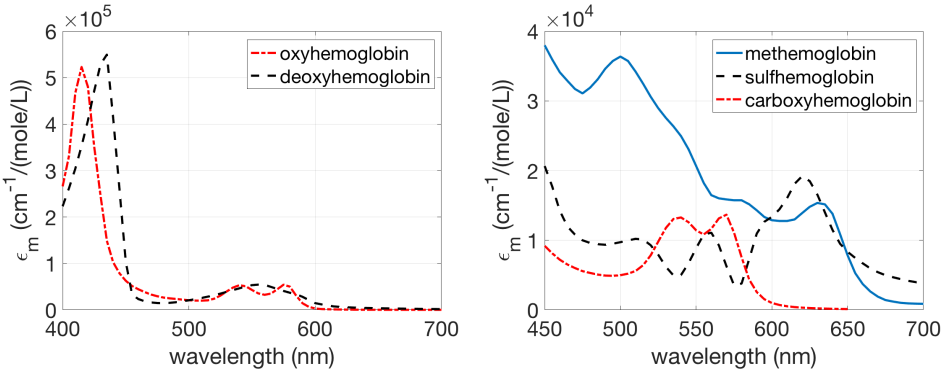

(a) (b)

Figure 2.2: Absorption spectra of the hemoglobins. (a) Molar extinction coefficient curves for the functional hemoglobins [76]. (b) Molar extinction coefficient curves for the dysfunctional hemoglobins [77, 82, 103].

2.3 Relevant Radiometric Concepts

Variations in the spectral distribution of the light propagated by a material, like a skin specimen, affect its appearance characteristics, particularly its hue (the attribute of color perception by means of which an object is judged to be red, yellow, green, blue, purple

and so forth [15]). Such variations, in turn, can be quantified in terms of reflectance. This radiometric quantity, denoted by $\rho(\lambda)$, represents the fraction of light at wavelength λ impinging on a material that is reflected by it. In general, reflectance measurements are performed using a spectrophotometer [47].

Alternatively, reflectance can be defined as the spectral power distribution of the reflected light, *i.e.*, the ratio of the reflected radiant power, Φ_r, to the incident radiant power, Φ_i [15]:

$$\rho(\lambda) = \frac{\Phi_r(\lambda)}{\Phi_i(\lambda)}. \tag{2.1}$$

There are nine different representations of reflectance. These representations depend on the incident and propagated (collected) light geometries, which are designated as directional, conical and hemispherical [67]. The directional geometry designates a differential solid angle $d\omega$ about a single direction ψ (represented by a pair of spherical coordinates θ and ϕ). The conical geometry designates a solid angle ω of any configuration (*e.g.*, a right circular cone). Finally, a hemispherical geometry designates a full hemispherical solid angle $\omega = 2\pi$ [15].

Considering a ray optics stochastic simulation framework, like the one employed in this research (Chapter 3), in which n rays are shot towards a specimen from a direction represented by $d\omega_i$ and at a given wavelength λ, we can assume that each ray carries the same amount of radiant power, denoted by Φ_{ray}. If the total radiant power to be shot is Φ_i, then the radiant power carried by each ray is given by [15]:

$$\Phi_{ray}(\lambda) = \frac{\Phi_i(\lambda)}{n}. \tag{2.2}$$

Hence, according to Equation 2.1, if n_r rays are reflected towards the upper hemisphere Ω_r, the directional-hemispherical reflectance of a specimen with respect to a wavelength λ can be quantified as [16]:

$$\rho(\lambda, d\omega_i, \Omega_r) = \frac{n_r}{n}. \tag{2.3}$$

Chapter 3

Investigation Framework

During the investigation described in this thesis, we performed controlled *in silico* experiments considering distinct severity levels of methemoglobinemia and sulfhemoglobinemia. More specifically, we used a predictive model of light and skin interactions (Section 3.1) and specimen characterization data a variable in the biomedical literature (Section 3.2) to compute directional-hemispherical reflectance curves for a cutaneous site considering variations in its dysfunctional hemoglobin (MetHb and SHb) levels and blood content. We then generate skin swatches (Section 3.3) to analyse the visual differences between the cyanotic appearances elicited by these disorders. These components of our investigation framework are described next.

3.1 In Silico Experimental Set-up

The model of light and skin interactions employed in our controlled *in silico* experiments, known as HyLIoS (*H*yperspectral *L*ight *I*mpingement on *S*kin) [25], employs a first-principles simulation approach. Accordingly, it accounts for all main light absorbers (keratin, DNA, uranic acid, melanins, functional and dysfunctional hemoglobins, beta-carotene, bilirubin, lipids and water) and scatterers (cells, melanosomes, fibers and fibrils) acting within the cutaneous tissues [11]. These correspond to the stratum corneum, the melanin-containing epidermis (subdivided into three main layers, the stratum granulosum, the stratum spinosum and the stratum basale) and the blood-perfused dermis (subdivided into the thin papillary layer and the dominant reticular layer (Fig. 2.1)).

Within the HyLIoS' geometrical-optics formulation, a ray interacting with a given skin specimen can be associated with any wavelength within a spectral region of interest. For

consistency, we considered a spectral resolution of 5 *nm* in all curves depicted in this work, which were computed using a virtual spectrophotometer [16]. In their computation, we employed 10^6 sample rays and, unless otherwise stated, considered an angle of incidence equal to 15°.

Clearly, the reliability of an *in silico* experimental framework is directly associated with the predictive capabilities of the computer model used in the simulations. Hence, it is important to note that HyLIoS was extensively evaluated through qualitative and quantitative comparisons of its outcomes with actual measured data [25]. Since then, it has been effectively employed in a number of related biomedical investigations (*e.g.*, [13, 17, 18, 90]).

For conciseness, we refer the reader interested in the full description of the HyLIoS model to the publications in which it was originally presented [24, 25]. Moreover, for the readers interested in the full reproduction of our *in silico* experimental results, we note that HyLIoS is available online [66] via a model distribution system [14] along with the supporting data (*e.g.*, refractive index and extinction coefficient curves of the light absorbers) [70] used in our investigation. This system enables researchers to specify the values to be assigned to the measurement variables (*e.g.*, angle of incidence and spectral range) and specimen characterization parameters (Tables 3.1, 3.2 and 3.3) using a web interface [66], and receive customized simulation results.

3.2 Specimen Characterization Data

We have elected the palmar fingertip as the testing site for our *in silico* experiments for the following reasons. This hypopigmented site is characterized by a reduced melanin content (more than fivefold lower than in the nonpalmoplantar regions [100]), which minimizes the masking effects of melanin on the visual assessment of cyanotic appearances [39, 18]. In addition, it is also characterized by an increased blood content [89, 18], making their spectral responses, and consequently, their cyanotic chromatic attributes more susceptible to changes in the contents of blood-borne pigments like MetHb and SHb. It is worth noting that the noninvasive measurement of blood related properties (*e.g.*, oxygen saturation levels measured using a pulse oximeter [31]) is usually performed at this site, which has also been considered in previous investigations involving peripheral cyanosis [17, 18].

Table 3.1: Parameters employed in the characterization of a palmar fingertip. The acronyms SC, SG, SS, SB, PD and RD refer to the skin layers considered by HyLIoS: stratum corneum, stratum granulosum, stratum spinosum, stratum basale, papillary dermis and reticular dermis, respectively.

Parameter	Value	Ref.
Ratio of Skin Surface Folds	0.1	[85][60]
SC Thickness (cm)	0.013	[3][2][75][78]
SG Thickness (cm)	0.0123	[97]
SS Thickness(cm)	0.0123	[97]
SB Thickness (cm)	0.0123	[97]
PD Thickness (cm)	0.02	[79]
RD Thickness (cm)	0.125	[5]
SC Melanosome Content (%)	0.0	[55][58]
SG Melanosome Content (%)	0.0	[55][58]
SS Melanosome Content (%)	0.0	[55][58]
SB Melanosome Content (%)	0.15	[103]
SC Colloidal Melanin Content (%)	0.06	[55][4][72]
SG Colloidal Melanin Content (%)	0.06	[55][4][72]
SS Colloidal Melanin Content (%)	0.06	[55][4][72]
SB Colloidal Melanin Content (%)	0.06	[103]
SB Melanosome Dimensions ($\mu m \times \mu m$)	0.41×0.17	[71]
Melanosome Eumelanin Concentration (g/L)	32.0	[87][45]
Melanosome Pheomelanin Concentration (g/L)	2.0	[87][45]
PD Blood Content (%)	0.5	[21]
RD Blood Content (%)	2.0	[68]
Dermal Oxygenated Hemoglobin Fraction (%)	90.0	[69]
Functional Hemoglobin Concentration in Blood (g/L)	147.0	[102]
MetHb Concentration in Blood (g/L)	1.5	[12]
COHb in Blood (g/L)	1.5	[12]
SHb Concentration in Blood (g/L)	0.0	[12]
Blood Bilirubin Concentration (g/L)	0.003	[107]
SC Beta-Carotene Concentration (g/L)	2.1E-4	[57]
Epidermis Beta-Carotene Concentration (g/L)	2.1E-4	[57]
Blood Beta-Carotene Concentration (g/L)	7.0E-5	[57]
SC Water Content (%)	35.0	[1][64]
Epidermis Water Content (%)	60.0	[1] [94]

Continues on the following page ...

Table 3.1 – Continuation

Parameter	Value	Ref.
PD Water Content (%)	75.0	[1] [94]
RD Water Content (%)	75.0	[1] [94]
SC Lipid Content (%)	20.0	[98]
Epidermis Lipid Content (%)	15.1	[1][83][22]
PD Lipid Content (%)	17.33	[1][83][22]
RD Lipid Content (%)	17.33	[1][83][22]
SC Keratin Content (%)	65.0	[33][81][34]
SC Urocanic Acid Density (mol/L)	0.01	[105]
Skin DNA Density (g/L)	0.185	[1][92][32]
SC Refractive Index	1.55	[86][29]
Epidermis Refractive Index	1.4	[88][60]
PD Refractive Index	1.39	[86][49]
RD Refractive Index	1.41	[86][49]
Melanin Refractive Index	1.7	[19]
PD Scatterers Refractive Index	1.5	[96]
Radius of PD Scatterers (nm)	40.0	[68]
PD Fraction Occupied by Scatterers (%)	22.0	[48]

Without loss of generality, we have characterized a palmar fingertip site in its normal (baseline) state using the dataset presented in Table 3.1. The selection of values for the parameters included in this dataset was based on physiologically valid ranges provided in related references, which are also listed in Table 3.1. We note that, for some of these parameters, the determination of physiologically valid ranges involved the use of multiple references.

Using HyLIoS and the dataset provided in Table 3.1, we then computed the baseline reflectance curve (Fig. 3.1 (b)) used as reference in our experiments. Subsequently, we computed reflectance curves associated with distinct severity levels of methemoglobinemia and sulfhemoglobinemia using modified versions of this dataset. These modified versions correspond to the dataset provided in Table 3.1, with the MetHb, SHb and functional hemoglobin (Hb) concentrations in blood replaced by the values provided in Tables 3.2 and 3.3. We remark that these dyshemoglobinemia disorders are associated with the abnormal presence of MetHb and SHb in the blood stream. Hence, in our experiments,

we also took into account variations in the blood content of the reticular dermis (denoted by v^{rd}_{blood}) from 2 to 15% [21].

In our baseline case, we considered COHb, MetHb and SHb concentrations in blood equal to 1.5, 1.5 and 0 g/L. It is worth noting that this selection of values was performed considering that, in normal physiological states, only small traces ($< 2\%$) of COHb and MetHb are found in human blood [44, 26, 103], while SHb is absent [103, 38].

Table 3.2: MetHb and functional hemoglobin concentrations (in g/L) used in the simulation of distinct levels (represented by percentages of MetHb with respect to total hemoglobin content) of methemoglobinemia severity.

	10%	20%	30%	40%	50%	60%	70%	80%
MetHb	15	30	45	60	75	90	105	120
Functional Hemoglobins	133.5	118.5	103.5	88.5	73.5	58.5	43.5	28.5

Table 3.3: SHb and functional hemoglobin concentrations (in g/L) used in the simulation of distinct levels (represented by percentages of SHb with respect to total hemoglobin content) of sulfhemoglobinemia severity.

	10%	20%	30%	40%	50%	60%	70%	80%
SHb	15	30	45	60	75	90	105	120
Functional Hemoglobins	132	117	102	87	72	57	42	27

3.3 Swatch Generation and Analysis

Our investigation also included the generation of skin swatches, henceforth referred to as MetHb and SHb swatches, to enable the analysis of the visual impact of distinct severity levels of methemoglobinemia and sulfhemoglobinemia, respectively, on cyanotic appearances elicited by these disorders. The swatches' chromatic attributes were obtained from the convolution of a selected illuminant's relative spectral power distribution, the modeled reflectance data and the broad spectral response of the human photoreceptors [46]. This last step was performed by employing a standard CIEXYZ to RGB color system conversion procedure [15, 56] and considering the CIE standard D65 (daylight) illuminant [46] (Fig. 3.1(a)). For the reader interested in reproducing this process, the corrresponding Matlab [8] code is provided in Appendix E. After computing the chromatic attributes of a swatch, we applied a greyscale texture (Fig. 3.1(c)) to make its depiction more realistic.

For comparison purposes, the skin swatch obtained using the baseline reflectance curve (Fig. 3.1(b)) computed for the selected specimen is presented in (Fig. 3.1(d)).

Besides visual inspection, we also employed a device-independent CIE-based metric to compare skin swatches associated with distinct severity levels of methemoglobinemia and sulfhemoglobinemia. More specifically, we computed the CIELAB differences between pairs of swatches using the following formula [84]:

$$\Delta E^*_{ab} = \sqrt{{d_L}^2 + {d_a}^2 + {d_b}^2}, \tag{3.1}$$

where d_L, d_a and d_b represent the differences $L^*_1 - L^*_2$, $a^*_1 - a^*_2$ and $b^*_1 - b^*_2$, respectively, in which L^*, a^* and b^* correspond to the CIELAB color space dimensions. These are calculated for the modeled chromatic attributes associated with the compared swatches (indicated by the subscripts 1 and 2, respectively). Again, we performed these calculations using standard formulas employed in colorimetry [20, 56] and considering the CIE standard D65 illuminant [46]. As before, for the reader interested in reproducing these calculations, the corresponding Matlab code is provided in Appendix E.

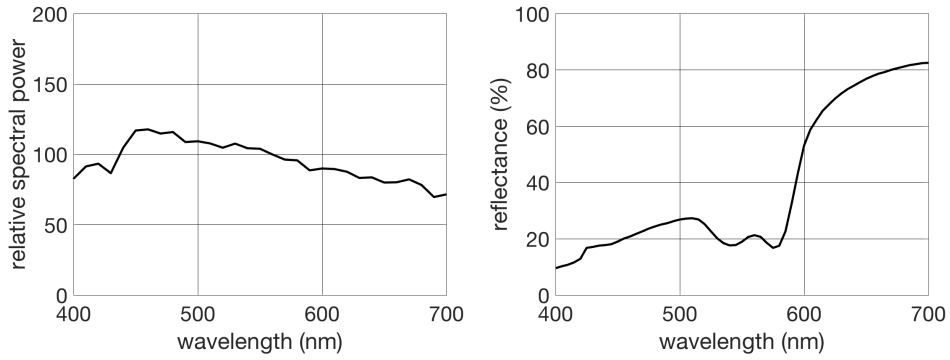

(a) (b)

(c) (d)

Figure 3.1: Components of the convolution process employed to generate a skin swatch depicting a palmar fingertip in its normal (baseline) state. (a) The relative spectral power distribution of the CIE standard D65 illuminant. (b) The baseline reflectance curve computed using the parameter values depicted in Table 3.1. (c) Greyscale texture of a palmar fingertip. (d) Resulting swatch.

Chapter 4

Investigation Findings

In this chapter, we present our findings and discuss their practical implications for the differentiation and monitoring of methemoglobinemia and sulfhemoglobinemia. We start with the examination of the reflectance curves obtained in our *in silico* experiments, henceforth referred to as dysfunctional (MetHb or SHb) reflectance curves. This is followed by a visual inspection and analysis of appearance changes resulting from distinct severity levels of methemoglobinemia and sulfhemoglobinemia. Building on the observations derived from our *in silico* experimental results, we then outline a cost-effective protocol for the noninvasive detection and differentiation of methemoglobinemia and sulfhemoglobinemia.

4.1 Methemoglobinemia and Sulfhemoglobinemia Spectral Responses

Initially, we performed experiments considering the blood content of the reticular dermis (v_{blood}^{rd}) equal to 2%. The results of these experiments are depicted in the graphs presented in Fig. 4.1. By examining these graphs, one can observe that the deviation of the dysfunctional reflectance curves from the baseline reflectance curve (Fig. 3.1 (b)) becomes more pronounced as the presence of MetHb and SHb increases, albeit with distinct deviation patterns being observed for the MetHb and SHb curves. More precisely, in the "blue" region (400 to 500 nm) of the visible light spectrum, one can observe a decrease in the MetHb curves and an increase in the SHb curves. In the "green" region (500 to 600 nm), one can observe an increase in both sets of curves. This increase, however, is more prominent for the MetHb curves. As a consequence, these curves show a more pronounced deviation

from the characteristic "w" shape (associated with a dominant presence of oxygenated hemoglobin [104]) discerned in the baseline reflectance curve (Fig. 3.1 (b)). Finally, in the "red" region (600 to 700 nm), one can observe a decrease in both sets of curves. This decrease, however, is more prominent for the SHb curves.

Afterwards, we performed experiments considering v_{blood}^{rd} equal to 5, 10 and 15%, whose results are presented in Fig. 4.2, Fig. 4.3, and Fig. 4.4, respectively. Although the same deviation patterns noted for the 2% case can be observed for the 5, 10 and 15% cases, the differences between the MetHb and SHb curves become smaller as v_{blood}^{rd} increases, particularly in the "blue" and "green" regions. In the "red" region, while both sets of curves become closer in the 600 to 650 nm interval, they remain relatively far apart in 650 to 700 nm interval. This can be explained by the relatively low absorption of light by both MetHb and SHb in this interval (Fig. 2.2 (b)). Thus, an increase in blood content will have a negligible impact on the reflectance values within this interval.

4.2 Cyanotic Appearance Changes

We remark that, as reported in the biomedical literature (*e.g.*, [36, 38, 41, 44]), skin spectral responses associated with methemoglobinemia and sulfhemoglobinemia lead to cyanotic skin appearances. One can expect that these appearances may vary according with the amounts of MetHb and SHb present in a subject's blood stream. In addition, it seems plausible that their characteristic chromatic attributes may be intensified as the blood content of the examined skin site increases. However, a quantitative investigation of the impact of these biophysical parameters on a subject's cyanotic appearance has not been performed to date.

In order to perform such an investigation, we employed the dysfunctional reflectance curves obtained from our *in silico* experiments (Section 4.1) to generate skin swatches depicting the appearance changes associated with these curves. In total, four sets of swatches were generated, one for each v_{blood}^{rd} value considered in our experiments, namely 2%, 5% 10% and 15%. These sets are presented in Figs. 4.5 to 4.8, respectively, along with the CIELAB $\Delta E_{ab}^{\star}$ differences computed for each pair of swatches generated for the same abnormal amounts of MetHb and SHb.

As it can be observed in Fig. 4.5, an increase in the methemoglobinemia and sulfhemoglobinemia severity levels led to a pale appearance when we considered v_{blood}^{rd} equal to 2%. In addition, it also led to more distinguishable $\Delta E_{ab}^{\star}$ differences between pairs of swatches generated considering the same amounts of MetHb and SHb.

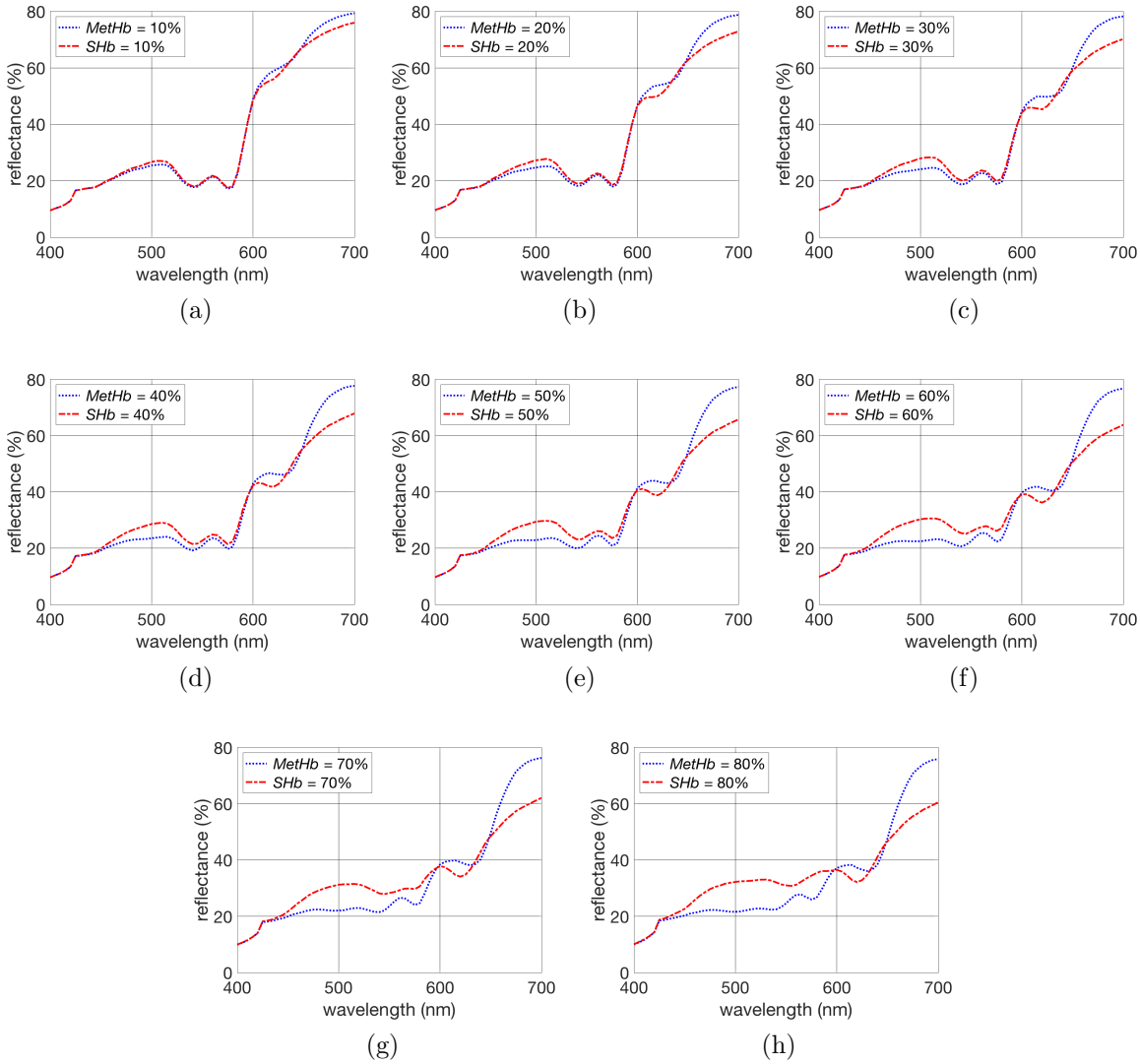

Figure 4.1: Graphs depicting reflectance curves resulting from increasing amounts of methemoglobin (MetHb) and sulfhemoglobin (SHb) in a skin specimen characterized by a reticular blood content (v_{blood}^{rd}) equal to 2%. These curves were obtained using the HyLIoS [25] model and considering an angle of incidence equal to 15°. Each graph corresponds to a distinct severity level of methemoglobinemia and sulfhemoglobinemia: (a) 10%, (b) 20%, (c) 30%, (d) 40%, (e) 50%, (f) 60%, (g) 70% and (h) 80%. The concentrations of dysfunctional and functional hemoglobins associated with these levels are provided in Tables 3.2 and 3.3. The remaining parameters values used in the specimen's characterization are provided in Table 3.1.

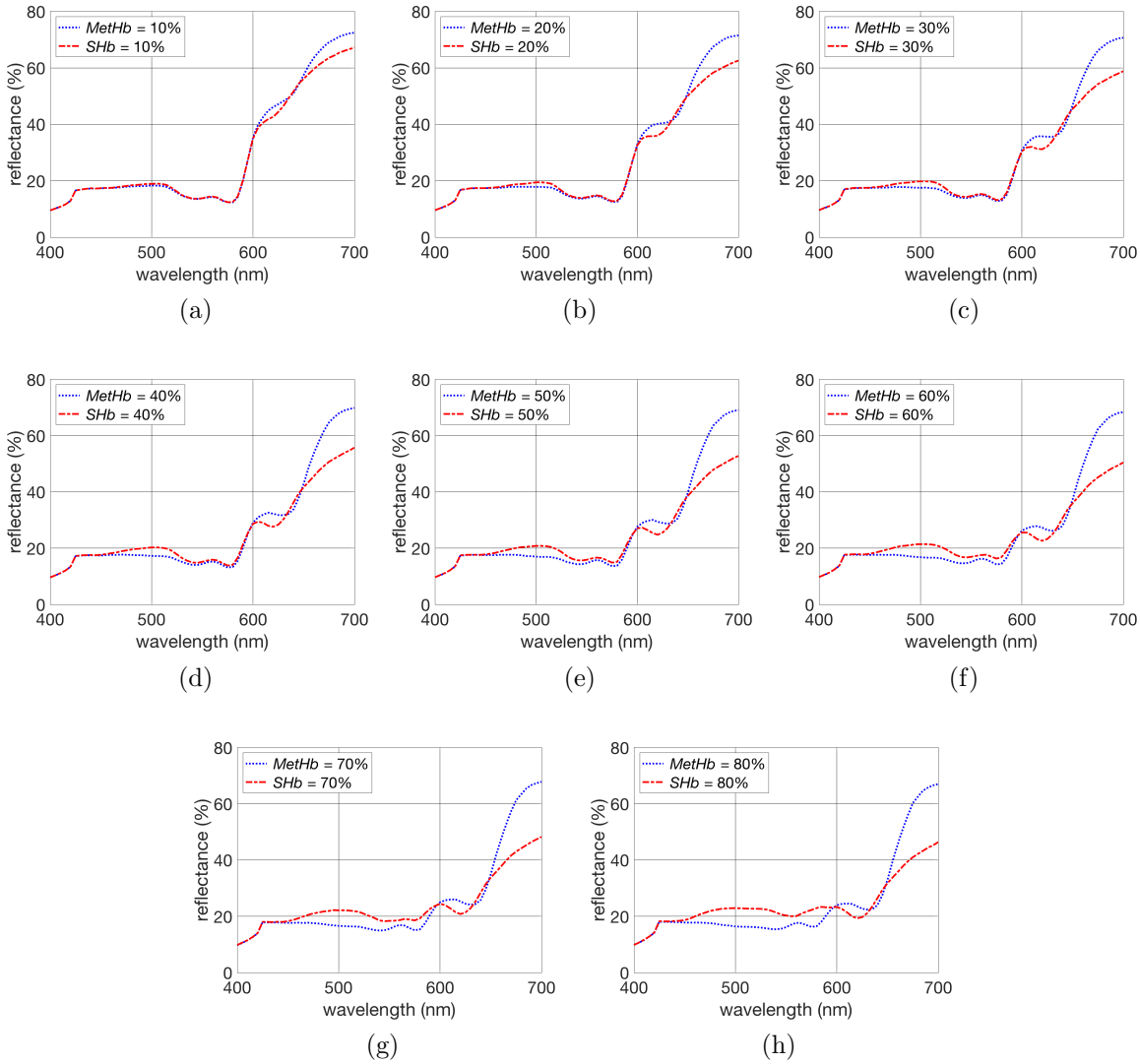

Figure 4.2: Graphs depicting reflectance curves resulting from increasing amounts of methemoglobin (MetHb) and sulfhemoglobin (SHb) in a skin specimen characterized by a reticular blood content (v^{rd}_{blood}) equal to 5%. These curves were obtained using the HyLIoS [25] model and considering an angle of incidence equal to 15°. Each graph corresponds to a distinct severity level of methemoglobinemia and sulfhemoglobinemia: (a) 10%, (b) 20%, (c) 30%, (d) 40%, (e) 50%, (f) 60%, (g) 70% and (h) 80%. The concentrations of dysfunctional and functional hemoglobins associated with these levels are provided in Tables 3.2 and 3.3. The remaining parameters values used in the specimen's characterization are provided in Table 3.1.

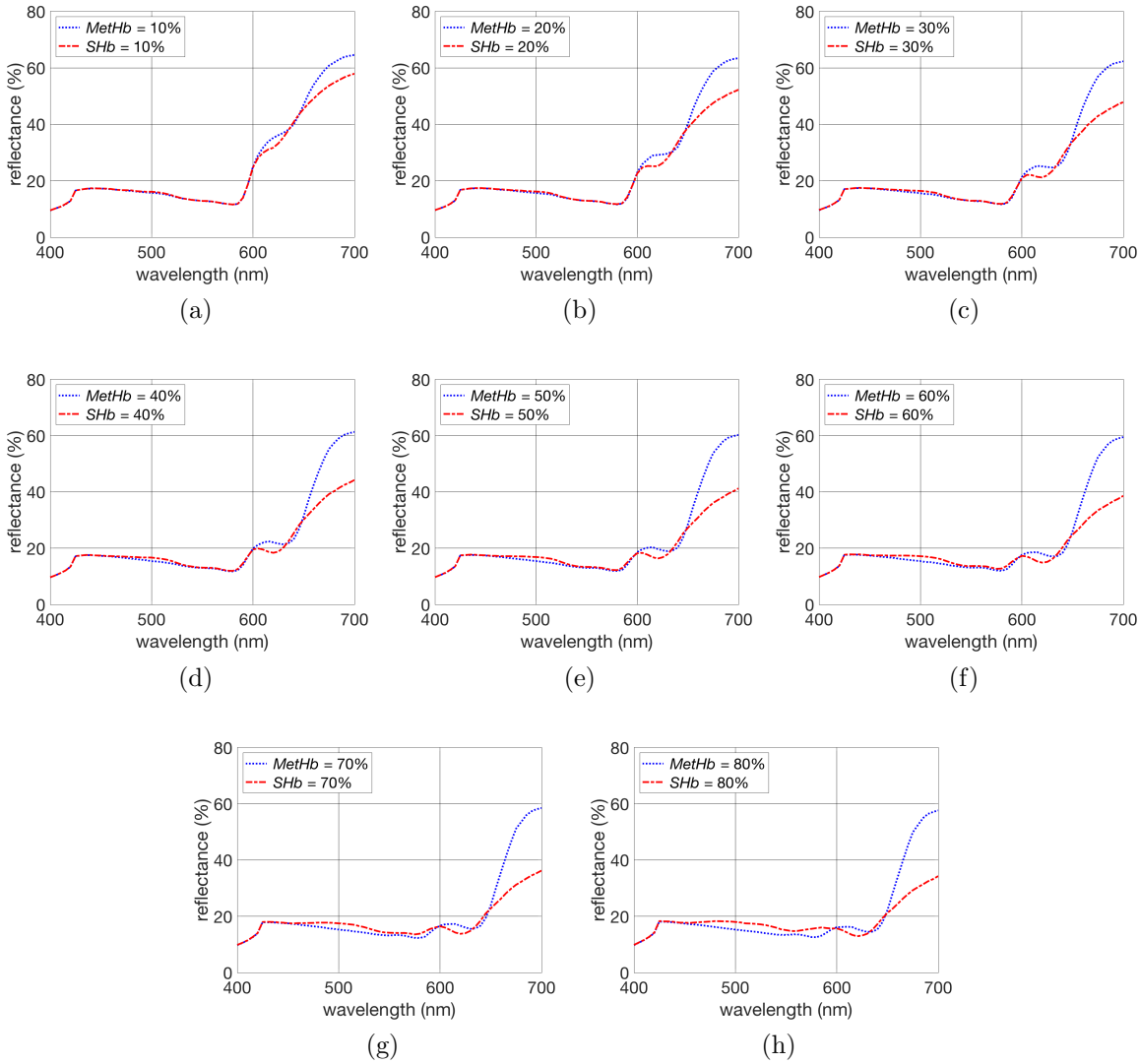

Figure 4.3: Graphs depicting reflectance curves resulting from increasing amounts of methemoglobin (MetHb) and sulfhemoglobin (SHb) in a skin specimen characterized by a reticular blood content (v_{blood}^{rd}) equal to 10%. These curves were obtained using the HyLIoS [25] model and considering an angle of incidence equal to 15°. Each graph corresponds to a distinct severity level of methemoglobinemia and sulfhemoglobinemia: (a) 10%, (b) 20%, (c) 30%, (d) 40%, (e) 50%, (f) 60%, (g) 70% and (h) 80%. The concentrations of dysfunctional and functional hemoglobins associated with these levels are provided in Tables 3.2 and 3.3. The remaining parameters values used in the specimen's characterization are provided in Table 3.1.

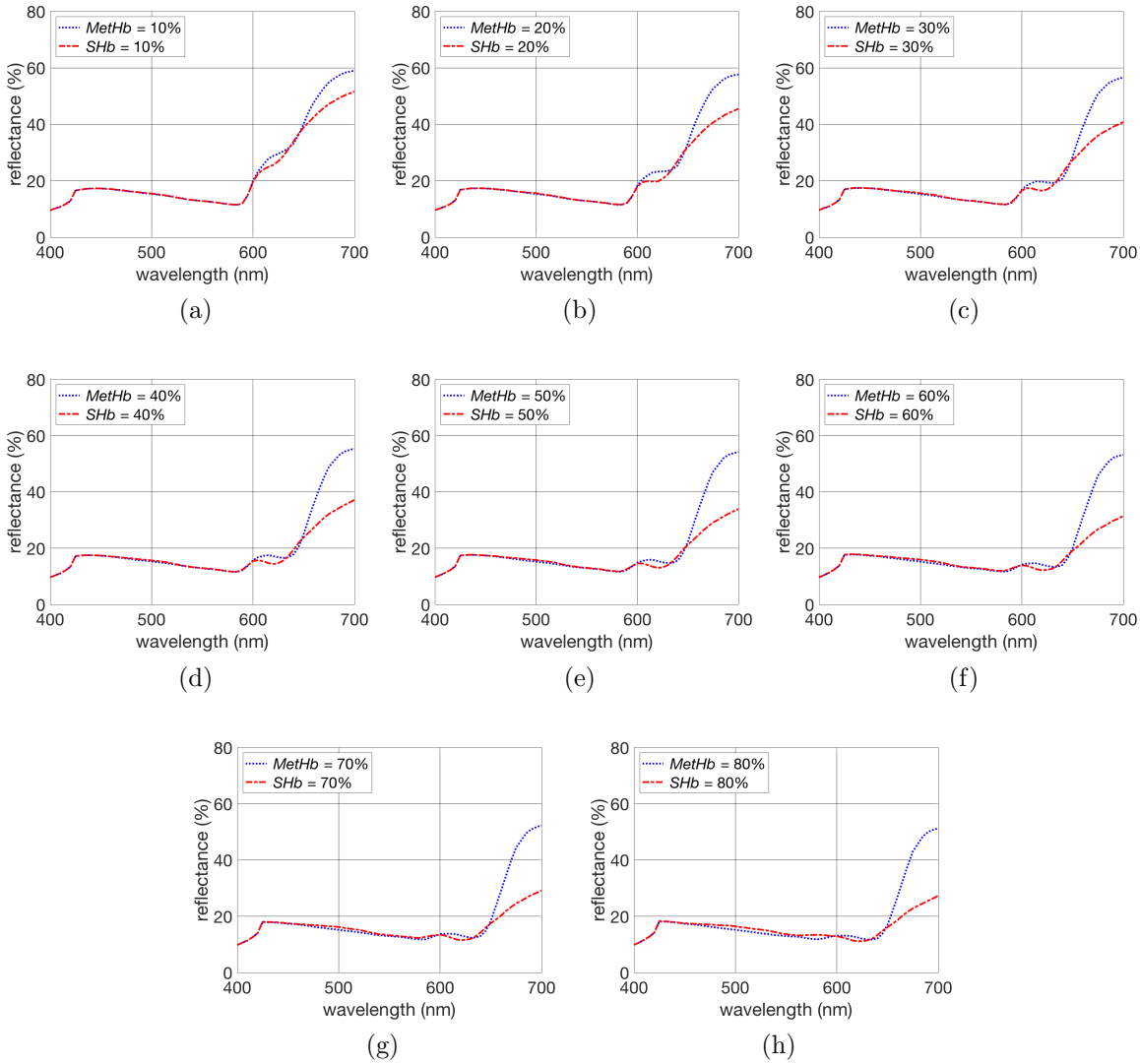

Figure 4.4: Graphs depicting reflectance curves resulting from increasing amounts of methemoglobin (MetHb) and sulfhemoglobin (SHb) in a skin specimen characterized by a reticular blood content (v_{blood}^{rd}) equal to 15%. These curves were obtained using the HyLIoS [25] model and considering an angle of incidence equal to 15°. Each graph corresponds to a distinct severity level of methemoglobinemia and sulfhemoglobinemia: (a) 10%, (b) 20%, (c) 30%, (d) 40%, (e) 50%, (f) 60%, (g) 70% and (h) 80%. The concentrations of dysfunctional and functional hemoglobins associated with these levels are provided in Tables 3.2 and 3.3.The remaining parameters values used in the specimen's characterization are provided in Table 3.1.

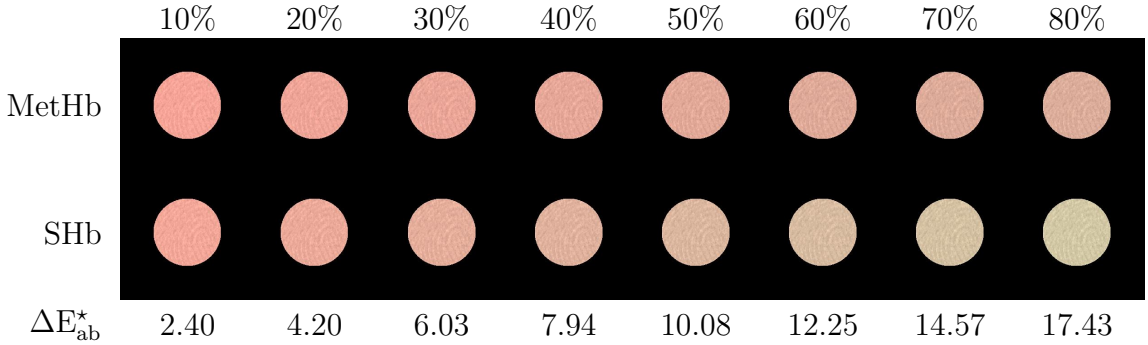

Figure 4.5: Skin swatches generated using the dysfunctional reflectance curves provided in Fig. 4.1, which were obtained considering skin specimen characterized by a reticular blood content (v^{rd}_{blood}) equal to 2% and increasing amounts of methemoglobin (MetHb) and sulfhemoglobin (SHb), from 10% to 80%. The bottom row presents the the CIELAB $\Delta E^{\star}_{ab}$ differences for each pair of MetHb and SHb swatches. The RGB values associated with each swatch depicted above can be found in Table A.1 in Appendix A.

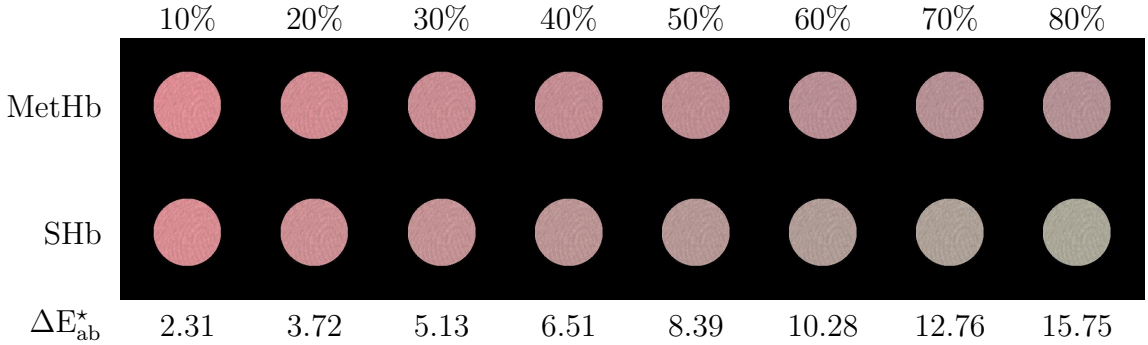

Figure 4.6: Skin swatches generated using the dysfunctional reflectance curves provided in Fig. 4.2, which were obtained considering skin specimen characterized by a reticular blood content (v^{rd}_{blood}) equal to 5% and increasing amounts of methemoglobin (MetHb) and sulfhemoglobin (SHb), from 10% to 80%. The bottom row presents the the CIELAB $\Delta E^{\star}_{ab}$ differences for each pair of MetHb and SHb swatches. The RGB values associated with each swatch depicted above can be found in Table A.2 in Appendix A.

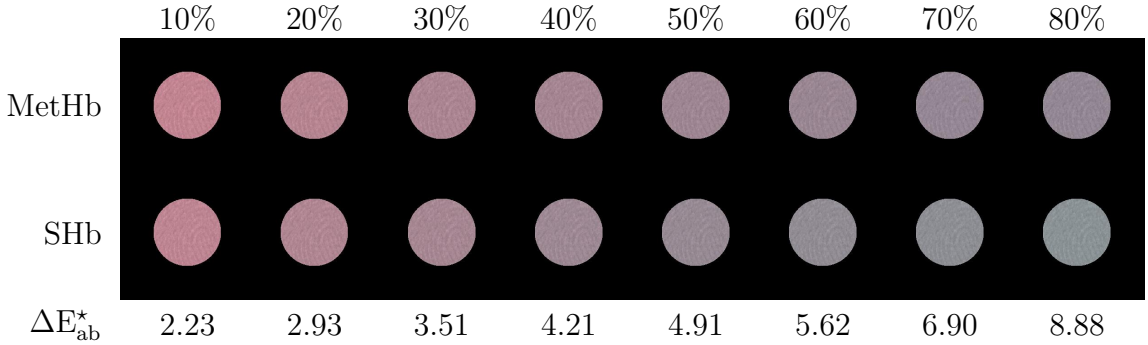

Figure 4.7: Skin swatches generated using the dysfunctional reflectance curves provided in Fig. 4.3, which were obtained considering skin specimen characterized by a reticular blood content (v^{rd}_{blood}) equal to 10% and increasing amounts of methemoglobin (MetHb) and sulfhemoglobin (SHb), from 10% to 80%. The bottom row presents the the CIELAB $\Delta E^{\star}_{ab}$ differences for each pair of MetHb and SHb swatches. The RGB values associated with each swatch depicted above can be found in Table A.3 in Appendix A.

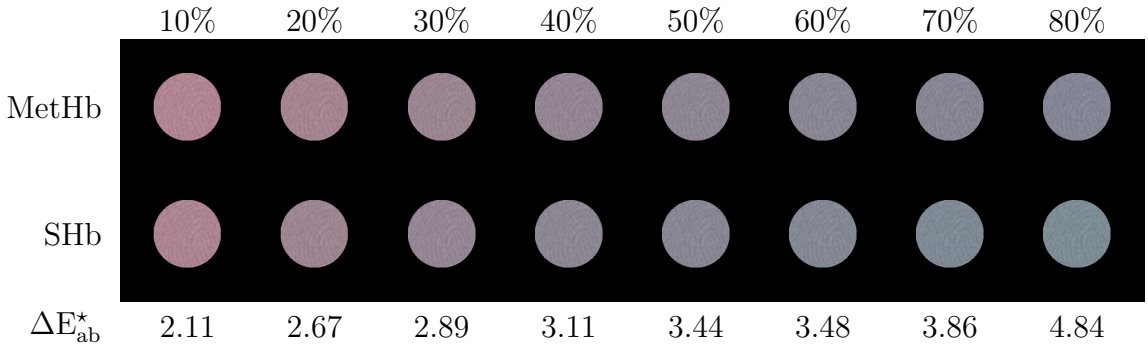

Figure 4.8: Skin swatches generated using the dysfunctional reflectance curves provided in Fig. 4.4, which were obtained considering skin specimen characterized by a reticular blood content (v^{rd}_{blood}) equal to 15% and increasing amounts of methemoglobin (MetHb) and sulfhemoglobin (SHb), from 10% to 80%. The bottom row presents the the CIELAB $\Delta E^{\star}_{ab}$ differences for each pair of MetHb and SHb swatches. The RGB values associated with each swatch depicted above can be found in Table A.4 in Appendix A.

As we employed higher values for v_{blood}^{rd}, the impact of increasing severity levels of methemoglobinemia and sulfhemoglobinemia on the swatches' appearance became more pronounced, with more characteristic cyanotic hues being elicited under these conditions. More specifically, one can observe a transition to red-purple (MetHb swatches) and grey (SHb swatches) hues in the 5% case (Fig. 4.6), to purple (MetHb swatches) and blue (SHb swatches) hues in the 10% case (Fig. 4.7), and to purple (MetHb swatches) and more saturated blue (SHb swatches) hues in the 15% case (Fig. 4.8).

The visual inspection of the swatches presented in Figs. 4.5 to 4.8 and the verification of their respective CIELAB $\Delta E_{ab}^{\star}$ differences reveal another relevant trend that can be summarized as follows. Although one can observe transitions to more characteristic cyanotic hues as higher v_{blood}^{rd} values are employed, the distinguishable CIELAB $\Delta E_{ab}^{\star}$ differences between pairs of swatches generated considering the same amounts of MetHb and SHb decreases. In practical terms, while a cyanotic appearance becomes more evident, the differentiation of their cause being an abnormal amount of MetHb or SHb becomes more problematic.

4.3 Proposed Detection and Differentiation Protocol

The observations reported in Section 4.2 indicate that the visual assessment of a patient's cyanotic appearance is not a reliable candidate for the differentiation of methemoglobinemia and sulfhemoglobinemia. However, it can be used to assist the detection of these disorders. More specifically, once a cyanotic appearance has been observed in a patient, other more common cyanosis-eliciting conditions may be ruled out using diagnosis-aiding tools usually available to the medical staff. For example, as mentioned earlier, cyanosis is normally associated with the presence of high levels of deoxygenated hemoglobin in the dermal tissues [17]. Thus, if a patient with a high level (above 90%) of oxygenated (saturated) arterial hemoglobin develops a cyanotic appearance, it is likely that such an appearance is being elicited by a dyshemoglobinemia disorder [39]. We remark that oxygen saturation levels can be quickly measured using a pulse oximeter [31], a device commonly available at the point of care of most medical settings.

After it has been detected that a patient is being subjected to either methemoglobinemia or sulfhemoglobinemia, the medical staff is left with the task of determining which of these conditions should be targeted for treatment. In order to accomplish this differentiation task in a cost-effective manner, ideally one would like to resort to a noninvasive procedure. Accordingly, we propose a procedure formulated using selected reflectance values obtained

at the patient's cyanotic fingertips. In the remainder of this chapter, we outline this procedure and evaluate its effectiveness.

From fundamental calculus [51], we know that the curve representing a differentiable function $y = f(x)$ is concave up on the interval where y' is increasing, and concave down on a interval where y' is decreasing. Moreover, assuming that $y = f(x)$ is twice differentiable on an interval I, then the curve representing $f(x)$ over I is concave up if $y'' > 0$, and concave down if $y'' < 0$.

In our investigation, $f(x)$ corresponds to a modeled reflectance curve $\rho(\lambda)$, where λ represents the wavelength of interest. Upon a closer examination of the dysfunctional reflectance curves (Section 4.1) obtained from our *in silico* experiments, one can observe a markedly distinct behavior of the MetHb and SHb curves on the 605 to 635 nm interval. More specifically, while the curves obtained considering abnormal amounts of MetHb are concave down on this interval, the curves obtained considering abnormal amounts of SHb are concave up. These observations suggested that the sign of the second derivative of $\rho(\lambda)$ at the center (620 nm) of this interval can be used to differentiate reflectance curves resulting from the presence of abnormal amounts of MetHb and SHb in blood-perfused cutaneous tissues, with a '-' sign indicating the former and a '+' sign indicating the latter.

We note that the second derivative of a dysfunctional reflectance curve at 620 nm can be numerically computed using the following three point central difference formula [37]:

$$y''(620) = \frac{\rho(605) - 2\,\rho(620) + \rho(635)}{225}, \tag{4.1}$$

where $\rho(605)$, $\rho(620)$ and $\rho(635)$ correspond to reflectance values at 605, 620 and 635 nm, respectively.

Since, for differentiation purposes, we are only interested in the sign of the second derivative, the denominator in Equation 4.1 can be omitted. Accordingly, we employed the following simplified formula to obtain the sign of the second derivative of the dysfunctional reflectance curves at 620 nm:

$$y''(620) = \rho(605) - 2\,\rho(620) + \rho(635). \tag{4.2}$$

Using Equation 4.2 and $\rho(605)$, $\rho(620)$ and $\rho(635)$ values extracted from the dysfunctional reflectance curves presented in Section 4.1, we computed the signs of their respective second derivative at 620 nm. We remark that these curves were computed considering an angle of incidence equal to 15°. It is appropriate, however, to account for possible changes in the measurement conditions that can take place when one employs an actual optical

device to collect reflectance data. For example, one can expect angular variations with respect to the angle of incidence due to slight curvature of the palmar fingertip. For this reason, we also repeated our *in silico* experiments considering angles of incidences equal to 0°, 30° and 45°, and extracted the $\rho(605)$, $\rho(620)$ and $\rho(635)$ values from the resulting dysfunctional reflectance curves (provided in Appendix B). We then used Equation 4.2 and these reflectance values to compute the signs of the second derivatives of these curves at 620 nm. As it can be observed in the aggregated outcomes of these sign computations presented in Tables 4.1 to 4.4, we were able to differentiate between methemoglobinemia and sulfhemoglobinemia in all tested instances.

	MetHb				SHb			
	0°	15°	30°	45°	0°	15°	30°	45°
10%	−	−	−	−	+	+	+	+
20%	−	−	−	−	+	+	+	+
30%	−	−	−	−	+	+	+	+
40%	−	−	−	−	+	+	+	+
50%	−	−	−	−	+	+	+	+
60%	−	−	−	−	+	+	+	+
70%	−	−	−	−	+	+	+	+
80%	−	−	−	−	+	+	+	+

Table 4.1: Second derivative signs (at 620 nm) of the dysfunctional reflectance curves resulting from our *in silico* experiments considering v^{rd}_{blood} equal to 2%. The signs were obtained using Equation 4.2 and the reflectance values extracted from these curves. These values are provided in Tables C.1 to C.4 (Appendix C). The curves were computed using the Hylios model [65], the specimen's characterization parameter values presented in Table 3.1 and considering four angles of incidence (0°, 15°, 30° and 45°) as well as distinct severity levels of methemoglobinemia and sulfhemoglobinemia (10% to 80%). The concentrations of dysfunctional (MetHb and SHb) and functional hemoglobins associated with these levels are provided in Tables 3.2 and 3.3.

	MetHb				SHb			
	0°	15°	30°	45°	0°	15°	30°	45°
10%	−	−	−	−	+	+	+	+
20%	−	−	−	−	+	+	+	+
30%	−	−	−	−	+	+	+	+
40%	−	−	−	−	+	+	+	+
50%	−	−	−	−	+	+	+	+
60%	−	−	−	−	+	+	+	+
70%	−	−	−	−	+	+	+	+
80%	−	−	−	−	+	+	+	+

Table 4.2: Second derivative signs (at 620 nm) of the dysfunctional reflectance curves resulting from our *in silico* experiments considering v^{rd}_{blood} equal to 5%. The signs were obtained using Equation 4.2 and the reflectance values extracted from these curves. These values are provided in Tables C.5 to C.8 (Appendix C). The curves were computed using the Hylios model [65], the specimen's characterization parameter values presented in Table 3.1 and considering four angles of incidence (0°, 15°, 30° and 45°) as well as distinct severity levels of methemoglobinemia and sulfhemoglobinemia (10% to 80%). The concentrations of dysfunctional (MetHb and SHb) and functional hemoglobins associated with these levels are provided in Tables 3.2 and 3.3.

	MetHb				SHb			
	0°	15°	30°	45°	0°	15°	30°	45°
10%	−	−	−	−	+	+	+	+
20%	−	−	−	−	+	+	+	+
30%	−	−	−	−	+	+	+	+
40%	−	−	−	−	+	+	+	+
50%	−	−	−	−	+	+	+	+
60%	−	−	−	−	+	+	+	+
70%	−	−	−	−	+	+	+	+
80%	−	−	−	−	+	+	+	+

Table 4.3: Second derivative signs (at 620 nm) of the dysfunctional reflectance curves resulting from our *in silico* experiments considering v^{rd}_{blood} equal to 10%. The signs were obtained using Equation 4.2 and the reflectance values extracted from these curves. These values are provided in Tables C.9 to C.12 (Appendix C). The curves were computed using the Hylios model [65], the specimen's characterization parameter values presented in Table 3.1 and considering four angles of incidence (0°, 15°, 30° and 45°) as well as distinct severity levels of methemoglobinemia and sulfhemoglobinemia (10% to 80%). The concentrations of dysfunctional (MetHb and SHb) and functional hemoglobins associated with these levels are provided in Tables 3.2 and 3.3.

	MetHb				SHb			
	0°	15°	30°	45°	0°	15°	30°	45°
10%	−	−	−	−	+	+	+	+
20%	−	−	−	−	+	+	+	+
30%	−	−	−	−	+	+	+	+
40%	−	−	−	−	+	+	+	+
50%	−	−	−	−	+	+	+	+
60%	−	−	−	−	+	+	+	+
70%	−	−	−	−	+	+	+	+
80%	−	−	−	−	+	+	+	+

Table 4.4: Second derivative signs (at 620 nm) of the dysfunctional reflectance curves resulting from our *in silico* experiments considering v^{rd}_{blood} equal to 15%. The signs were obtained using Equation 4.2 and the reflectance values extracted from these curves. These values are provided in Tables C.13 to C.16 (Appendix C). The curves were computed using the Hylios model [65], the specimen's characterization parameter values presented in Table 3.1 and considering four angles of incidence (0°, 15°, 30° and 45°) as well as distinct severity levels of methemoglobinemia and sulfhemoglobinemia (10% to 80%). The concentrations of dysfunctional (MetHb and SHb) and functional hemoglobins associated with these levels are provided in Tables 3.2 and 3.3.

It is worth noting that reflectance values measured using actual devices, such as spectrophotometers, may be subjected to uncertainties associated with the device. A high precision device will have an uncertainty of ±0.001 or 0.1% [52]. A low precision device may have an uncertainty close to 1% [52, 106]. In order to assess the consistency of our observations with respect to these random fluctuations, we also performed a set of simulations considering the presence of random noise (±1%) in our simulations. Again, we were able to differentiate between methemoglobinemia and sulfhemoglobinemia in all tested instances. All reflectance datasets associated with these instances are provided in Appendix C.

For conciseness, we selected to present in the remainder of this section the reflectance values used to obtain the signs associated with the most difficult differentiation instances found in our experiments. These instances, in which one can observe the closest proximity between MetHb and SHb in the selected spectral interval, correspond to the case where we set v^{rd}_{blood} equal to 15%. The $\rho(605)$, $\rho(620)$ and $\rho(635)$ values extracted from the curves associated with these test instances are presented in Table 4.5, and the corresponding second derivative signed values (to enable the quantitative verification of the correctness of our calculations) computed using Equation 4.2 are provided in Table 4.6.

	MetHb			SHb		
	605	620	635	605	620	635
10%	0.2320	0.2890	0.3141	0.2246	0.2578	0.3160
20%	0.2047	0.2330	0.2419	0.1940	0.1986	0.2427
30%	0.1828	0.1964	0.1973	0.1723	0.1634	0.2038
40%	0.1681	0.1707	0.1693	0.1574	0.1440	0.1724
50%	0.1566	0.1533	0.1477	0.1455	0.1308	0.1530
60%	0.1457	0.1415	0.1328	0.1378	0.1210	0.1393
70%	0.1374	0.1337	0.1248	0.1322	0.1150	0.1278
80%	0.1310	0.1256	0.1172	0.1263	0.1108	0.1208

Table 4.5: Reflectance values at 605, 620 and 635 nm extracted from dysfunctional curves computed using the HyLIoS model [25], the specimen's characterization parameter values presented in Table 3.1 and accounting for the presence of random noise ($\pm 1\%$) in our simulations. In the computation of these curves, we considered an angle of incidence of 15°, a reticular blood content (v^{rd}_{blood}) equal to 15% and distinct severity levels of methemoglobinemia and sulfhemoglobinemia (10% to 80%). The concentrations of dysfunctional (MetHb and SHb) and functional hemoglobins associated with these levels are provided in Tables 3.2 and 3.3.

	10%	20%	30%	40%	50%	60%	70%	80%
MetHb	-0.0319	-0.0194	-0.0127	-0.0040	-0.0023	-0.0045	-0.0052	-0.0030
SHb	+0.0250	+0.0395	+0.0493	+0.0418	+0.0369	+0.0351	+0.0300	+0.0255

Table 4.6: Second derivative values computed using the reflectance values provided in Table 4.5 and Equation 4.2 for distinct severity levels of methemoglobinemia and sulfhemoglobinemia (10% to 80%). The concentrations of dysfunctional (MetHb and SHb) and functional hemoglobins associated with these levels are provided in Tables 3.2 and 3.3.

Previously, Baranoski et al. [12] have also proposed five-point and three-point central difference formulas for differentiating between methemoglobinemia and sulfhemoglobinemia. In their work, they were able to differentiate these disorders within a severity level range between 20% and 70% and considering the reticular blood content equal to 5%. Using the proposed formula, we were able to differentiate these disorders within a broader severity level range (from 10% to 80%) and considering observed [21] physiological variations in the reticular blood content (from 2% to 15%). These observations indicate that the proposed three-point formula enables a wider range of sensitivity in the differentiation of methemoglobinemia and sulfhemoglobinemia without incurring into additional computational costs.

In summary, based on our *in silico* experimental findings, we propose a protocol in which

a subject's cyanotic appearance is employed to assist the detection of methemoglobinemia and sulfhemoglobinemia, and an optical procedure is used to differentiate these disorders. This procedure, in turn, would consist in the noninvasive measurement of three reflectance values at the patient's cyanotic fingertips followed by the sign computation using Equation 4.2. We note that the proposed differentiation procedure would require only three measurements, which could be obtained *in situ* (without the need, for example, of sending blood samples for analysis elsewhere) using a hand-held spectrophotometer, a relatively inexpensive device in comparison with co-oximeters and blood gas analysers. Moreover, these measurements would be performed at wavelengths within the visible (harmless) region of the light spectrum. These aspects would likely make it attractive for use at the point of care of low-resources medical settings.

Since other noninvasive optical monitoring procedures, such as pulse oximetry [31], also rely on light and skin interactions in the near-infrared domain, one might question the reason why we have not extended our investigation to this spectral domain. Although our *in silico* experimental framework can be used to obtain skin reflectance readings from the ultraviolet to the infrared domain, our investigation was centered at the visible domain for the following reasons. First, one of the focal points of our investigation, cyanosis, is directly associated with skin spectral responses in this spectral domain. Second, there is a relative scarcity of reliable data with respect to the extinction coefficients of MetHb and SHb outside the visible domain. The available data (*e.g.*, [82, 103]) indicates that the extinction coefficients of MetHb and SHb in the near-infrared domain may be one order of magnitude lower than their visible domain counterparts. This, in turn, suggests that the chances of finding significant spectral features to allow a reliable differentiation of methemoglobinemia and sulfhemoglobinemia are small in the near-infrared domain. Nonetheless, as reliable near-infrared extinction coefficient data for MetHb and SHb become available, it will be worthwhile to investigate the possibility of finding differentiation features for methemoglobinemia and sulfhemoglobinemia in this spectral domain as well.

Chapter 5

Conclusion and Future Prospects

In this work, we have quantitatively examined the connection between the onset of cyanosis and distinct severity levels of methemoglobinemia and sulfhemoglobinemia. More specifically, we have demonstrated the impact of different amounts of MetHb and SHb on cyanotic chromatic attributes of a specimen also subjected to variations on dermal blood content. We have also assessed the impact of these biophysical parameters on the specimen's spectral responses. Building on the findings derived from our *in silico* findings, we have proposed a cost-effective protocol for the detection and differentiation of methemoglobinemia and sulfhemoglobinemia. Our *in silico* evaluation of its effectiveness and sensitivity range suggests that it can represent a promising alternative to the technologies currently used in the detection and differentiation of these dyshemoglobinemia disorders.

It has been long recognized [93, 95] that *in silico* experiments performed through predictive computer simulations can be successfully employed to predict the quantitative behaviour of complex biological systems, to accelerate the hypothesis generation and validation cycles of biomedical research, notably those that cannot be performed using traditional "wet" laboratory technologies, and to drive new scientific investigations. It is important to keep in mind, however, that a computer simulation has a limited value if it is not being supported and verified against reliable data obtained through actual experiments performed under *in vivo* and/or *in vitro* conditions. Furthermore, the pairing of computer simulations with actual experiments can contribute to a more straightforward translation of research outcomes obtained *in silico* to clinical practice. These experiments, for example, could consist in reflectance measurements performed (*in vivo*) on a patient subjected to a dyshemoglobinemia disease, followed by a collection of a blood sample to determine (*in vitro*) the MetHb and SHb levels in his/her blood stream.

Viewed in this context, our *in silico* findings and, in particular, the verification of the proposed protocol's effectiveness would certainly benefit from confirmation through *in vivo* and/or *in vitro* experiments. We note, however, that the scarcity of *in vivo* and *in vitro* experiments involving the measurement of chromatic and spectral data associated with the onset of methemoglobinemia and sulfhemoglobinemia has motivated our use of an *in silico* approach in the first place. Moreover, we remark that our *in silico* experiments were performed using a first-principles model of light and skin interactions, whose predictive capabilities have been extensively evaluated in previous works [13, 17, 18, 25, 90]. Also, to the best of our knowledge, we have employed the most reliable supporting biophysical data, such as the spectral extinction coefficients for methemoglobin [77] and sulfhemoglobin [103], provided in the biomedical literature. Hence, we are confident that our findings can be corroborated by *in vivo* and/or *in vitro* measured data as it becomes available.

As outlined above, the investigation presented in this thesis also highlighted the need for databases depicting measured chromatic and spectral data obtained from skin specimens subject to pathological conditions, particularly those affecting the patients' appearance and posing a high risk of morbidity and mortality for them. In order to improve this situation, we believe that the biomedical community should support efforts directed to the creation of such databases. These should include, but not be limited to data related to dyshemoglobinemia disorders. These efforts would likely involve the establishment of synergistic cooperations between researchers and medical institutions involved in the diagnosis and treatment of the targeted pathological conditions. Once the databases are created, it would be essential that they are made publicly accessible so that they can be fully verified and employed by the entire biomedical community.

References

[1] P. Agache. Main skin biological constants. In P. Agache and P. Humbert, editors, *Measuring the Skin*, pages 727–746. Springer-Berlag, Berlin, Germany, 2004.

[2] P. Agache. Metrology of the stratum corneum. In P. Agache and P. Humbert, editors, *Measuring the Skin*, pages 101–111. Springer-Berlag, Berlin, Germany, 2004.

[3] P. Agache. Stratum corneum histophysiology. In P. Agache and P. Humbert, editors, *Measuring the Skin*, pages 95–100. Springer-Berlag, Berlin, Germany, 2004.

[4] S. Alaluf, D. Atkins, K. Barret, M. Blount, N. Carter, and A. Heath. Ethnic variation in melanin content and composition in photoexposed and photoprotected human skin. *Pigment Cell Res.*, 15:112–118, 2002.

[5] R.R. Anderson and J.A. Parrish. The optics of human skin. *J. Investig. Dermatol.*, 77(1):13–9, 1981.

[6] R.R. Anderson and J.A. Parrish. Optical properties of human skin. In J.D. Regan and J.A. Parrish, editors, *The Science of Photomedicine*, pages 147–194, N.Y., USA, 1982. Plenun Press.

[7] S.W. Askew and G.V.G. Baranoski. On the dysfunctional hemoglobins and cyanosis connection: Practical implications for the clinical detection and differentiation of methemoglobinemia and sulfhemoglobinemia. *Biomed. Opt. Express*, 9(7), 2018.

[8] S. Attaway. *MATLAB: A Practical Introduction to Programming and Problem Solving.* Butterworth-Heinmann Inc, 2018.

[9] N.F. Azmi, F. Delbressine, and L. Feijs. Conceptual determination and assessment of cyanosis. *Int. J. Bioscience, Biochemistry and Bioinformatics*, 6(3):75–83, 2016.

[10] A. Baernstein, K.M. Smith, and J.G. Elmore. Singing the blues: is it really cyanosis? *Resp. Care*, 53(8):1081–1084, 2008.

[11] G.V.G Baranoski and T.F. Chen. Optical properties of skin surface. In P. Humbert, H. Maibach, F. Fanian, and P. Agache, editors, *Agache's Measuring Skin*, volume 1, pages 85–98, Cham, Switzerland, 2017. Springer International Publishing.

[12] G.V.G. Baranoski, T.F. Chen, B.W. Kimmel, E. Miranda, and D. Yim. On the noninvasive optical monitoring and differentiation of methemoglobinemia and sulfhemoglobinemia. *J. Biomed. Opt.*, 17(9):097005–1–14, 2012.

[13] G.V.G. Baranoski, A. Dey, and T.F. Chen. Assessing the sensitivity of human skin hyperspectral responses to increasing anemia severity levels. *J. Biomed. Opt.*, 9(20):095002–1–14, 2015.

[14] G.V.G. Baranoski, T. Dimson, T.F. Chen, B. Kimmel, D. Yim, and E. Miranda. Rapid dissemination of light transport models on the web. *IEEE Comput. Graph.*, 32:10–15, 2012.

[15] G.V.G. Baranoski and A. Krishnaswamy. *Light & Skin Interactions: Simulations for Computer Graphics Applications*. Morgan Kaufmann/Elsevier, Burlington, MA, USA, 2010.

[16] G.V.G. Baranoski, J.G. Rokne, and G. Xu. Virtual spectrophotometric measurements for biologically and physically-based rendering. *The Visual Computer*, 17(8):506–518, 2001.

[17] G.V.G Baranoski, S.R. Van Leeuwen, and T.F. Chen. Elucidating the biophysical processes responsible for the chromatic attributes of peripheral cyanosis. In *39th Annual International Conference of the IEEE Engineering in Medicine and Biology Society (EMBC)*, pages 90–95, Jeju Island, South Korea, August 2017.

[18] G.V.G Baranoski, S.R. Van Leeuwen, and T.F. Chen. On the detection of peripheral cyanosis in individuals with distinct levels of cutaneous pigmentation. In *39th Annual International Conference of the IEEE Engineering in Medicine and Biology Society (EMBC)*, pages 4260–4264, Jeju Island, South Korea, August 2017.

[19] A.N. Bashkatov, E.A. Genina, V.I. Kochubey, and V.V. Tuchin. Optical properties of human skin, subcutaneous and mucous tissues in the wavelength range from 400 to 2000 nm. *J. of Physics D: Applied Physics*, 38:2543–2555, 2005.

[20] D.H. Brainard. Color appearance and color difference specification. *The Science of Color*, 2:191–216, 2003.

[21] A. Caduff, M.S. Talary, and P. Zakharov. Cutaneous blood perfusion as a perturbing factor for noninvasive glucose monitoring. *Diabetes Technology & Therapeutics*, 12(1):1–9, 2010.

[22] A.E. Cerussi, A.J. Berger, F. Bevilacqua, N. Shah, D. Jakubowski, J. Butler, R. Holcombe, and B. J. Tromberg. Sources of absorption and scattering contrast for near-infrared optical mammography. *Academic radiology*, 8(3):211–218, March 2001.

[23] M.R. Chedekel. Photophysics and photochemistry of melanin. In M.R. Chedekel L. Zeise and T.B. Fitzpatrick, editors, *Melanin: Its Role in Human Photoprotection*, pages 11–22, Overland Park, Kansas, USA, 1995. Valdenmar Publishing Co. 2223b.

[24] T.F. Chen. *On the Modelling of Hyperspectral Light and Skin Interactions and the Simulation of Skin Appearance Changes Due to Tanning*. PhD thesis, D.R. Cheriton School of Computer Science, University of Waterloo, 2015.

[25] T.F. Chen, G.V.G. Baranoski, B.W. Kimmel, and E. Miranda. Hyperspectral modeling of skin appearance. *ACM Trans. Graph.*, 34(3):31:1–14, 2015.

[26] S.F.W. Cunnington A. J., Kendrick, B. Wamola, B. Lowe, and C. R. J. C. Newton. Carboxyhemoglobin levels in kenyan children with plasmodium falciparum malaria. *The American Journal of Tropical Medicine and Hygiene*, 71(1):43–47, 2004.

[27] K.M. Van de Graaff. *Human Anatomy*. W. C. Brown Publishers, Dubuque, IO, USA, 4th edition, 1995.

[28] L. Derbas, M. Warsame, M.A. Oma, Y. Zafar, and G. Howell. Sulfhaemoglobinaemia caused by ferrous sulfate. *BMJ Case REp.*, pages 56:1–13, May 2017.

[29] B.L. Diffey. A mathematical model for ultraviolet optics in skin. *Phys. Med. Biol.*, 28(6):647–657, 1983.

[30] C.A. Finch. Methemoglobinemia and sulfhemoglobinemia. *New England Journal of Medicine*, 239(13):470–478, 1948.

[31] R. Flewelling. Noninvasive optical monitoring. In Joseph D. Bronzino, editor, *The Biomedical Engineering Handbook*, pages 1346–1356. CRC Press LLC, 1 edition, 1995.

[32] R. Flindt. *Amazing Numbers in Biology*. Springer-Verlag, Berlin, Germany, 2006.

[33] E. Fuchs. Keratins and the skin. *Annual Review of Cell and Developmental Biology*, 11(1):123–154, 1995.

[34] D.J. Gawkrodger and M.R. Ardern-Jones. *Dermatology An Illustrated Colour Text*. Churchill Livingstone, Elsevier, 3rd edition, 2002.

[35] G.Casey. Oxygen transport and the use of pulse oxymetry. *Nursing Standard*, 15(47):46–53, 2001.

[36] A. George and D. Goetz. A case of sulfhemoglobinemia in a child with chronic constipation. *Resp Med Case Reports*, 21:21–24, 2017.

[37] C.F. Gerald and P.O. Wheatley. *Applied Numerical Analysis*. Addison-Wesley Publishing Company, Reading, Massachusetts, USA, 5 edition, 1999.

[38] L Gharahbaghian, B Massoudian, and G Dimassa. Methemoglobinemia and sulfhemoglobinemia in two pediatric patients after ingestion of hydroxylamine sulfate. *West. J. Emerg. Med.*, 10(3):197–201, August 2009.

[39] G. Giangreco, D. Campbell, and M. Cowan. A 32-year-old female with aids, *Pneumocystis jiroveci* pneumonia, and methemoglobinemia. *Case Reports in Critical Care*, 2013:1–5, 2013.

[40] P.R. Ginimuge and S.D. Jyothi. Methylene blue: revisited. *J. Anaesthesiol. Clin. Pharmacol.*, 26(4):517–520, 2010.

[41] A.S. Gopalachar, V.L. Bowie, and P. Bharadwaj. Phenazopyridine-induced sulfhemoglobinemia. *Ann. Pharmacol.*, 39:1128–1130, 2005.

[42] S. Guiducci and M. Matucci-Cerenic. Definition, nomenclature and diagnostic criteria. In F.M.Wigley, A.L. Herrick, and N.A Flavahan, editors, *Raynaud's Phenomenon, A Guide to Pathogenesis and Treatment*, pages 13–20. Springer, New York, NY, USA, 2015.

[43] N.B. Hampson, C.A. Piantadosi, S.R. Thom, and L.K. Weaver. Practice recommendations in the diagnosis, management, and prevention of carbon monoxide poisoning. *Am. J. Resp. Crit. Care*, 186(11):1095–1101, 2012.

[44] S. Haymond, R. Cariappa, C.S. Eby, and M.G. Scott. Laboratory assessment of oxygenation in methemoglobinemia. *Clinical Chemistry*, 51(2):434–444, 2005.

[45] A. Hennessy, C. Oh, B. Diffey, K. Wakamatsu, S. Ito, and J. Rees. Eumelanin and pheomelanin concentrations in human epidermis before and after UVB irradiation. *Pigment Cell Res.*, 18:220–223, 2005.

[46] R.W.G. Hunt. *Measuring Colour*. Ellis Horwood Limited, Chichester, England, 2nd edition, 1991.

[47] R.S. Hunter and R.W. Harold. *The Measurement of Appearance*. John Wiley & Sons, New York, NY, USA, second edition, 1987.

[48] S.L. Jacques. Origins of tissue optical properties in the UVA, visible, and NIR regions. *OSA TOPS on Adv. in Opt. Imaging and Photon Migration*, 2:364–369, 1996.

[49] S.L. Jacques, C.A. Alter, and S.A. Prahl. Angular dependence of HeNe laser light scattering by human dermis. *Lasers Life Sci.*, 1:309–333, 1987.

[50] K.K. Jain. Carbon monoxide and other tissue poisons. In K.K. Jain, editor, *Textbook of Hyperbaric Medicine*, pages 131–154, Cham, Switzerland, 2017. Springer International Publishing.

[51] G.B. Thomas Jr, R.L. Finney, and M.D. Weir. *Calculus and Analytic Geometry*. Addison-Wesley Publishing Company, Reading, Massachusetts, USA, 9 edition, 1996.

[52] D.B. Judd and G. Wyszecki. *Color in Business, Science and Industry*. John Wiley & Sons, New York, NY, USA, third edition, 1975.

[53] T. Karen, H.U. Bucher, and J. Fauchére. Comparison of a new transcutaneous bilirubinometer (bilimed) with serum bilirubin measurments in preterm and full-term infants. *BMC Pediatrics*, 9(70):1–7, 2009.

[54] A. Kienle, L. Lilge, A. Vitkin, M.S. Patterson, B.C. Wilson, R. Hibst, and R. Steiner. Why do veins appear blue? A new look at an old question. *Applied Optics*, 35(7):1151–1160, 1996.

[55] N. Kollias, R.M. Sayre, L. Zeise, and M.R. Chedekel. Photoprotection by melanin. *J. Photoch. Photobio. B.*, 9(2):135–60, 1991.

[56] B. Kravchenko. Balancing fidelity and performance in iridal light transport simulations aimed at interactive applications. Master's thesis, D.R. Cheriton School of Computer Science, University of Waterloo, 2016.

[57] R. Lee, M.M. Mathews-Roth, M.A. Pathak, and J.A. Parrish. The detection of carotenoid pigments in human skin. *J. Investig. Dermatol.*, 64(3):175–177, 1975.

[58] T.S. Lister. *Simulating the Color of Port Wine Stain Skin.* PhD thesis, University of Southampton,U.K., February 2013.

[59] C. Lundsgaard and D. Van Slyke. Cyanosis. In *Medicine Monographs*, pages 1–80. Wlliams & Wilkins Company, The Rockfeller Institute for Medical Research, Baltimore, USA, 1923.

[60] N. Magnenat-Thalmann, P. Kalra, J. L. Leveque, R. Bazin, D. Batisse, and B. Querleux. A computational skin model: fold and wrinkle formation. *IEEE T. Inf. Technol. B.*, 6(4):317–323, 2002.

[61] C.D. Marple. Cyanosis. *The American Journal of Nursing*, 58(2):222–235, 1958.

[62] S.M. McMullen and W. Patrick. Cyanosis. *The American Journal of Medicine*, 126(3):210–212, 2013.

[63] K. Murphy, C. Ryan, E.M. Dempsey, P. W. Otoole, R.P. Ross, C. Stanton, and C.A. Ryan. Neonatal sulfhemoglobinemia and hemolytic anemia associated with intestinal morganella morganii. *Pediatrics*, 136(6), 2015.

[64] N. Nakagawa, M. Matsumoto, and S. Sakai. *In vivo* measurement of the water content in the dermis by confocal Raman spectroscopy. *Skin Research and Technology*, 16(2):137–141, 2010.

[65] Natural Phenomena Simulation Group (NPSG). *Run HyLIoS Online.* School of Computer Science, University of Waterloo, Ontario, Canada, 2014. http://www.npsg.uwaterloo.ca/models/hylios.php.

[66] Natural Phenomena Simulation Group (NPSG). *Run HyLIoS Online.* School of Computer Science, University of Waterloo, Ontario, Canada, 2017. http://www.npsg.uwaterloo.ca/models/hyliosEx.php.

[67] F.E. Nicodemus, J.C. Richmond, J.J. Hsia, I.W. Ginsberg, and T. Limperis. Geometrical considerations and nomenclature for reflectance. In L.B. Wolff, S.A. Shafer, and G.E. Healey, editors, *Physics-Based Vision Principles and Practice: Radiometry*, pages 94–145, Boston, 1992. Jones and Bartlett Publishers.

[68] G.E. Nilsson, T. Tenland, and P.A. Öberg. Evaluation of a laser Doppler flowmeter for measuring of tissue blood flow. *IEEE Transactions on Biomedical Engineering*, 27(10):597–604, 1980.

[69] M.L. Noll and J.F. Byers. Usefulness of measures of Svo_2, Spo_2, vital signs, and derived dual oximetry parameters as indicators of arterial blood gas variables during weaning of cardiac surgery patients from mechanical ventilation. *Heart & Lung*, 24(3):220–227, 1995.

[70] NPSG. *Human Skin Data*. Natural Phenomena Simulation Group (NPSG), School of Computer Science, University of Waterloo, Ontario, Canada, 2014. http://www.npsg.uwaterloo.ca/data/skin.php.

[71] R.L. Olson, J. Gaylor, and M.A. Everett. Skin color, melanin, and erythema. *Arch. Dermatol.*, 108(4):541–544, 1973.

[72] M.A. Pathak. Functions of melanin and protection by melanin. In M.R. Chedekel L. Zeise and T.B. Fitzpatrick, editors, *Melanin: Its Role in Human Photoprotection*, pages 125–134, Overland Park, Kansas, USA, 1995. Valdenmar Publishing Co.

[73] S. Patnaik, M.M. Natarajan, E.J. James, and K. Ebenezer. Methylene blue unresponsive methemoglobinemia. *Indian J. Crit. Care Med.*, 18(4):253–255, 2014.

[74] R.W. Peterson, K. Kadugodinandareddy, V. Karunakaran, C. Whitney, J. Ling, and J.Y. Ye. Utilizing an open-microcavity optoacoustic sensor for spectroscopic determination of methemoglobin concentration. In *SPIE BIOS, Optical Tomography and Spectroscopy of Tissue XI*, pages 93191N–1–8. SPIE, vol. 9319, 2015.

[75] G. Plewig, E. Scheuber, B. Reuter, and W. Waidelich. Thickness of the corneocytes. In R. Marks and G. Plewig, editors, *Stratum Corneum*, pages 171–174, Berlin, 1983. Springer-Verlag.

[76] S.A. Prahl. Optical absorption of hemoglobin. Technical report, Oregon Medical Laser Center, 1999.

[77] L.L. Randeberg, J.H. Bonesrønning, M. Dalaker, J.S. Nelson, and L.O. Svaasand. Methemoglobin formation during laser induced photothermolysis of vascular skin lesions. *Lasers in Surgery and Medicine*, 34(5):414–419, 2004.

[78] K. Robertson and J.L. Rees. Variation in epidermal morphology in human skin at different body sites as measured by reflectance confocal microscopy. *Acta Derm. Venereol.*, 90:368–373, 2010.

[79] M. Schwarz, M. Omar, A. Buehler, J. Aguirre, and V. Ntziachristos. Implications of ultrasound frequency in optoacoustic mesoscopy of the skin. *IEEE Trans. Med. Imaging*, 34(2):672–677, 2015.

[80] S. Shadnia, K. Soltaninejad, H. Hassanian-Moghada, A. Sadeghi, H. Rahimzadeh, N. Zamani, A. Ghasemi-toussi, and M. Abdollahi. Methemoglobinemia in aluminium phosphide poisoning. *Human and Experimental Toxicology*, 30(3):250–253, 2010.

[81] H. Shimizu. *Shimizu's Textbook of Dermatology*. Hokkaido University Press, 2007.

[82] O. Siggaard-Andersen, B. Nrgaard-Pedersen, and J. Rem. Hemoglobin pigments. spectrophotometric determination of oxy-, carboxy-, met-, and sulfhemoglobin in capillary blood. *Clinica Chimica Acta*, 42(1):85 – 100, 1972.

[83] C.A. Squier, P. Cox, and P. Wertz. Lipid content and water permeability of skin and oral mucosa. *Journal of Investigative Dermatology*, 96(1):123–126, 1991.

[84] M. Stokes, M.D. Fairchild, and R.S. Berns. Precision requirements for digital color reproduction. *ACM Trans. Graph.*, 11(4):406–422, 1992.

[85] P.S. Talreja, G.B. Kasting, N.K. Kleene, W.L. Pickens, and T. Wang. Visualization of the lipid barrier and measurement of lipid pathlength in human stratum corneum. *AAPS PharmSci.*, 3(2):48–56, 2001.

[86] G.J. Tearney, M.E. Brezinski, J.F. Southern, B.E. Bouma, M.R. Hee, and J.G. Fujimoto. Determination of the refractive index of highly scattering human tissue by optical coherence tomography. *Opt. Lett.*, 20(21):2258–2260, Nov 1995.

[87] A.J. Thody, E.M. Higgins, K. Wakamatsu, S. Ito, S.A. Burchill, and J. Marks. Pheomelanin as well as eumelanin is present in human epidermis. *J. Investig. Dermatol.*, 97(2):340–344, 08 1991.

[88] V.V. Tuchin. *Tissue optics: light scattering methods and instruments for medical diagnosis*. SPIE PM. SPIE/International Society for Optical Engineering, Bellingham, WA, USA, 2007.

[89] R.H. Turner, G.E. Burch, and W.A. Sodeman. Studies in the physiology of blood vessels in man. III. Some effects of raising and lowering the arm upon the pulse volume and blood volume of the human finger tip in health and in certain diseases of the blood vessels. *J. Clin. Invest.*, 16(5):789–798, 1937.

[90] S.R. Van Leeuwen and G.V.G Baranoski. Elucidating the contribution of Rayleigh scattering to the bluish appearance of veins. *J. Biomed. Opt.*, 23(2):025001–1–17, 2018.

[91] S.R. Van Leeuwen, G.V.G Baranoski, and B.W. Kimmel. Three-wavelength method for the optical differentiation of methemoglobin and sulfhemoglobin in oxygenated blood. In *39th Annual International Conference of the IEEE Engineering in Medicine and Biology Society (EMBC)*, pages 4570–4573, Jeju Island, South Korea, August 2017.

[92] J.S. Varcoe. *Clinical Biochemistry: Techniques and Instrumentation A Practical Course*. World Scientific, Singapore, 2001.

[93] B.D. Ventura, C. Lemerle, K. Michalodimitrakis, and L. Serrano. From *in vivo* to *in silico* biology and back. *Nature*, 443:527–553, 2006.

[94] J.A. Viator, J. Komadina, L.O. Svaasand, G. Aguilar, B. Choi, and N.J. Stuart. A comparative study of photoacoustic and reflectance methods for determination of epidermal melanin content. *J. Investig. Dermatol.*, 122(6):1432–1439, 06 2004.

[95] M. Viceconti, A. Henney, and E. Morley-Fletcher. In silico clinical trials: how computer simulation will transform the biomedical industry. *Int. J. Clin. Trials*, 3(2):37–46, 2016.

[96] X. Wang, T.E. Milner, and M.C. Chang anf J.S. Nelson. Group refractive index measurement of dry and hydrated type I collagen films using optical low-coherence reflectometry. *J. Biomed. Opt.*, 12:212–216, 1996.

[97] J.T. Whitton and J.D. Everall. The thickness of the epidermis. *British Journal of Dermatology*, 89:467–476, 1973.

[98] M.L. Williams, M. Hincenbergs, and K.A. Holbrook. Skin lipid content during early fetal development. *J. Investig. Dermatol.*, 91(3):263–268, 09 1988.

[99] E. Wolak, F.L. Byerly, T. Mason, and B.A. Cairns. Methemoglobinemia in critically ill burned patients. *Am. J. Crit. Care*, 14(2):104–1018, 2005.

[100] Y. Yamaguchi, S. Itami, H. Watabe, K. Yasumoto, Z. A. Abdel-Malek, T. Kubo, F. Rouzaud, A. Tanemura, K. Yoshikawa, and V.J. Hearing. Mesenchymal-epithelial interactions in the skin: increased expression of dickkopf1 by palmoplantar fibroblast inhibits melanocyte growth and differentiation. *J. Cell Biol.*, 165(2):275–285, 2004.

[101] M.F. Yang, V.V. Tuchin, and A.N. Yaroslavsky. Principles of light-skin interactions. In E.D. Baron, editor, *Light-Based Therapies for Skin of Color*, pages 1–44, London, 2009. Springer-Verlag.

[102] A.N. Yaroslavsky, A.V. Priezzhev, J. Rodriques, I.V. Yarolavsky, and H. Battarbee. Optics of blood. In V.V. Tuchin, editor, *Handbook of Optical Biomedical Engineering*, pages 169–216, Bellingham, USA, 2002. SPIE-Press.

[103] I.H. Yarynovska and A. Bilyi. Absorption spectra of sulfhemoglobin derivatives of human blood. In G.L. Cote and A.V. Priezzhev, editors, *Optical Diagnostics and Sensing VI*, volume 6094, pages 1–6. SPIE, 2006.

[104] D. Yim, G.V.G. Baranoski, B.W. Kimmel, T.F. Chen, and E. Miranda. A cell-based light interaction model for human blood. *Computer Graphics Forum*, 31(2):845–854, 2012.

[105] A.R. Young. Chromophores in human skin. *Phys. Med. Biol.*, 42(5):789, 1997.

[106] G.A. Zerlaut and T.E. Anderson. Multiple-integrating sphere spectrophotometer for measuring absolute spectral reflectance and transmittance. *Applied Optics*, 20(21):3797–3804, November 1981.

[107] S.D. Zucker, P.S. Horn, and K.E. Sherman. Serum bilirubin levels in the US population: Gender effect and inverse correlation with colorectal cancer. *Hepatology*, 40(4):827–835, 2004.

Alphabetical Index

reflected radiant power, 9

beta-carotene, 7
bilirubin, 7
blood gas analysers, 2
blood-perfused cutaneous tissues, 26

CIELAB differences, 15
co-oximeters, 2
collagen fibrils, 7
concave down, 26
concave up, 26
controlled in silico experiments, 3
cyanosis, 1
cyanotic appearance, 25
cyanotic hues, 25

dermis, 5
differential solid angle, 9
directional-hemispherical reflectance, 9
DNA, 7
dysfunctional, 17
dysfunctional forms of hemoglobin, 1
dyshemoglobinemia, 3
dyshemoglobinemia disorders, 1

epidermis, 5, 10
eumelanin, 7

functional forms of hemoglobin, 1

geometrical-optics formulation, 10

heme, 7
hemoglobin, 7
hue, 8
hypodermis, 7
hypopigmented, 11

incident radiant power, 9

keratin, 7

lipid droplets, 7

methemoblobinemia, 1
methemoglobin, 1
methemoglobinemia, 2
methylene blue, 2

nonpalmoplantar regions, 11

oxygen saturation levels, 25

palmar fingertip, 13
peripheral cyanosis, 11
pheomelanin, 7
porphyrin rings, 7
pulse oximeter, 25

ray optics stochastic simulation, 9
Rayleigh scattering, 7
red blood cells, 7
reflectance, 9
reticular dermis, 14

spectral power distribution, 9
spectrophotometer, 9
stratum basale, 5
stratum corneum, 5
stratum granulosum, 5
stratum lucidum, 5
stratum spinosum, 5
sulfhemoglobin, 1
sulfhemoglobinemia, 1, 2

three point central difference formula, 26

urocanic, 7

virtual spectrophotometer, 11

APPENDICES

Appendix A

RGB Data

In this appendix, we provide the RGB values computed for the swatches presented in Chapter 4.

Table A.1: RGB values computed for the swatches depicted in Fig. 4.5.

	MetHb			SHb		
	R	G	B	R	G	B
10%	247	165	152	244	167	152
20%	240	165	152	236	170	154
30%	235	166	152	229	174	155
40%	230	167	153	224	178	157
50%	227	169	153	219	183	159
60%	224	170	153	216	188	161
70%	222	172	154	213	193	163
80%	220	173	155	211	200	166

Table A.2: RGB values computed for the swatches depicted in Fig. 4.6.

	MetHb			SHb		
	R	G	B	R	G	B
10%	219	140	146	215	141	146
20%	209	140	146	204	143	147
30%	202	141	147	195	146	148
40%	195	142	147	188	149	149
50%	190	142	147	181	152	150
60%	185	143	147	176	156	151
70%	182	144	148	173	161	152
80%	179	146	148	170	168	154

Table A.3: RGB values computed for the swatches depicted in Fig. 4.7.

	MetHb			SHb		
	R	G	B	R	G	B
10%	194	133	145	190	133	146
20%	181	133	146	176	135	146
30%	172	134	146	165	136	147
40%	165	134	147	157	137	147
50%	159	134	147	151	138	148
60%	154	135	147	146	140	149
70%	150	135	148	142	143	149
80%	146	136	148	140	147	150

Table A.4: RGB values computed for the swatches depicted in Fig. 4.8.

	MetHb			SHb		
	R	G	B	R	G	B
10%	178	132	146	173	133	146
20%	164	133	146	159	133	146
30%	155	133	146	149	134	147
40%	148	134	147	141	135	147
50%	142	134	147	135	135	148
60%	137	134	147	131	136	148
70%	134	134	148	128	137	149
80%	131	134	148	126	139	149

Appendix B

Additional Dysfunctional Reflectance Curves

In this appendix, we provide the dysfunctional reflectance curves resulting from repeating our *in silico* experiments (described in Sections 3.1, 3.2 and 4.1) for distinct angles of incidence, namely 0° (Figs. B.1 to B.4), 30° (Figs. B.5 to B.8) and 45° (Figs. B.9 to B.12).

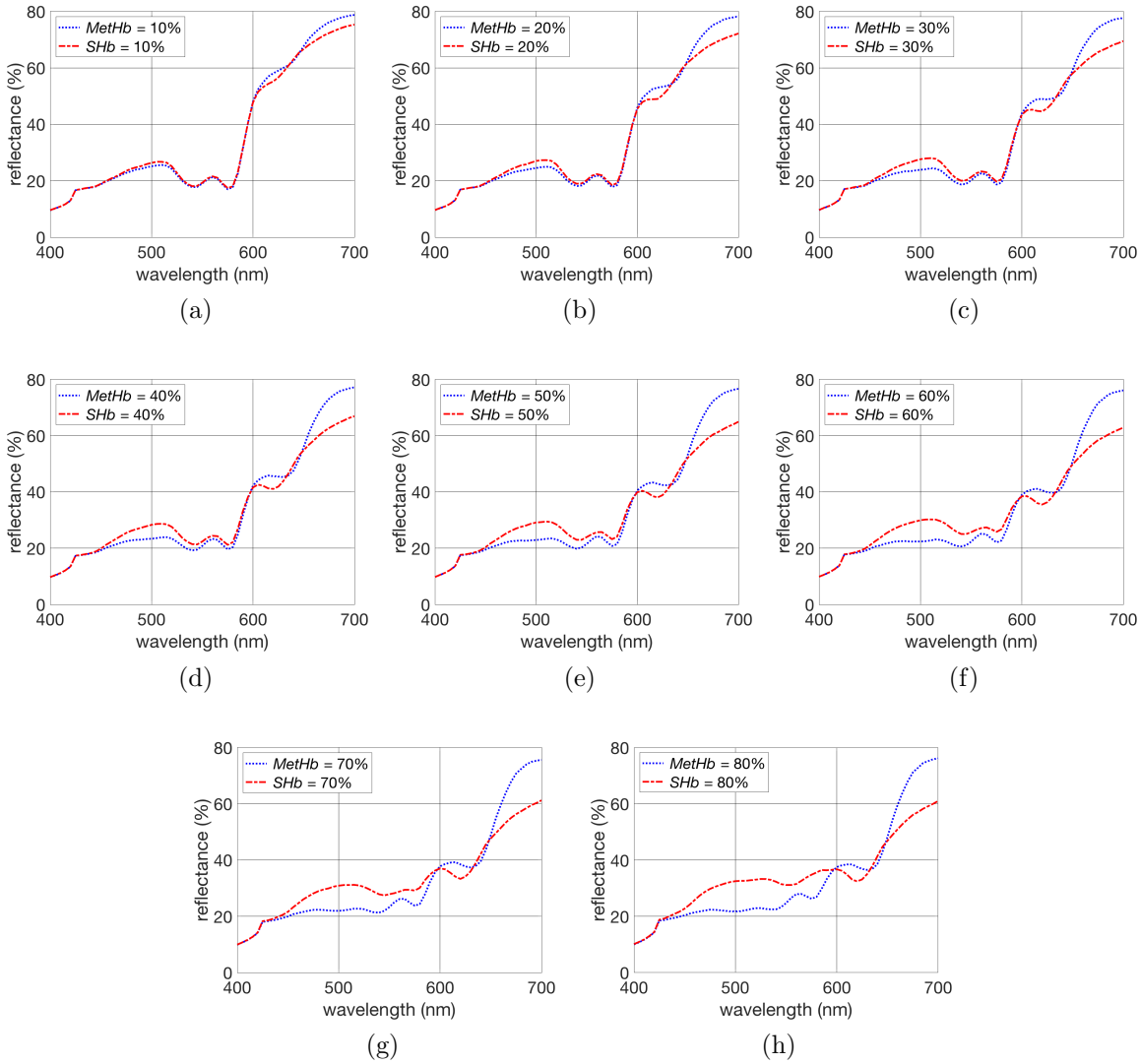

Figure B.1: Graphs depicting reflectance curves resulting from increasing amounts of methemoglobin (MetHb) and sulfhemoglobin (SHb) in a skin specimen characterized by a reticular blood content (v_{blood}^{rd}) equal to 2%. These curves were obtained using the HyLIoS [25] model and considering an angle of incidence equal to 0°. Each graph corresponds to a distinct severity level of methemoglobinemia and sulfhemoglobinemia: (a) 10%, (b) 20%, (c) 30%, (d) 40%, (e) 50%, (f) 60%, (g) 70% and (h) 80%. The concentrations of dysfunctional and functional hemoglobins associated with these levels are provided in Tables 3.2 and 3.3. The remaining parameters values used in the specimen's characterization are provided in Table 3.1.

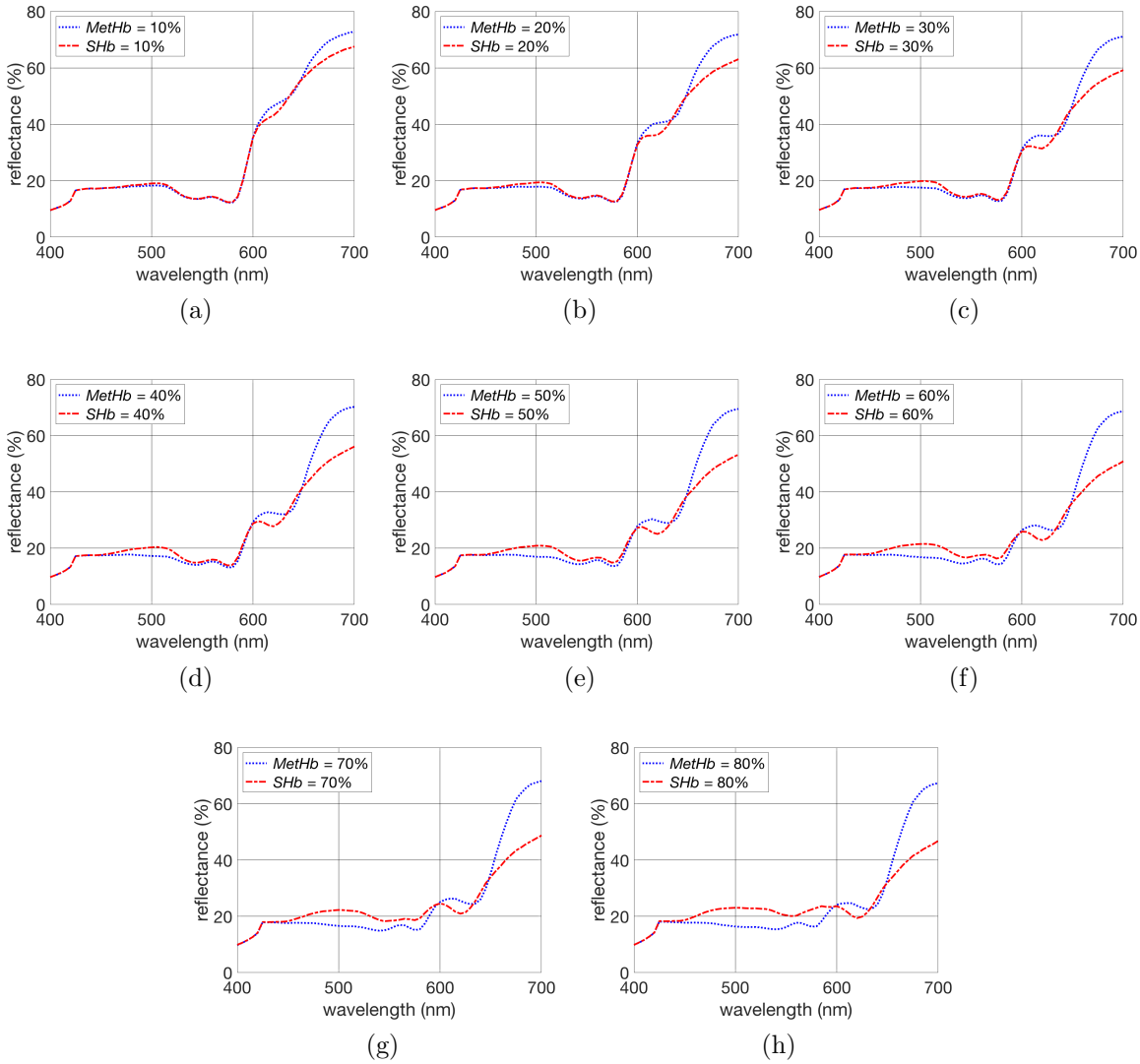

Figure B.2: Graphs depicting reflectance curves resulting from increasing amounts of methemoglobin (MetHb) and sulfhemoglobin (SHb) in a skin specimen characterized by a reticular blood content (v_{blood}^{rd}) equal to 5%. These curves were obtained using the HyLIoS [25] model and considering an angle of incidence equal to 0°. Each graph corresponds to a distinct severity level of methemoglobinemia and sulfhemoglobinemia: (a) 10%, (b) 20%, (c) 30%, (d) 40%, (e) 50%, (f) 60%, (g) 70% and (h) 80%. The concentrations of dysfunctional and functional hemoglobins associated with these levels are provided in Tables 3.2 and 3.3. The remaining parameters values used in the specimen's characterization are provided in Table 3.1.

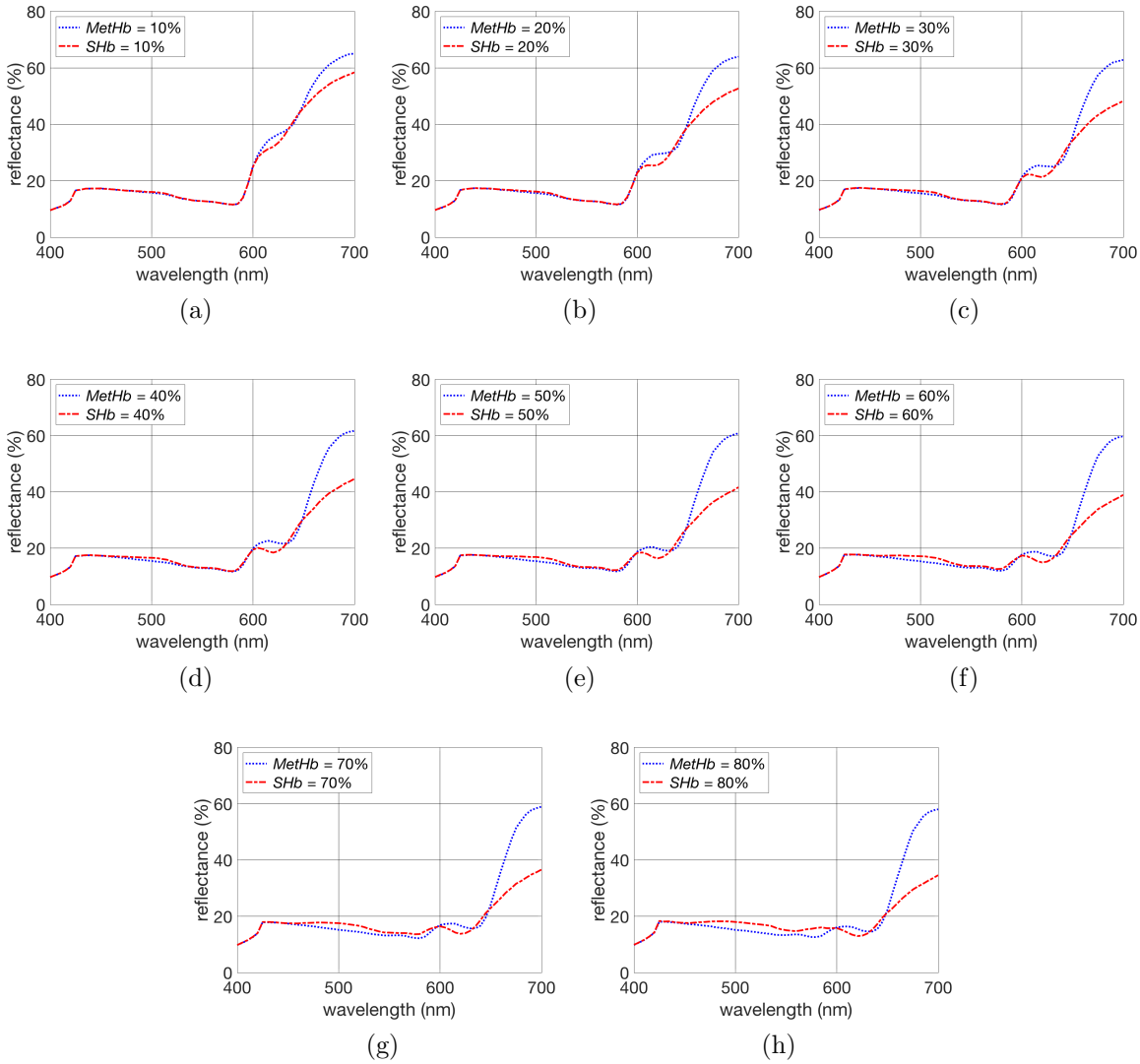

Figure B.3: Graphs depicting reflectance curves resulting from increasing amounts of methemoglobin (MetHb) and sulfhemoglobin (SHb) in a skin specimen characterized by a reticular blood content (v_{blood}^{rd}) equal to 10%. These curves were obtained using the HyLIoS [25] model and considering an angle of incidence equal to 0°. Each graph corresponds to a distinct severity level of methemoglobinemia and sulfhemoglobinemia: (a) 10%, (b) 20%, (c) 30%, (d) 40%, (e) 50%, (f) 60%, (g) 70% and (h) 80%. The concentrations of dysfunctional and functional hemoglobins associated with these levels are provided in Tables 3.2 and 3.3. The remaining parameters values used in the specimen's characterization are provided in Table 3.1.

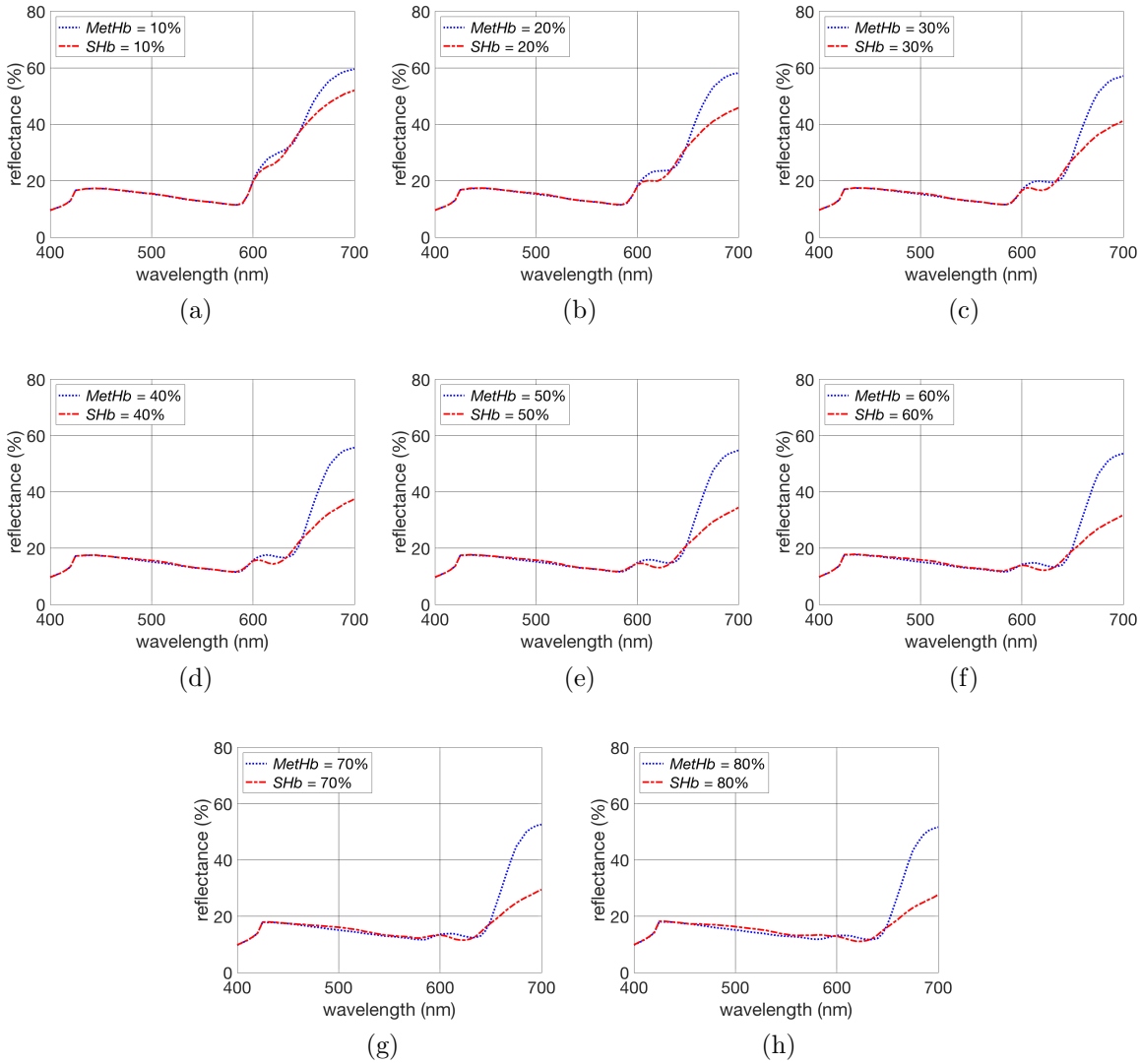

Figure B.4: Graphs depicting reflectance curves resulting from increasing amounts of methemoglobin (MetHb) and sulfhemoglobin (SHb) in a skin specimen characterized by a reticular blood content (v_{blood}^{rd}) equal to 15%. These curves were obtained using the HyLIoS [25] model and considering an angle of incidence equal to 0°. Each graph corresponds to a distinct severity level of methemoglobinemia and sulfhemoglobinemia: (a) 10%, (b) 20%, (c) 30%, (d) 40%, (e) 50%, (f) 60%, (g) 70% and (h) 80%. The concentrations of dysfunctional and functional hemoglobins associated with these levels are provided in Tables 3.2 and 3.3. The remaining parameters values used in the specimen's characterization are provided in Table 3.1.

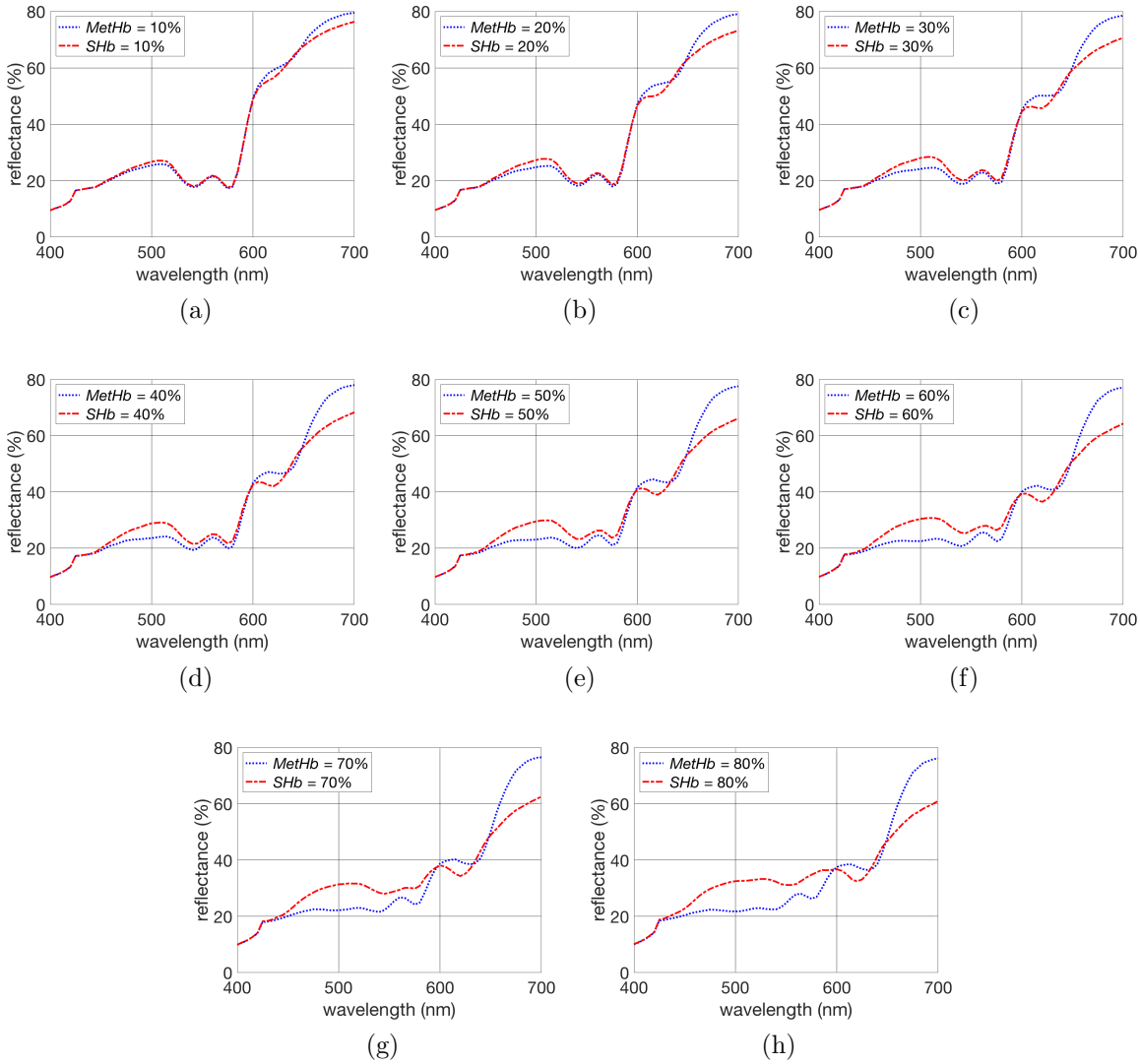

Figure B.5: Graphs depicting reflectance curves resulting from increasing amounts of methemoglobin (MetHb) and sulfhemoglobin (SHb) in a skin specimen characterized by a reticular blood content (v_{blood}^{rd}) equal to 2%. These curves were obtained using the HyLIoS [25] model and considering an angle of incidence equal to 30°. Each graph corresponds to a distinct severity level of methemoglobinemia and sulfhemoglobinemia: (a) 10%, (b) 20%, (c) 30%, (d) 40%, (e) 50%, (f) 60%, (g) 70% and (h) 80%. The concentrations of dysfunctional and functional hemoglobins associated with these levels are provided in Tables 3.2 and 3.3. The remaining parameters values used in the specimen's characterization are provided in Table 3.1.

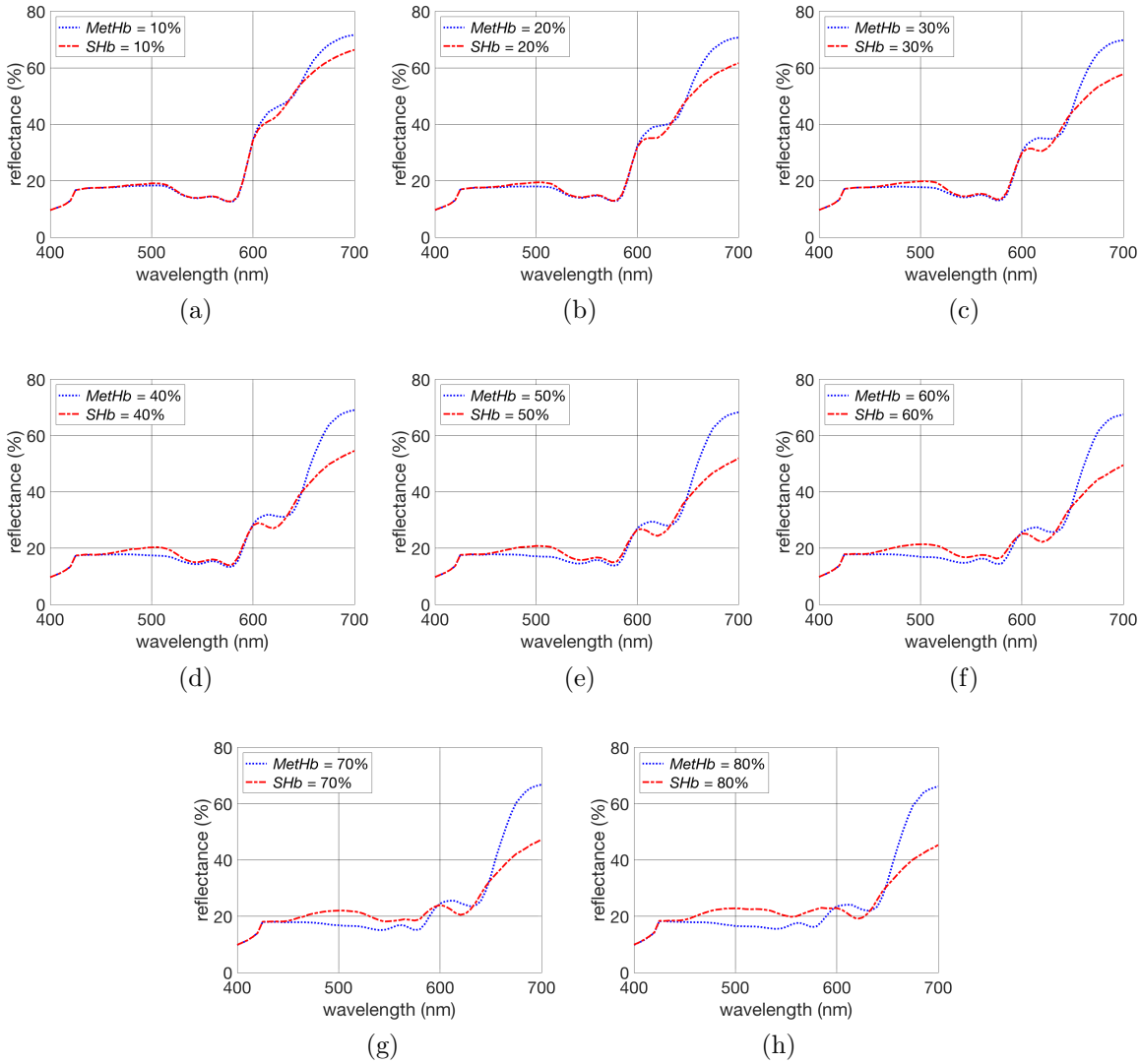

Figure B.6: Graphs depicting reflectance curves resulting from increasing amounts of methemoglobin (MetHb) and sulfhemoglobin (SHb) in a skin specimen characterized by a reticular blood content (v_{blood}^{rd}) equal to 5%. These curves were obtained using the HyLIoS [25] model and considering an angle of incidence equal to 30°. Each graph corresponds to a distinct severity level of methemoglobinemia and sulfhemoglobinemia: (a) 10%, (b) 20%, (c) 30%, (d) 40%, (e) 50%, (f) 60%, (g) 70% and (h) 80%. The concentrations of dysfunctional and functional hemoglobins associated with these levels are provided in Tables 3.2 and 3.3. The remaining parameters values used in the specimen's characterization are provided in Table 3.1.

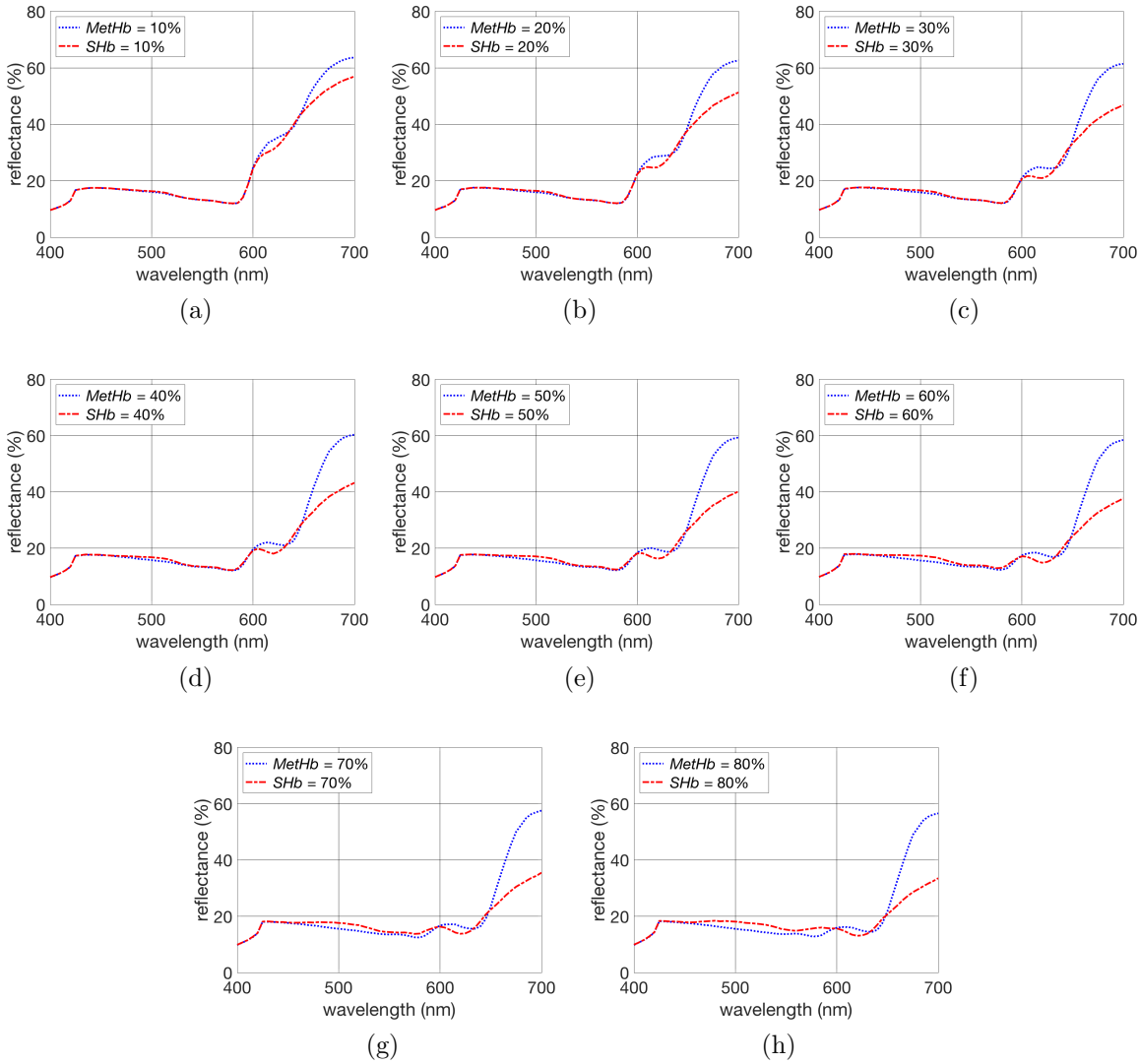

Figure B.7: Graphs depicting reflectance curves resulting from increasing amounts of methemoglobin (MetHb) and sulfhemoglobin (SHb) in a skin specimen characterized by a reticular blood content (v_{blood}^{rd}) equal to 10%. These curves were obtained using the HyLIoS [25] model and considering an angle of incidence equal to 30°. Each graph corresponds to a distinct severity level of methemoglobinemia and sulfhemoglobinemia: (a) 10%, (b) 20%, (c) 30%, (d) 40%, (e) 50%, (f) 60%, (g) 70% and (h) 80%. The concentrations of dysfunctional and functional hemoglobins associated with these levels are provided in Tables 3.2 and 3.3. The remaining parameters values used in the specimen's characterization are provided in Table 3.1.

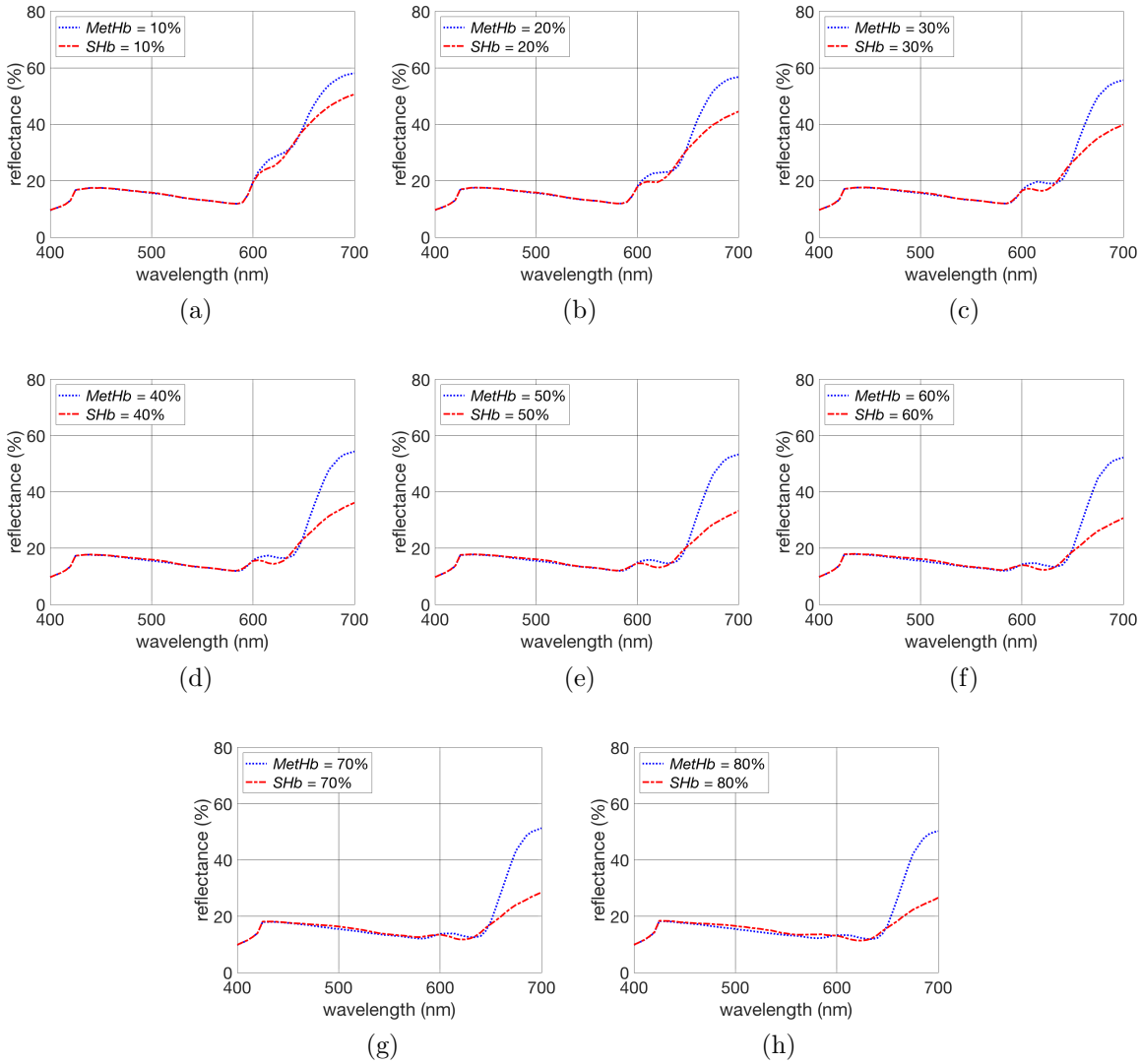

Figure B.8: Graphs depicting reflectance curves resulting from increasing amounts of methemoglobin (MetHb) and sulfhemoglobin (SHb) in a skin specimen characterized by a reticular blood content (v_{blood}^{rd}) equal to 15%. These curves were obtained using the HyLIoS [25] model and considering an angle of incidence equal to 30°. Each graph corresponds to a distinct severity level of methemoglobinemia and sulfhemoglobinemia: (a) 10%, (b) 20%, (c) 30%, (d) 40%, (e) 50%, (f) 60%, (g) 70% and (h) 80%. The concentrations of dysfunctional and functional hemoglobins associated with these levels are provided in Tables 3.2 and 3.3. The remaining parameters values used in the specimen's characterization are provided in Table 3.1.

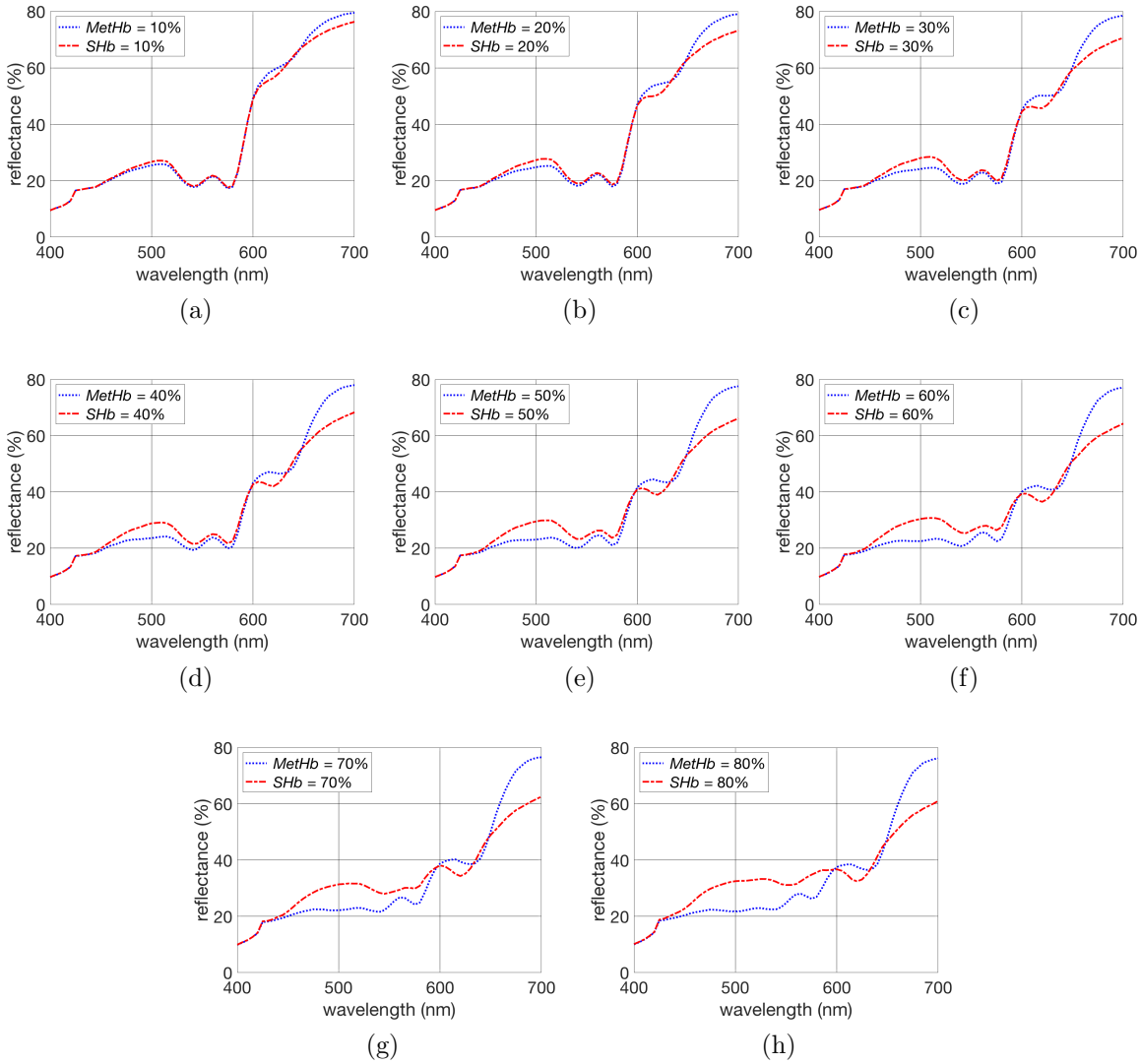

Figure B.9: Graphs depicting reflectance curves resulting from increasing amounts of methemoglobin (MetHb) and sulfhemoglobin (SHb) in a skin specimen characterized by a reticular blood content (v_{blood}^{rd}) equal to 2%. These curves were obtained using the HyLIoS [25] model and considering an angle of incidence equal to 45°. Each graph corresponds to a distinct severity level of methemoglobinemia and sulfhemoglobinemia: (a) 10%, (b) 20%, (c) 30%, (d) 40%, (e) 50%, (f) 60%, (g) 70% and (h) 80%. The concentrations of dysfunctional and functional hemoglobins associated with these levels are provided in Tables 3.2 and 3.3. The remaining parameters values used in the specimen's characterization are provided in Table 3.1.

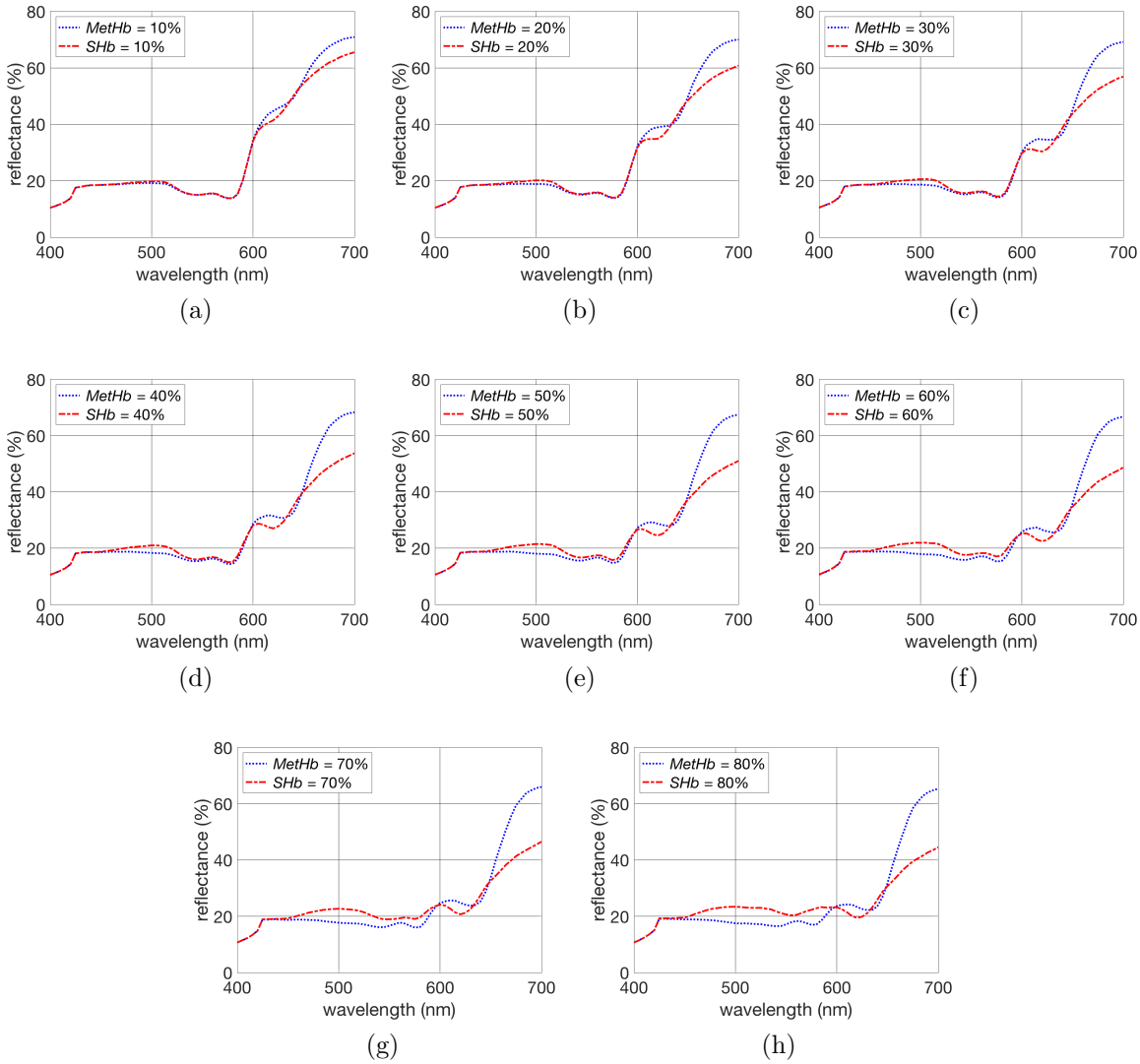

Figure B.10: Graphs depicting reflectance curves resulting from increasing amounts of methemoglobin (MetHb) and sulfhemoglobin (SHb) in a skin specimen characterized by a reticular blood content (v^{rd}_{blood}) equal to 5%. These curves were obtained using the HyLIoS [25] model and considering an angle of incidence equal to 45°. Each graph corresponds to a distinct severity level of methemoglobinemia and sulfhemoglobinemia: (a) 10%, (b) 20%, (c) 30%, (d) 40%, (e) 50%, (f) 60%, (g) 70% and (h) 80%. The concentrations of dysfunctional and functional hemoglobins associated with these levels are provided in Tables 3.2 and 3.3. The remaining parameters values used in the specimen's characterization are provided in Table 3.1.

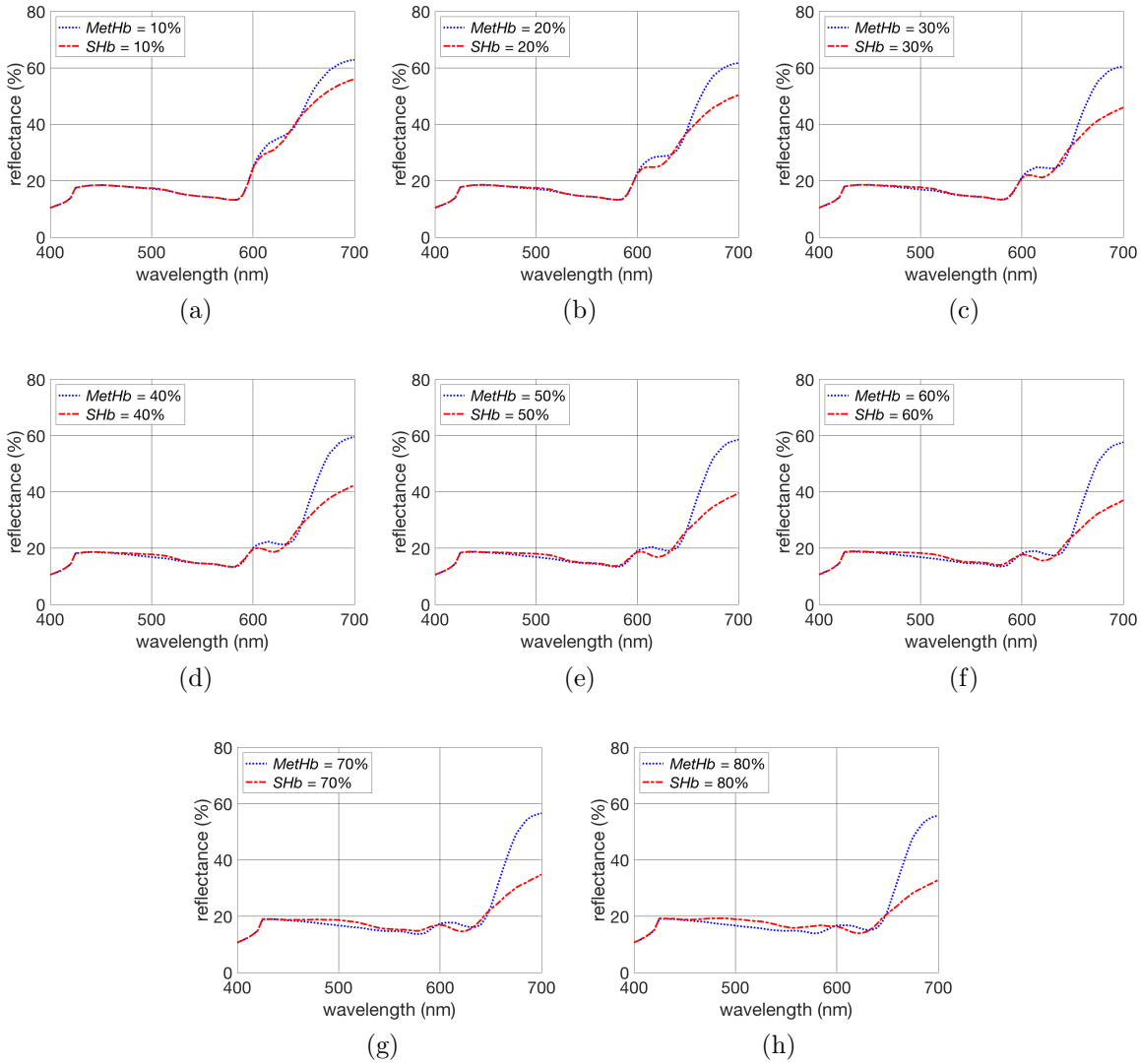

Figure B.11: Graphs depicting reflectance curves resulting from increasing amounts of methemoglobin (MetHb) and sulfhemoglobin (SHb) in a skin specimen characterized by a reticular blood content (v_{blood}^{rd}) equal to 10%. These curves were obtained using the HyLIoS [25] model and considering an angle of incidence equal to 45°. Each graph corresponds to a distinct severity level of methemoglobinemia and sulfhemoglobinemia: (a) 10%, (b) 20%, (c) 30%, (d) 40%, (e) 50%, (f) 60%, (g) 70% and (h) 80%. The concentrations of dysfunctional and functional hemoglobins associated with these levels are provided in Tables 3.2 and 3.3. The remaining parameters values used in the specimen's characterization are provided in Table 3.1.

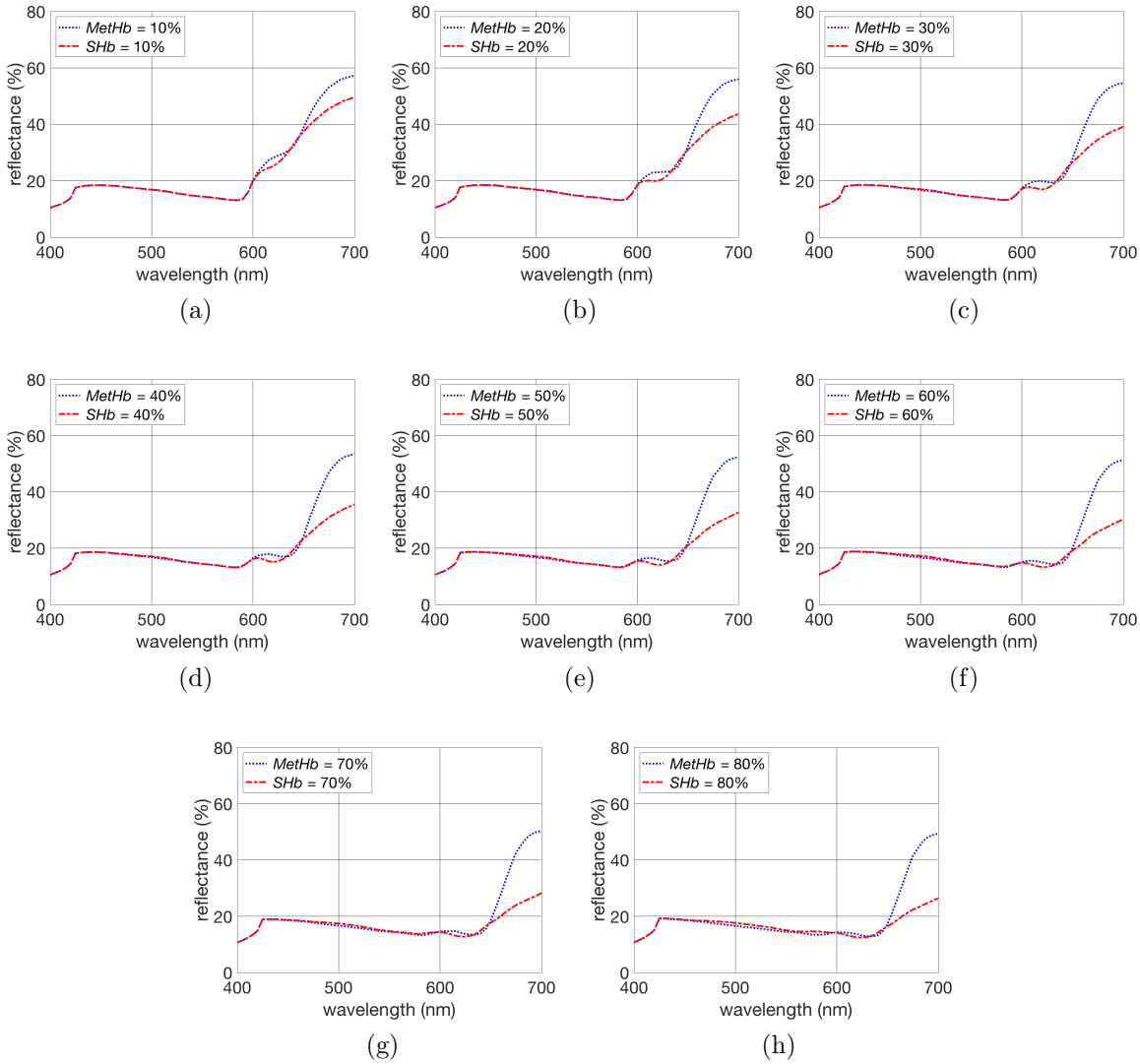

Figure B.12: Graphs depicting reflectance curves resulting from increasing amounts of methemoglobin (MetHb) and sulfhemoglobin (SHb) in a skin specimen characterized by a reticular blood content (v_{blood}^{rd}) equal to 15%. These curves were obtained using the HyLIoS [25] model and considering an angle of incidence equal to 45°. Each graph corresponds to a distinct severity level of methemoglobinemia and sulfhemoglobinemia: (a) 10%, (b) 20%, (c) 30%, (d) 40%, (e) 50%, (f) 60%, (g) 70% and (h) 80%. The concentrations of dysfunctional and functional hemoglobins associated with these levels are provided in Tables 3.2 and 3.3. The remaining parameters values used in the specimen's characterization are provided in Table 3.1.

Appendix C

Reflectance Data

In this appendix, we provide the reflectance values used to compute the signs depicted in Tables 4.1 to 4.4 in (Chapter 4) considering different values for the blood content of the reticular dermis (v^{rd}_{blood}) and distinct angles of incidence.

Table C.1: Reflectance values extracted from dysfunctional curves obtained considering the blood content of the reticular dermis (v^{rd}_{blood}) equal to 2% and the angle of incidence equal to 0°.

	MetHb			SHb		
	605	620	635	605	620	635
10%	0.5360	0.5921	0.6220	0.5270	0.5638	0.6194
20%	0.5046	0.5410	0.5574	0.4909	0.5042	0.5608
30%	0.4781	0.5017	0.5093	0.4606	0.4572	0.5163
40%	0.4529	0.4693	0.4724	0.4361	0.4200	0.4798
50%	0.4321	0.4406	0.4391	0.4137	0.3899	0.4491
60%	0.4132	0.4165	0.4122	0.3938	0.3652	0.4231
70%	0.3963	0.3943	0.3896	0.3771	0.3432	0.3993
80%	0.3817	0.3757	0.3682	0.3620	0.3245	0.3786

Table C.2: Reflectance values extracted from dysfunctional curves obtained considering the blood content of the reticular dermis (v^{rd}_{blood}) equal to 2% and the angle of incidence equal to 15°.

	MetHb			SHb		
	605	620	635	605	620	635
10%	0.5327	0.5888	0.6183	0.5235	0.5595	0.6163
20%	0.4998	0.5378	0.5551	0.4882	0.4997	0.5574
30%	0.4737	0.4980	0.5057	0.4584	0.4532	0.5119
40%	0.4492	0.4645	0.4672	0.4327	0.4180	0.4758
50%	0.4289	0.4378	0.4362	0.4111	0.3881	0.4454
60%	0.4107	0.4136	0.4087	0.3920	0.3624	0.4200
70%	0.3939	0.3928	0.3862	0.3744	0.3411	0.3967
80%	0.3782	0.3727	0.3660	0.3591	0.3215	0.3765

Table C.3: Reflectance values extracted from dysfunctional curves obtained considering the blood content of the reticular dermis (v^{rd}_{blood}) equal to 2% and the angle of incidence equal to 30°.

	MetHb			SHb		
	605	620	635	605	620	635
10%	0.5239	0.5810	0.6095	0.5153	0.5522	0.6084
20%	0.4934	0.5300	0.5457	0.4789	0.4898	0.5486
30%	0.4642	0.4898	0.4976	0.4500	0.4458	0.5035
40%	0.4421	0.4562	0.4595	0.4263	0.4110	0.4663
50%	0.4207	0.4289	0.4282	0.4045	0.3806	0.4360
60%	0.4028	0.4059	0.4003	0.3852	0.3553	0.4100
70%	0.3863	0.3847	0.3786	0.3674	0.3332	0.3885
80%	0.3710	0.3666	0.3581	0.3525	0.3152	0.3681

Table C.4: Reflectance values extracted from dysfunctional curves obtained considering the blood content of the reticular dermis (v^{rd}_{blood}) equal to 2% and the angle of incidence equal to 45°.

	MetHb			SHb		
	605	620	635	605	620	635
10%	0.5176	0.5742	0.6025	0.5090	0.5451	0.6023
20%	0.4877	0.5232	0.5381	0.4743	0.4852	0.5412
30%	0.4594	0.4829	0.4900	0.4462	0.4410	0.4969
40%	0.4370	0.4509	0.4523	0.4209	0.4048	0.4616
50%	0.4171	0.4234	0.4218	0.3996	0.3759	0.4304
60%	0.3981	0.4000	0.3950	0.3799	0.3518	0.4060
70%	0.3821	0.3802	0.3732	0.3634	0.3307	0.3830
80%	0.3674	0.3622	0.3536	0.3496	0.3122	0.3646

Table C.5: Reflectance values extracted from dysfunctional curves obtained considering the blood content of the reticular dermis (v^{rd}_{blood}) equal to 5% and the angle of incidence equal to 0°.

	MetHb			SHb		
	605	620	635	605	620	635
10%	0.4020	0.4646	0.4963	0.3916	0.4308	0.4946
20%	0.3665	0.4045	0.4189	0.3535	0.3624	0.4233
30%	0.3372	0.3600	0.3643	0.3222	0.3141	0.3718
40%	0.3137	0.3255	0.3252	0.2964	0.2778	0.3329
50%	0.2924	0.2974	0.2938	0.2757	0.2507	0.3019
60%	0.2744	0.2746	0.2670	0.2579	0.2288	0.2761
70%	0.2596	0.2550	0.2458	0.2418	0.2095	0.2555
80%	0.2459	0.2376	0.2276	0.2285	0.1940	0.2368

Table C.6: Reflectance values extracted from dysfunctional curves obtained considering the blood content of the reticular dermis (v^{rd}_{blood}) equal to 5% and the angle of incidence equal to 15°.

	MetHb			SHb		
	605	620	635	605	620	635
10%	0.3991	0.4617	0.4937	0.3884	0.4267	0.4917
20%	0.3645	0.4015	0.4161	0.3503	0.3594	0.4203
30%	0.3341	0.3573	0.3619	0.3184	0.3117	0.3694
40%	0.3103	0.3229	0.3223	0.2947	0.2765	0.3306
50%	0.2903	0.2941	0.2903	0.2730	0.2479	0.2987
60%	0.2715	0.2733	0.2646	0.2557	0.2265	0.2743
70%	0.2573	0.2529	0.2435	0.2400	0.2081	0.2535
80%	0.2445	0.2360	0.2253	0.2265	0.1932	0.2351

Table C.7: Reflectance values extracted from dysfunctional curves obtained considering the blood content of the reticular dermis (v^{rd}_{blood}) equal to 5% and the angle of incidence equal to 30°.

	MetHb			SHb		
	605	620	635	605	620	635
10%	0.3918	0.4538	0.4838	0.3811	0.4191	0.4818
20%	0.3570	0.3932	0.4077	0.3437	0.3520	0.4116
30%	0.3293	0.3506	0.3553	0.3137	0.3051	0.3609
40%	0.3057	0.3167	0.3157	0.2897	0.2706	0.3231
50%	0.2847	0.2904	0.2845	0.2683	0.2438	0.2938
60%	0.2669	0.2673	0.2594	0.2510	0.2222	0.2686
70%	0.2531	0.2470	0.2388	0.2358	0.2053	0.2483
80%	0.2392	0.2320	0.2224	0.2235	0.1908	0.2299

Table C.8: Reflectance values extracted from dysfunctional curves obtained considering the blood content of the reticular dermis (v^{rd}_{blood}) equal to 5% and the angle of incidence equal to 45°.

	MetHb			SHb		
	605	620	635	605	620	635
10%	0.3866	0.4475	0.4777	0.3781	0.4144	0.4749
20%	0.3534	0.3891	0.4026	0.3412	0.3485	0.4063
30%	0.3266	0.3467	0.3508	0.3113	0.3038	0.3583
40%	0.3045	0.3145	0.3126	0.2875	0.2706	0.3208
50%	0.2842	0.2870	0.2823	0.2679	0.2451	0.2908
60%	0.2680	0.2655	0.2593	0.2525	0.2244	0.2679
70%	0.2533	0.2482	0.2402	0.2384	0.2072	0.2483
80%	0.2411	0.2332	0.2232	0.2253	0.1945	0.2320

Table C.9: Reflectance values extracted from dysfunctional curves obtained considering the blood content of the reticular dermis (v^{rd}_{blood}) equal to 10% and the angle of incidence equal to 0°.

	MetHb			SHb		
	605	620	635	605	620	635
10%	0.2937	0.3549	0.3843	0.2846	0.3204	0.3831
20%	0.2603	0.2948	0.3058	0.2492	0.2551	0.3103
30%	0.2345	0.2524	0.2554	0.2223	0.2125	0.2615
40%	0.2152	0.2227	0.2190	0.2012	0.1845	0.2262
50%	0.1974	0.1992	0.1930	0.1848	0.1638	0.2003
60%	0.1841	0.1810	0.1731	0.1716	0.1495	0.1803
70%	0.1729	0.1670	0.1578	0.1602	0.1380	0.1653
80%	0.1636	0.1559	0.1461	0.1516	0.1300	0.1525

Table C.10: Reflectance values extracted from dysfunctional curves obtained considering the blood content of the reticular dermis (v_{blood}^{rd}) equal to 10% and the angle of incidence equal to 15°.

	MetHb			SHb		
	605	620	635	605	620	635
10%	0.2916	0.3522	0.3812	0.2816	0.3172	0.3798
20%	0.2588	0.2915	0.3036	0.2468	0.2514	0.3070
30%	0.2340	0.2509	0.2525	0.2210	0.2115	0.2584
40%	0.2125	0.2210	0.2185	0.1994	0.1838	0.2249
50%	0.1970	0.1975	0.1923	0.1834	0.1632	0.1989
60%	0.1836	0.1799	0.1723	0.1706	0.1489	0.1795
70%	0.1716	0.1667	0.1573	0.1599	0.1380	0.1643
80%	0.1623	0.1548	0.1458	0.1513	0.1294	0.1522

Table C.11: Reflectance values extracted from dysfunctional curves obtained considering the blood content of the reticular dermis (v_{blood}^{rd}) equal to 10% and the angle of incidence equal to 30°.

	MetHb			SHb		
	605	620	635	605	620	635
10%	0.2854	0.3440	0.3736	0.2769	0.3113	0.3718
20%	0.2543	0.2867	0.2971	0.2425	0.2476	0.3003
30%	0.2301	0.2467	0.2481	0.2167	0.2094	0.2539
40%	0.2107	0.2165	0.2150	0.1979	0.1807	0.2202
50%	0.1935	0.1955	0.1887	0.1823	0.1628	0.1962
60%	0.1811	0.1785	0.1707	0.1695	0.1484	0.1772
70%	0.1710	0.1640	0.1561	0.1598	0.1382	0.1627
80%	0.1623	0.1544	0.1449	0.1514	0.1310	0.1509

Table C.12: Reflectance values extracted from dysfunctional curves obtained considering the blood content of the reticular dermis (v^{rd}_{blood}) equal to 10% and the angle of incidence equal to 45°.

	MetHb			SHb		
	605	620	635	605	620	635
10%	0.2854	0.3408	0.3696	0.2762	0.3085	0.3678
20%	0.2558	0.2852	0.2953	0.2439	0.2494	0.2977
30%	0.2317	0.2465	0.2480	0.2205	0.2114	0.2533
40%	0.2142	0.2188	0.2160	0.2008	0.1862	0.2225
50%	0.1982	0.1985	0.1936	0.1874	0.1683	0.1989
60%	0.1878	0.1832	0.1752	0.1761	0.1559	0.1820
70%	0.1772	0.1707	0.1624	0.1671	0.1464	0.1681
80%	0.1681	0.1616	0.1526	0.1590	0.1396	0.1581

Table C.13: Reflectance values extracted from dysfunctional curves obtained considering the blood content of the reticular dermis (v^{rd}_{blood}) equal to 15% and the angle of incidence equal to 0°.

	MetHb			SHb		
	605	620	635	605	620	635
10%	0.2359	0.2894	0.3190	0.2265	0.2580	0.3164
20%	0.2068	0.2345	0.2428	0.1964	0.1990	0.2461
30%	0.1847	0.1979	0.1977	0.1751	0.1658	0.2039
40%	0.1689	0.1727	0.1688	0.1585	0.1440	0.1744
50%	0.1562	0.1550	0.1490	0.1464	0.1306	0.1538
60%	0.1460	0.1420	0.1350	0.1377	0.1216	0.1403
70%	0.1380	0.1327	0.1249	0.1310	0.1157	0.1287
80%	0.1321	0.1250	0.1177	0.1251	0.1109	0.1215

Table C.14: Reflectance values extracted from dysfunctional curves obtained considering the blood content of the reticular dermis (v_{blood}^{rd}) equal to 15% and the angle of incidence equal to 15°.

	MetHb			SHb		
	605	620	635	605	620	635
10%	0.2336	0.2883	0.3161	0.2250	0.2560	0.3131
20%	0.2055	0.2321	0.2406	0.1948	0.1975	0.2444
30%	0.1838	0.1965	0.1963	0.1734	0.1646	0.2020
40%	0.1682	0.1719	0.1677	0.1575	0.1436	0.1737
50%	0.1550	0.1545	0.1482	0.1459	0.1300	0.1537
60%	0.1459	0.1413	0.1336	0.1374	0.1219	0.1384
70%	0.1382	0.1325	0.1245	0.1313	0.1156	0.1290
80%	0.1317	0.1257	0.1177	0.1255	0.1117	0.1209

Table C.15: Reflectance values extracted from dysfunctional curves obtained considering the blood content of the reticular dermis (v_{blood}^{rd}) equal to 15% and the angle of incidence equal to 30°.

	MetHb			SHb		
	605	620	635	605	620	635
10%	0.2307	0.2823	0.3096	0.2220	0.2507	0.3071
20%	0.2023	0.2280	0.2364	0.1927	0.1949	0.2401
30%	0.1816	0.1946	0.1933	0.1721	0.1643	0.1992
40%	0.1670	0.1698	0.1668	0.1573	0.1441	0.1713
50%	0.1556	0.1536	0.1484	0.1463	0.1311	0.1514
60%	0.1461	0.1410	0.1351	0.1384	0.1230	0.1390
70%	0.1391	0.1328	0.1258	0.1318	0.1176	0.1301
80%	0.1333	0.1264	0.1192	0.1275	0.1142	0.1226

Table C.16: Reflectance values extracted from dysfunctional curves obtained considering the blood content of the reticular dermis (v^{rd}_{blood}) equal to 15% and the angle of incidence equal to 45°.

	MetHb			SHb		
	605	620	635	605	620	635
10%	0.2328	0.2819	0.3062	0.2248	0.2516	0.3040
20%	0.2061	0.2303	0.2367	0.1970	0.1987	0.2405
30%	0.1872	0.1985	0.1973	0.1789	0.1693	0.2020
40%	0.1742	0.1759	0.1712	0.1653	0.1512	0.1762
50%	0.1626	0.1610	0.1548	0.1549	0.1403	0.1595
60%	0.1549	0.1500	0.1427	0.1467	0.1335	0.1472
70%	0.1480	0.1418	0.1347	0.1416	0.1279	0.1376
80%	0.1428	0.1371	0.1286	0.1380	0.1251	0.1318

Appendix D

Reflectance Data Subjected to Random Fluctuations

In this appendix, we provide the reflectance values accounting for the ±1% random noise in our simulations.

Table D.1: Reflectance values extracted from dysfunctional curves obtained considering the blood content of the reticular dermis equal to 2% and the angle of incidence equal to 0°.

	MetHb			SHb		
	605	620	635	605	620	635
10%	0.5353	0.5946	0.6203	0.5309	0.5588	0.6256
20%	0.5045	0.5424	0.5523	0.4937	0.5011	0.5626
30%	0.4763	0.5015	0.5124	0.4625	0.4614	0.5132
40%	0.4533	0.4709	0.4734	0.4343	0.4201	0.4801
50%	0.4333	0.4423	0.4400	0.4170	0.3861	0.4518
60%	0.4162	0.4131	0.4128	0.3976	0.3643	0.4258
70%	0.3925	0.3905	0.3857	0.3774	0.3426	0.4025
80%	0.3808	0.3773	0.3656	0.3615	0.3237	0.3780

Table D.2: Reflectance values extracted from dysfunctional curves obtained considering the blood content of the reticular dermis equal to 2% and the angle of incidence equal to 15°.

	MetHb			SHb		
	605	620	635	605	620	635
10%	0.5327	0.5888	0.6183	0.5235	0.5595	0.6163
20%	0.4998	0.5378	0.5551	0.4882	0.4997	0.5574
30%	0.4737	0.4980	0.5057	0.4584	0.4532	0.5119
40%	0.4492	0.4645	0.4672	0.4327	0.4180	0.4758
50%	0.4289	0.4378	0.4362	0.4111	0.3881	0.4454
60%	0.4107	0.4136	0.4087	0.3920	0.3624	0.4200
70%	0.3939	0.3928	0.3862	0.3744	0.3411	0.3967
80%	0.3782	0.3727	0.3660	0.3591	0.3215	0.3765

Table D.3: Reflectance values extracted from dysfunctional curves obtained considering the blood content of the reticular dermis equal to 2% and the angle of incidence equal to 30°.

	MetHb			SHb		
	605	620	635	605	620	635
10%	0.5196	0.5847	0.6147	0.5117	0.5514	0.6068
20%	0.4942	0.5315	0.5449	0.4819	0.4931	0.5521
30%	0.4634	0.4865	0.4967	0.4535	0.4487	0.4988
40%	0.4419	0.4605	0.4581	0.4284	0.4138	0.4657
50%	0.4176	0.4291	0.4273	0.4015	0.3815	0.4368
60%	0.4006	0.4089	0.4034	0.3863	0.3584	0.4087
70%	0.3849	0.3867	0.3779	0.3689	0.3299	0.3911
80%	0.3699	0.3699	0.3587	0.3545	0.3181	0.3664

Table D.4: Reflectance values extracted from dysfunctional curves obtained considering the blood content of the reticular dermis equal to 2% and the angle of incidence equal to 45°.

	MetHb			SHb		
	605	620	635	605	620	635
10%	0.5183	0.5735	0.6046	0.5060	0.5481	0.6070
20%	0.4877	0.5230	0.5336	0.4709	0.4855	0.5436
30%	0.4569	0.4840	0.4947	0.4443	0.4432	0.4928
40%	0.4407	0.4522	0.4540	0.4234	0.4036	0.4623
50%	0.4199	0.4269	0.4218	0.4012	0.3764	0.4276
60%	0.3970	0.3990	0.3985	0.3827	0.3508	0.4079
70%	0.3837	0.3776	0.3752	0.3671	0.3318	0.3846
80%	0.3653	0.3620	0.3570	0.3507	0.3106	0.3637

Table D.5: Reflectance values extracted from dysfunctional curves obtained considering the blood content of the reticular dermis equal to 5% and the angle of incidence equal to 0°.

	MetHb			SHb		
	605	620	635	605	620	635
10%	0.3990	0.4644	0.4957	0.3944	0.4338	0.4941
20%	0.3662	0.4041	0.4165	0.3544	0.3650	0.4267
30%	0.3340	0.3607	0.3666	0.3198	0.3150	0.3692
40%	0.3166	0.3244	0.3269	0.2948	0.2752	0.3322
50%	0.2904	0.2955	0.2922	0.2756	0.2512	0.2993
60%	0.2771	0.2768	0.2694	0.2592	0.2298	0.2745
70%	0.2585	0.2557	0.2437	0.2399	0.2080	0.2573
80%	0.2453	0.2389	0.2296	0.2284	0.1936	0.2380

Table D.6: Reflectance values extracted from dysfunctional curves obtained considering the blood content of the reticular dermis equal to 5% and the angle of incidence equal to 15°.

	MetHb			SHb		
	605	620	635	605	620	635
10%	0.3981	0.4648	0.4940	0.3863	0.4274	0.4885
20%	0.3615	0.4049	0.4119	0.3532	0.3628	0.4204
30%	0.3326	0.3570	0.3609	0.3200	0.3093	0.3700
40%	0.3092	0.3256	0.3203	0.2927	0.2792	0.3309
50%	0.2888	0.2919	0.2898	0.2706	0.2470	0.2996
60%	0.2729	0.2748	0.2672	0.2541	0.2271	0.2755
70%	0.2574	0.2544	0.2458	0.2394	0.2060	0.2547
80%	0.2432	0.2341	0.2236	0.2253	0.1917	0.2359

Table D.7: Reflectance values extracted from dysfunctional curves obtained considering the blood content of the reticular dermis equal to 5% and the angle of incidence equal to 30°.

	MetHb			SHb		
	605	620	635	605	620	635
10%	0.3936	0.4568	0.4850	0.3833	0.4200	0.4774
20%	0.3588	0.3912	0.4063	0.3472	0.3522	0.4099
30%	0.3320	0.3504	0.3577	0.3138	0.3052	0.3643
40%	0.3066	0.3194	0.3188	0.2914	0.2695	0.3254
50%	0.2855	0.2876	0.2824	0.2707	0.2446	0.2925
60%	0.2649	0.2651	0.2575	0.2513	0.2223	0.2662
70%	0.2551	0.2473	0.2394	0.2378	0.2055	0.2480
80%	0.2375	0.2334	0.2221	0.2233	0.1915	0.2318

Table D.8: Reflectance values extracted from dysfunctional curves obtained considering the blood content of the reticular dermis equal to 5% and the angle of incidence equal to 45°.

	MetHb			SHb		
	605	620	635	605	620	635
10%	0.3842	0.4519	0.4807	0.3816	0.4132	0.4745
20%	0.3539	0.3917	0.4041	0.3442	0.3499	0.4088
30%	0.3273	0.3497	0.3539	0.3133	0.3045	0.3608
40%	0.3020	0.3165	0.3131	0.2892	0.2699	0.3226
50%	0.2833	0.2854	0.2840	0.2654	0.2432	0.2924
60%	0.2681	0.2649	0.2602	0.2509	0.2225	0.2683
70%	0.2516	0.2499	0.2425	0.2375	0.2092	0.2459
80%	0.2422	0.2332	0.2233	0.2250	0.1929	0.2310

Table D.9: Reflectance values extracted from dysfunctional curves obtained considering the blood content of the reticular dermis equal to 10% and the angle of incidence equal to 0°.

	MetHb			SHb		
	605	620	635	605	620	635
10%	0.2936	0.3576	0.3877	0.2819	0.3196	0.3834
20%	0.2614	0.2924	0.3078	0.2468	0.2560	0.3076
30%	0.2350	0.2526	0.2570	0.2207	0.2130	0.2595
40%	0.2138	0.2245	0.2204	0.2022	0.1860	0.2252
50%	0.1967	0.2010	0.1943	0.1842	0.1631	0.2016
60%	0.1841	0.1806	0.1746	0.1731	0.1495	0.1795
70%	0.1745	0.1672	0.1587	0.1610	0.1381	0.1638
80%	0.1621	0.1574	0.1465	0.1512	0.1304	0.1525

Table D.10: Reflectance values extracted from dysfunctional curves obtained considering the blood content of the reticular dermis equal to 10% and the angle of incidence equal to 15°.

	MetHb			SHb		
	605	620	635	605	620	635
10%	0.2910	0.3534	0.3798	0.2795	0.3181	0.3807
20%	0.2595	0.2935	0.3006	0.2490	0.2519	0.3090
30%	0.2347	0.2494	0.2528	0.2195	0.2103	0.2580
40%	0.2113	0.2219	0.2187	0.1994	0.1838	0.2234
50%	0.1977	0.1988	0.1909	0.1828	0.1645	0.1996
60%	0.1831	0.1804	0.1735	0.1711	0.1474	0.1780
70%	0.1719	0.1664	0.1559	0.1583	0.1385	0.1632
80%	0.1622	0.1552	0.1449	0.1519	0.1294	0.1518

Table D.11: Reflectance values extracted from dysfunctional curves obtained considering the blood content of the reticular dermis equal to 10% and the angle of incidence equal to 30°.

	MetHb			SHb		
	605	620	635	605	620	635
10%	0.2830	0.3429	0.3718	0.2745	0.3122	0.3753
20%	0.2529	0.2873	0.2991	0.2408	0.2484	0.3003
30%	0.2293	0.2472	0.2484	0.2165	0.2103	0.2558
40%	0.2104	0.2185	0.2139	0.1968	0.1793	0.2186
50%	0.1946	0.1974	0.1877	0.1839	0.1612	0.1947
60%	0.1825	0.1783	0.1697	0.1700	0.1482	0.1758
70%	0.1694	0.1655	0.1571	0.1588	0.1378	0.1615
80%	0.1632	0.1554	0.1438	0.1518	0.1311	0.1494

Table D.12: Reflectance values extracted from dysfunctional curves obtained considering the blood content of the reticular dermis equal to 10% and the angle of incidence equal to 45°.

	MetHb			SHb		
	605	620	635	605	620	635
10%	0.2846	0.3403	0.3732	0.2771	0.3064	0.3679
20%	0.2563	0.2825	0.2930	0.2454	0.2519	0.2976
30%	0.2295	0.2444	0.2486	0.2204	0.2132	0.2525
40%	0.2142	0.2180	0.2148	0.2011	0.1878	0.2209
50%	0.1963	0.1986	0.1939	0.1856	0.1688	0.1981
60%	0.1890	0.1832	0.1753	0.1764	0.1554	0.1809
70%	0.1767	0.1714	0.1621	0.1666	0.1459	0.1686
80%	0.1695	0.1620	0.1538	0.1600	0.1407	0.1568

Table D.13: Reflectance values extracted from dysfunctional curves obtained considering the blood content of the reticular dermis equal to 15% and the angle of incidence equal to 0°.

	MetHb			SHb		
	605	620	635	605	620	635
10%	0.2374	0.2868	0.3213	0.2256	0.2601	0.3176
20%	0.2055	0.2356	0.2436	0.1967	0.1971	0.2474
30%	0.1863	0.1970	0.1990	0.1742	0.1660	0.2021
40%	0.1674	0.1716	0.1689	0.1599	0.1428	0.1727
50%	0.1551	0.1539	0.1484	0.1466	0.1318	0.1548
60%	0.1450	0.1423	0.1359	0.1375	0.1227	0.1400
70%	0.1378	0.1322	0.1243	0.1300	0.1156	0.1282
80%	0.1311	0.1251	0.1186	0.1248	0.1108	0.1222

Table D.14: Reflectance values extracted from dysfunctional curves obtained considering the blood content of the reticular dermis equal to 15% and the angle of incidence equal to 15°.

	MetHb			SHb		
	605	620	635	605	620	635
10%	0.2355	0.2909	0.3185	0.2234	0.2548	0.3124
20%	0.2042	0.2306	0.2415	0.1967	0.1991	0.2421
30%	0.1853	0.1983	0.1944	0.1734	0.1646	0.2013
40%	0.1679	0.1718	0.1667	0.1589	0.1431	0.1736
50%	0.1557	0.1557	0.1476	0.1468	0.1296	0.1530
60%	0.1456	0.1418	0.1348	0.1369	0.1213	0.1371
70%	0.1377	0.1322	0.1234	0.1302	0.1162	0.1301
80%	0.1326	0.1263	0.1187	0.1265	0.1115	0.1208

Table D.15: Reflectance values extracted from dysfunctional curves obtained considering the blood content of the reticular dermis equal to 15% and the angle of incidence equal to 30°.

	MetHb			SHb		
	605	620	635	605	620	635
10%	0.2303	0.2812	0.3079	0.2200	0.2486	0.3093
20%	0.2007	0.2263	0.2380	0.1909	0.1948	0.2402
30%	0.1804	0.1956	0.1943	0.1724	0.1646	0.1988
40%	0.1659	0.1691	0.1670	0.1581	0.1454	0.1717
50%	0.1558	0.1537	0.1498	0.1463	0.1308	0.1521
60%	0.1449	0.1409	0.1342	0.1395	0.1224	0.1379
70%	0.1396	0.1333	0.1266	0.1322	0.1166	0.1305
80%	0.1341	0.1267	0.1187	0.1270	0.1153	0.1224

Table D.16: Reflectance values extracted from dysfunctional curves obtained considering the blood content of the reticular dermis equal to 15% and the angle of incidence equal to 45°.

	MetHb			SHb		
	605	620	635	605	620	635
10%	0.2342	0.2802	0.3070	0.2248	0.2509	0.3040
20%	0.2075	0.2297	0.2367	0.1959	0.1988	0.2420
30%	0.1876	0.1986	0.1984	0.1789	0.1689	0.2014
40%	0.1737	0.1771	0.1712	0.1637	0.1513	0.1770
50%	0.1621	0.1602	0.1562	0.1550	0.1415	0.1602
60%	0.1537	0.1492	0.1427	0.1480	0.1339	0.1470
70%	0.1466	0.1420	0.1339	0.1409	0.1276	0.1380
80%	0.1418	0.1370	0.1290	0.1391	0.1242	0.1326

Appendix E

Matlab Code for Generating Swatches and Computing CIELAB Differences

In this appendix, we present the Matlab [8] code used in the generation of the swatches and in the computation of the CIELAB difference presented in Figs. 4.5 to 4.8.

```
% Make sure all csv files are placed one directory back. cd ..
% Files should follow the naming convention as follows:
% MetHb: sHB_00_mHB_100_VRD_150_Angle_150.csv
% sHB: sHB_10_mHB_15_VRD_150_Angle_150.csv

function swatch_creation

files = dir('../*.csv');
rgb_array = {};
cielab_array = {};
figure(1);clf;
for file = 1:size(files,1)
    figure(1);
    figsPerRow = 8;
    subplot(ceil(size(files,1)/figsPerRow),figsPerRow,file);
    showRGBFile(['../',files(file).name]);
end
```

```
18
19 function image = showRGBFile(filename)
20     rgb = getRGBFile(filename);
21     image = showRGB(rgb);
22     title(filename);
23     outname = strsplit(filename,'/');
24     outname = outname{end};
25     outname = strsplit(outname,'.');
26     outname = outname{1};
27
28     s={filename};
29     r=strrep(s,'.csv','.jpg');
30     r=strrep(r,'../','');
31     str=strjoin(r);
32     figure(2);
33     clf;
34     % This adds black around swatch from the make_circle file.
35     image = make_circle(image, 300, 300);
36     imshow(image);
37     imwrite(image, str);
38 end
39
40 function image = showRGB(rgb)
41     type = 'finger';
42     cropping = false;
43
44     if(strcmp(type,'finger'))
45         id = '';
46         x  = '';
47         % Reads in image file to give finger print texture.
48         finger_print_texture = double(imread(['
               finger_print_texture',id,'.png']))/255;
49         d2f = double(imread(['d2',x,'f',id,'.png']))/255;
50         image(1,1,:) = rgb;
51         image = imresize(image,[size(finger_print_texture,1) size
               (finger_print_texture,2)]);
52         image = image.*finger_print_texture./d2f;
53         offset = 15;
```

```
54          image = image((1:355)+offset,:,:);
55      end
56
57      image = imresize(image,[300 300]);
58
59      if(cropping)
60          cropOffset = 0*strcmp(type,'finger');
61          image = image(1+cropOffset:end/2+cropOffset,:,:);
62      end
63
64      imshow(image);
65      xlabel(num2str(round(rgb*255)));
66  end
67
68  function rgb = getRGBFile(filename)
69      % read in csv data and interpolate waves 400-700 by 10's and
            reflectance
70      % with 400 to 700 by 5's to interpolate the reflectance
            between.
71      data = getCSVData(filename);
72      waves = data(:,1);
73      refls = data(:,2);
74      w = 400:5:700;
75      r = interp1(waves,refls,w);
76      rgb = getRGB(w,r);
77  end
78
79  function rgb = getRGB(waves, refls)
80      % speify the illuminant to use. Daylight D65.
81      ill = 'd65';
82      if(strcmp(ill,'d65'))
83          [wI, iI] = illuminant('d65');
84          XYZ2sRGB = makecform('xyz2srgb','AdaptedWhitePoint',
                whitepoint('d65'));
85      end
86      % interpolate illuminant with 400-700 by 5's.
87      iI = interp1(wI,iI,waves);
88      refls = refls .* iI;
```

```
89      % use color matching function
90      [~, xyz] = spectrumRGB(waves);
91      % use trapezoidal rule to approximate the area under the
            curve.
92       X = trapz(waves,xyz(1,:,1).*refls);
93       Y = trapz(waves,xyz(1,:,2).*refls);
94       Z = trapz(waves,xyz(1,:,3).*refls);
95      % put into array.
96      XYZ(1,:,1) = X;
97      XYZ(1,:,2) = Y;
98      XYZ(1,:,3) = Z;
99      % color match values divided by integration of waves with
            illumninant.
100     XYZ = XYZ/(trapz(waves,iI)*0.23);
101     rgb = applycform(XYZ, XYZ2sRGB);
102     rgb_array = [rgb_array, rgb*255 ];
103 end
104
105 function data = getCSVData(filename)
106     % read in every other line from csv files.
107     f = csvread(filename,1,0);
108     waves = f(1:2:end,1);
109     ref = f(1:2:end,2);
110     data = waves;
111     data(:,2) = ref;
112 end
113
114 % Since there are 16 files in the directory (8 SHb and 8 MetHb)
        we need to seperate them.
115 % Since the first 8 files that are read in are MetHb files and
        the next 8 are SHb files
116 % we offset the index by 8 each on each iteration of the while
        loop in order to output
117 % the RGB values of each swatch to a new csv file as well as
        determine the
118 % CIELAB difference between the SHb and MetHb swatches.
119 n = 1;
120 rgb_to_file = {};
```

```
121 while n < 9
122     methb_rgb=rgb_array{n}
123     sulfhb_rgb=rgb_array{n+8}
124
125     methb_r=methb_rgb(1,1);
126     methb_g=methb_rgb(1,2);
127     methb_b=methb_rgb(1,3);
128
129     sulfhb_r=sulfhb_rgb(1,1);
130     sulfhb_g=sulfhb_rgb(1,2);
131     sulfhb_b=sulfhb_rgb(1,3);
132
133     file_name=str(15:29)
134     rgb_string=strcat(methb_r,methb_g, methb_b, sulfhb_r,
          sulfhb_g, sulfhb_b)
135
136     rgb_to_file = [rgb_to_file, methb_r];
137     rgb_to_file = [rgb_to_file, methb_g];
138     rgb_to_file = [rgb_to_file, methb_b];
139     rgb_to_file = [rgb_to_file, sulfhb_r];
140     rgb_to_file = [rgb_to_file, sulfhb_g];
141     rgb_to_file = [rgb_to_file, sulfhb_b];
142
143     file_name = strcat(file_name, '.csv');
144
145     dlmwrite(file_name,rgb_to_file,'-append')
146
147     first=rgb_array{n}
148     second=rgb_array{n + 8}
149
150     r1=first(1,1);
151     g1=first(1,2);
152     b1=first(1,3);
153
154     r1=r1/255;
155     g1=g1/255;
156     b1=b1/255;
157
```

```
158       rb=second(1,1);
159       gb=second(1,2);
160       bb=second(1,3);
161
162       rb=rb/255;
163       gb=gb/255;
164       bb=bb/255;
165
166       c1 = rgb2lab([r1 g1 b1],'whitepoint','d65');
167       c3 = rgb2lab([r1 g1 b1]);
168       c2 = rgb2lab([rb gb bb],'whitepoint','d65');
169
170      % Final step in the computation of CIELAB Differences.
171       val = sqrt((c1(1)-c2(1))^2 + (c1(2)-c2(2))^2 + (c1(3)-c2(3))
             ^2)
172       cielab_array = [cielab_array, val];
173
174      n = n+1;
175  end
```

```
1  % Create black circle around matlab square swatch.
2  function result = make_circle(image, width, height)
3       blackout = ones(width, height, 3);
4
5       for i = 1 : width
6           for j = 1 : height
7             % Change last number between 0 and 1. Lowering adds
                 black raising lowers black.
8               %if sqrt((i - width/2)^2 + (j - height/2)^2) >= (min(
                   width, height) * 0.25)
9               if sqrt((i - width/2)^2 + (j - height/2)^2) >= (min(
                   width, height))
10                for k = 1 : 3
11                    blackout(i, j, k) = 0;
12                end
13              end
14          end
15      end
```

```
16
17      result = image.*blackout;
18  end
```